

# The IceCube Neutrino Observatory

## Contributions to ICRC 2017 Part I: Searches for the Sources of Astrophysical Neutrinos

### Contents

<b>1 Searching for VHE gamma-ray emission associated with IceCube astrophysical neutrinos using FACT, H.E.S.S., MAGIC, and VERITAS</b>	
PoS (ICRC2017) 618	arXiv:1708.08945
<b>2 Search for point-like sources in the astrophysical muon neutrino flux with IceCube</b>	7
— PoS (ICRC2017) 997	
<b>3 Search for weak neutrino point sources using angular auto-correlation analyses in IceCube</b>	15
— PoS (ICRC2017) 1014	
<b>4 All-sky search for correlations in the arrival directions of astrophysical neutrino candidates and ultrahigh-energy cosmic rays</b>	23
— PoS (ICRC2017) 961	
<b>5 Results of IceCube searches for neutrinos from blazars using seven years of through-going muon data</b>	31
— PoS (ICRC2017) 994	
<b>6 IceCube Search for Neutrinos from 1ES 1959+650: Completing the Picture</b>	39
PoS (ICRC2017) 969	
<b>7 Using all-flavor and all-sky event selections by IceCube to search for neutrino emission from the Galactic plane</b>	47
— PoS (ICRC2017) 995	
<b>8 Constraints on diffuse neutrino emission from the Galactic Plane with 7 years of IceCube data</b>	55
— PoS (ICRC2017) 1011	
<b>9 Search for extended sources of neutrino emission with 7 years of IceCube data</b>	63
— PoS (ICRC2017) 963	
<b>10 Search for a cumulative neutrino signal from blazar flares using IceCube data</b>	71
— PoS (ICRC2017) 957	
<b>11 Investigation of Obscured Flat Spectrum Radio AGN with the IceCube Neutrino Observatory</b>	79
— PoS (ICRC2017) 1000	
<b>12 Realtime neutrino alerts and follow-up in IceCube</b>	87
— PoS (ICRC2017) 982	

<b>13 Search for High-Energy Neutrino Emission from Fast Radio Bursts</b>	<b>95</b>
PoS (ICRC2017) 980	
<b>14 IceCube as a Neutrino Follow-up Observatory for Astronomical Transients</b>	<b>103</b>
PoS (ICRC2017) 1007	

## IceCube Collaboration Member List

M. G. Aartsen<sup>2</sup>, M. Ackermann<sup>52</sup>, J. Adams<sup>16</sup>, J. A. Aguilar<sup>12</sup>, M. Ahlers<sup>20</sup>, M. Ahrens<sup>44</sup>, I. Al Samarai<sup>25</sup>, D. Altmann<sup>24</sup>, K. Andeen<sup>33</sup>, T. Anderson<sup>49</sup>, I. Anseau<sup>12</sup>, G. Anton<sup>24</sup>, C. Argüelles<sup>14</sup>, J. Auffenberg<sup>1</sup>, S. Axani<sup>14</sup>, H. Bagherpour<sup>16</sup>, X. Bai<sup>41</sup>, J. P. Barron<sup>23</sup>, S. W. Barwick<sup>27</sup>, V. Baum<sup>32</sup>, R. Bay<sup>8</sup>, J. J. Beatty<sup>18,19</sup>, J. Becker Tjus<sup>11</sup>, K.-H. Becker<sup>51</sup>, S. BenZvi<sup>43</sup>, D. Berley<sup>17</sup>, E. Bernardini<sup>52</sup>, D. Z. Besson<sup>28</sup>, G. Binder<sup>9,8</sup>, D. Bindig<sup>51</sup>, E. Blaufuss<sup>17</sup>, S. Blot<sup>52</sup>, C. Boehm<sup>44</sup>, M. Börner<sup>21</sup>, F. Bos<sup>11</sup>, D. Bose<sup>46</sup>, S. Böser<sup>32</sup>, O. Botner<sup>50</sup>, J. Bourbeau<sup>31</sup>, F. Bradascio<sup>52</sup>, J. Braun<sup>31</sup>, L. Brayeur<sup>13</sup>, M. Brenzke<sup>1</sup>, H.-P. Bretz<sup>52</sup>, S. Bron<sup>25</sup>, J. Brostean-Kaiser<sup>52</sup>, A. Burgman<sup>50</sup>, T. Carver<sup>25</sup>, J. Casey<sup>31</sup>, M. Casier<sup>13</sup>, E. Cheung<sup>17</sup>, D. Chirkin<sup>31</sup>, A. Christov<sup>25</sup>, K. Clark<sup>29</sup>, L. Classen<sup>36</sup>, S. Coenders<sup>35</sup>, G. H. Collin<sup>14</sup>, J. M. Conrad<sup>14</sup>, D. F. Cowen<sup>49,48</sup>, R. Cross<sup>43</sup>, M. Day<sup>31</sup>, J. P. A. M. de André<sup>22</sup>, C. De Clercq<sup>13</sup>, J. J. DeLaunay<sup>49</sup>, H. Dembinski<sup>37</sup>, S. De Ridder<sup>26</sup>, P. Desiati<sup>31</sup>, K. D. de Vries<sup>13</sup>, G. de Wasseige<sup>13</sup>, M. de With<sup>10</sup>, T. DeYoung<sup>22</sup>, J. C. Díaz-Vélez<sup>31</sup>, V. di Lorenzo<sup>32</sup>, H. Dujmovic<sup>46</sup>, J. P. Dumm<sup>44</sup>, M. Dunkman<sup>49</sup>, B. Eberhardt<sup>32</sup>, T. Ehrhardt<sup>32</sup>, B. Eichmann<sup>11</sup>, P. Eller<sup>49</sup>, P. A. Evenson<sup>37</sup>, S. Fahey<sup>31</sup>, A. R. Fazely<sup>7</sup>, J. Felde<sup>17</sup>, K. Filimonov<sup>8</sup>, C. Finley<sup>44</sup>, S. Flis<sup>44</sup>, A. Franckowiak<sup>52</sup>, E. Friedman<sup>17</sup>, T. Fuchs<sup>21</sup>, T. K. Gaisser<sup>37</sup>, J. Gallagher<sup>30</sup>, L. Gerhardt<sup>9</sup>, K. Ghorbani<sup>31</sup>, W. Giang<sup>23</sup>, T. Glauch<sup>1</sup>, T. Glüsenkamp<sup>24</sup>, A. Goldschmidt<sup>9</sup>, J. G. Gonzalez<sup>37</sup>, D. Grant<sup>23</sup>, Z. Griffith<sup>31</sup>, C. Haack<sup>1</sup>, A. Hallgren<sup>50</sup>, F. Halzen<sup>31</sup>, K. Hanson<sup>31</sup>, D. Hebecker<sup>10</sup>, D. Heereman<sup>12</sup>, K. Helbing<sup>51</sup>, R. Hellauer<sup>17</sup>, S. Hickford<sup>51</sup>, J. Hignight<sup>22</sup>, G. C. Hill<sup>2</sup>, K. D. Hoffman<sup>17</sup>, R. Hoffmann<sup>51</sup>, B. Hokanson-Fasig<sup>31</sup>, K. Hoshina<sup>31,a</sup>, F. Huang<sup>49</sup>, M. Huber<sup>35</sup>, K. Hultqvist<sup>44</sup>, M. Hünnefeld<sup>21</sup>, S. In<sup>46</sup>, A. Ishihara<sup>15</sup>, E. Jacobi<sup>52</sup>, G. S. Japaridze<sup>5</sup>, M. Jeong<sup>46</sup>, K. Jero<sup>31</sup>, B. J. P. Jones<sup>4</sup>, P. Kalaczynski<sup>1</sup>, W. Kang<sup>46</sup>, A. Kappes<sup>36</sup>, T. Karg<sup>52</sup>, A. Karle<sup>31</sup>, U. Katz<sup>24</sup>, M. Kauer<sup>31</sup>, A. Keivani<sup>49</sup>, J. L. Kelley<sup>31</sup>, A. Kheirandish<sup>31</sup>, J. Kim<sup>46</sup>, M. Kim<sup>15</sup>, T. Kintscher<sup>52</sup>, J. Kiryluk<sup>45</sup>, T. Kittler<sup>24</sup>, S. R. Klein<sup>9,8</sup>, G. Kohnen<sup>34</sup>, R. Koirala<sup>37</sup>, H. Kolanoski<sup>10</sup>, L. Köpke<sup>32</sup>, C. Kopper<sup>23</sup>, S. Kopper<sup>47</sup>, J. P. Koschinsky<sup>1</sup>, D. J. Koskinen<sup>20</sup>, M. Kowalski<sup>10,52</sup>, K. Krings<sup>35</sup>, M. Kroll<sup>11</sup>, G. Krückl<sup>32</sup>, J. Kunnen<sup>13</sup>, S. Kunwar<sup>52</sup>, N. Kurahashi<sup>40</sup>, T. Kuwabara<sup>15</sup>, A. Kyriacou<sup>2</sup>, M. Labare<sup>26</sup>, J. L. Lanfranchi<sup>49</sup>, M. J. Larson<sup>20</sup>, F. Lauber<sup>51</sup>, D. Lennarz<sup>22</sup>, M. Lesiak-Bzdak<sup>45</sup>, M. Leuermann<sup>1</sup>, Q. R. Liu<sup>31</sup>, L. Lu<sup>15</sup>, J. Lünemann<sup>13</sup>, W. Luszczak<sup>31</sup>, J. Madsen<sup>42</sup>, G. Maggi<sup>13</sup>, K. B. M. Mahn<sup>22</sup>, S. Mancina<sup>31</sup>, R. Maruyama<sup>38</sup>, K. Mase<sup>15</sup>, R. Maunu<sup>17</sup>, F. McNally<sup>31</sup>, K. Meagher<sup>12</sup>, M. Medici<sup>20</sup>, M. Meier<sup>21</sup>, T. Menne<sup>21</sup>, G. Merino<sup>31</sup>, T. Meures<sup>12</sup>, S. Miarecki<sup>9,8</sup>, J. Micallef<sup>22</sup>, G. Momenté<sup>32</sup>, T. Montaruli<sup>25</sup>, R. W. Moore<sup>23</sup>, M. Moulai<sup>14</sup>, R. Nahnauer<sup>52</sup>, P. Nakarmi<sup>47</sup>, U. Naumann<sup>51</sup>, G. Neer<sup>22</sup>, H. Niederhausen<sup>45</sup>, S. C. Nowicki<sup>23</sup>, D. R. Nygren<sup>9</sup>, A. Obertacke Pollmann<sup>51</sup>, A. Olivás<sup>17</sup>, A. O'Murchadha<sup>12</sup>, T. Palczewski<sup>9,8</sup>, H. Pandya<sup>37</sup>, D. V. Pankova<sup>49</sup>, P. Peiffer<sup>32</sup>, J. A. Pepper<sup>47</sup>, C. Pérez de los Heros<sup>50</sup>, D. Pieloth<sup>21</sup>, E. Pinat<sup>12</sup>, M. Plum<sup>33</sup>, P. B. Price<sup>8</sup>, G. T. Przybylski<sup>9</sup>, C. Raab<sup>12</sup>, L. Rädcl<sup>1</sup>, M. Rameez<sup>20</sup>, K. Rawlins<sup>3</sup>, I. C. Rea<sup>35</sup>, R. Reimann<sup>1</sup>, B. Relethford<sup>40</sup>, M. Relich<sup>15</sup>, E. Resconi<sup>35</sup>, W. Rhode<sup>21</sup>, M. Richman<sup>40</sup>, S. Robertson<sup>2</sup>, M. Rongen<sup>1</sup>, C. Rott<sup>46</sup>, T. Ruhe<sup>21</sup>, D. Ryckbosch<sup>26</sup>, D. Rysewyk<sup>22</sup>, T. Sälzer<sup>1</sup>, S. E. Sanchez Herrera<sup>23</sup>, A. Sandrock<sup>21</sup>, J. Sandroos<sup>32</sup>, S. Sarkar<sup>20,39</sup>, S. Sarkar<sup>23</sup>, K. Satalecka<sup>52</sup>, P. Schlunder<sup>21</sup>, T. Schmidt<sup>17</sup>, A. Schneider<sup>31</sup>, S. Schoenen<sup>1</sup>, S. Schöneberg<sup>11</sup>, L. Schumacher<sup>1</sup>, D. Seckel<sup>37</sup>, S. Seunarine<sup>42</sup>, J. Soedingrekso<sup>21</sup>, D. Soldin<sup>51</sup>, M. Song<sup>17</sup>, G. M. Spiczak<sup>42</sup>,

C. Spiering<sup>52</sup>, J. Stachurska<sup>52</sup>, M. Stamatikos<sup>18</sup>, T. Stanev<sup>37</sup>, A. Stasik<sup>52</sup>, J. Stettner<sup>1</sup>, A. Steuer<sup>32</sup>, T. Stezelberger<sup>9</sup>, R. G. Stokstad<sup>9</sup>, A. Stöbl<sup>15</sup>, N. L. Strotjohann<sup>52</sup>, G. W. Sullivan<sup>17</sup>, M. Sutherland<sup>18</sup>, I. Taboada<sup>6</sup>, J. Tatar<sup>9,8</sup>, F. Tenholt<sup>11</sup>, S. Ter-Antonyan<sup>7</sup>, A. Terliuk<sup>52</sup>, G. Tešić<sup>49</sup>, S. Tilav<sup>37</sup>, P. A. Toale<sup>47</sup>, M. N. Tobin<sup>31</sup>, S. Toscano<sup>13</sup>, D. Tosi<sup>31</sup>, M. Tselengidou<sup>24</sup>, C. F. Tung<sup>6</sup>, A. Turcati<sup>35</sup>, C. F. Turley<sup>49</sup>, B. Ty<sup>31</sup>, E. Unger<sup>50</sup>, M. Usner<sup>52</sup>, J. Vandenbroucke<sup>31</sup>, W. Van Driessche<sup>26</sup>, N. van Eijndhoven<sup>13</sup>, S. Vanheule<sup>26</sup>, J. van Santen<sup>52</sup>, M. Vehring<sup>1</sup>, E. Vogel<sup>1</sup>, M. Vraeghe<sup>26</sup>, C. Walck<sup>44</sup>, A. Wallace<sup>2</sup>, M. Wallraff<sup>1</sup>, F. D. Wandler<sup>23</sup>, N. Wandkowsky<sup>31</sup>, A. Waza<sup>1</sup>, C. Weaver<sup>23</sup>, M. J. Weiss<sup>49</sup>, C. Wendt<sup>31</sup>, J. Werthebach<sup>21</sup>, S. Westerhoff<sup>31</sup>, B. J. Whelan<sup>2</sup>, S. Wickmann<sup>1</sup>, K. Wiebe<sup>32</sup>, C. H. Wiebusch<sup>1</sup>, L. Wille<sup>31</sup>, D. R. Williams<sup>47</sup>, L. Wills<sup>40</sup>, M. Wolf<sup>31</sup>, J. Wood<sup>31</sup>, T. R. Wood<sup>23</sup>, E. Woolsey<sup>23</sup>, K. Woschnagg<sup>8</sup>, D. L. Xu<sup>31</sup>, X. W. Xu<sup>7</sup>, Y. Xu<sup>45</sup>, J. P. Yanez<sup>23</sup>, G. Yodh<sup>27</sup>, S. Yoshida<sup>15</sup>, T. Yuan<sup>31</sup>, M. Zoll<sup>44</sup>

<sup>1</sup>III. Physikalisches Institut, RWTH Aachen University, D-52056 Aachen, Germany

<sup>2</sup>Department of Physics, University of Adelaide, Adelaide, 5005, Australia

<sup>3</sup>Dept. of Physics and Astronomy, University of Alaska Anchorage, 3211 Providence Dr., Anchorage, AK 99508, USA

<sup>4</sup>Dept. of Physics, University of Texas at Arlington, 502 Yates St., Science Hall Rm 108, Box 19059, Arlington, TX 76019, USA

<sup>5</sup>CTSPS, Clark-Atlanta University, Atlanta, GA 30314, USA

<sup>6</sup>School of Physics and Center for Relativistic Astrophysics, Georgia Institute of Technology, Atlanta, GA 30332, USA

<sup>7</sup>Dept. of Physics, Southern University, Baton Rouge, LA 70813, USA

<sup>8</sup>Dept. of Physics, University of California, Berkeley, CA 94720, USA

<sup>9</sup>Lawrence Berkeley National Laboratory, Berkeley, CA 94720, USA

<sup>10</sup>Institut für Physik, Humboldt-Universität zu Berlin, D-12489 Berlin, Germany

<sup>11</sup>Fakultät für Physik & Astronomie, Ruhr-Universität Bochum, D-44780 Bochum, Germany

<sup>12</sup>Université Libre de Bruxelles, Science Faculty CP230, B-1050 Brussels, Belgium

<sup>13</sup>Vrije Universiteit Brussel (VUB), Dienst ELEM, B-1050 Brussels, Belgium

<sup>14</sup>Dept. of Physics, Massachusetts Institute of Technology, Cambridge, MA 02139, USA

<sup>15</sup>Dept. of Physics and Institute for Global Prominent Research, Chiba University, Chiba 263-8522, Japan

<sup>16</sup>Dept. of Physics and Astronomy, University of Canterbury, Private Bag 4800, Christchurch, New Zealand

<sup>17</sup>Dept. of Physics, University of Maryland, College Park, MD 20742, USA

<sup>18</sup>Dept. of Physics and Center for Cosmology and Astro-Particle Physics, Ohio State University, Columbus, OH 43210, USA

<sup>19</sup>Dept. of Astronomy, Ohio State University, Columbus, OH 43210, USA

<sup>20</sup>Niels Bohr Institute, University of Copenhagen, DK-2100 Copenhagen, Denmark

<sup>21</sup>Dept. of Physics, TU Dortmund University, D-44221 Dortmund, Germany

<sup>22</sup>Dept. of Physics and Astronomy, Michigan State University, East Lansing, MI 48824, USA

<sup>23</sup>Dept. of Physics, University of Alberta, Edmonton, Alberta, Canada T6G 2E1

<sup>24</sup>Erlangen Centre for Astroparticle Physics, Friedrich-Alexander-Universität Erlangen-Nürnberg,

D-91058 Erlangen, Germany

<sup>25</sup>Département de physique nucléaire et corpusculaire, Université de Genève, CH-1211 Genève, Switzerland

<sup>26</sup>Dept. of Physics and Astronomy, University of Gent, B-9000 Gent, Belgium

<sup>27</sup>Dept. of Physics and Astronomy, University of California, Irvine, CA 92697, USA

<sup>28</sup>Dept. of Physics and Astronomy, University of Kansas, Lawrence, KS 66045, USA

<sup>29</sup>SNOLAB, 1039 Regional Road 24, Creighton Mine 9, Lively, ON, Canada P3Y 1N2

<sup>30</sup>Dept. of Astronomy, University of Wisconsin, Madison, WI 53706, USA

<sup>31</sup>Dept. of Physics and Wisconsin IceCube Particle Astrophysics Center, University of Wisconsin, Madison, WI 53706, USA

<sup>32</sup>Institute of Physics, University of Mainz, Staudinger Weg 7, D-55099 Mainz, Germany

<sup>33</sup>Department of Physics, Marquette University, Milwaukee, WI, 53201, USA

<sup>34</sup>Université de Mons, 7000 Mons, Belgium

<sup>35</sup>Physik-department, Technische Universität München, D-85748 Garching, Germany

<sup>36</sup>Institut für Kernphysik, Westfälische Wilhelms-Universität Münster, D-48149 Münster, Germany

<sup>37</sup>Bartol Research Institute and Dept. of Physics and Astronomy, University of Delaware, Newark, DE 19716, USA

<sup>38</sup>Dept. of Physics, Yale University, New Haven, CT 06520, USA

<sup>39</sup>Dept. of Physics, University of Oxford, 1 Keble Road, Oxford OX1 3NP, UK

<sup>40</sup>Dept. of Physics, Drexel University, 3141 Chestnut Street, Philadelphia, PA 19104, USA

<sup>41</sup>Physics Department, South Dakota School of Mines and Technology, Rapid City, SD 57701, USA

<sup>42</sup>Dept. of Physics, University of Wisconsin, River Falls, WI 54022, USA

<sup>43</sup>Dept. of Physics and Astronomy, University of Rochester, Rochester, NY 14627, USA

<sup>44</sup>Oskar Klein Centre and Dept. of Physics, Stockholm University, SE-10691 Stockholm, Sweden

<sup>45</sup>Dept. of Physics and Astronomy, Stony Brook University, Stony Brook, NY 11794-3800, USA

<sup>46</sup>Dept. of Physics, Sungkyunkwan University, Suwon 440-746, Korea

<sup>47</sup>Dept. of Physics and Astronomy, University of Alabama, Tuscaloosa, AL 35487, USA

<sup>48</sup>Dept. of Astronomy and Astrophysics, Pennsylvania State University, University Park, PA 16802, USA

<sup>49</sup>Dept. of Physics, Pennsylvania State University, University Park, PA 16802, USA

<sup>50</sup>Dept. of Physics and Astronomy, Uppsala University, Box 516, S-75120 Uppsala, Sweden

<sup>51</sup>Dept. of Physics, University of Wuppertal, D-42119 Wuppertal, Germany

<sup>52</sup>DESY, D-15738 Zeuthen, Germany

<sup>a</sup>Earthquake Research Institute, University of Tokyo, Bunkyo, Tokyo 113-0032, Japan

**Acknowledgment:** The authors gratefully acknowledge the support from the following agencies and institutions: USA - U.S. National Science Foundation-Office of Polar Programs, U.S. National Science Foundation-Physics Division, University of Wisconsin Alumni Research Foundation, the Center for High Throughput Computing (CHTC) at the University of Wisconsin - Madison, the Open Science Grid (OSG) grid infrastructure and the Extreme Science and Engineering Discovery Environment (XSEDE); U.S. Department of Energy, and National Energy Research Scientific Computing Center; Particle Astrophysics research computing center at the University of Maryland; Institute for Cyber-Enabled Research at Michigan State University; Astroparticle Physics Computational Facility at Marquette University; Belgium - Funds for Scientific Research (FRS-FNRS and FWO), FWO Odysseus and Big Science programs, Belgian Federal Science Policy Office (Belspo); Germany - Bundesministerium für Bildung und Forschung (BMBF), Deutsche Forschungsgemeinschaft (DFG), Helmholtz Alliance for Astroparticle Physics (HAP), Initiative and Networking Fund of the Helmholtz Association; Deutsches Elektronen Synchrotron (DESY); Cluster of Excellence (PRISMA ? EXC 1098); High Performance Computing Cluster of the IT-Center of the RWTH Aachen; Sweden - Swedish Research Council, Swedish Polar Research Secretariat, Swedish National Infrastructure for Computing (SNIC), and Knut and Alice Wallenberg Foundation; Canada - Natural Sciences and Engineering Research Council of Canada, Calcul Québec, Compute Ontario, WestGrid and Compute Canada; Denmark - Villum Fonden, Danish National Research Foundation (DNRF); New Zealand - Marsden Fund, New Zealand; Australian Research Council; Japan - Japan Society for Promotion of Science (JSPS) and Institute for Global Prominent Research (IGPR) of Chiba University; Korea - National Research Foundation of Korea (NRF); Switzerland - Swiss National Science Foundation (SNSF).

## Search for point-like sources in the astrophysical muon neutrino flux with IceCube

---

### The IceCube Collaboration<sup>†</sup>

<sup>†</sup> [http://icecube.wisc.edu/collaboration/authors/icrc17\\_icecube](http://icecube.wisc.edu/collaboration/authors/icrc17_icecube)

E-mail: [reimann@physik.rwth-aachen.de](mailto:reimann@physik.rwth-aachen.de)

The IceCube Collaboration has observed a high-energy diffuse astrophysical neutrino flux consistently in two detection channels: first using high-energy events interacting inside the detector and secondly with through-going muon-neutrino induced muons. In order to identify the sources of this flux, these muon-neutrino events are ideal messenger particles because of their excellent angular resolution. Here we present a search for point-like neutrino sources based on the same sample that was used to measure the diffuse high-energy astrophysical muon-neutrino flux with a live-time of six years. This high purity sample is restricted to the Northern hemisphere and consists of  $\sim 340\,000$  events with a median angular resolution of  $\sim 1^\circ$  at 1 TeV that decreases to  $\sim 0.3^\circ$  at 1 PeV. In this analysis an unbinned likelihood maximization is used that is optimized for point-like neutrino emission with the same characteristics as the diffuse muon neutrino flux. The sensitivity improves by  $\sim 20\%$  compared to previous analyses and is at a level of  $E^2 \partial\phi/\partial E = 4 \cdot 10^{-13} \text{ TeV cm}^{-2} \text{ s}^{-1}$ . No significant source was found in an unbiased sky scan on the Northern hemisphere and in a search based on a standard candidate source list of IceCube and ANTARES.

**Corresponding author:** R. Reimann<sup>\*1</sup>

<sup>1</sup> *III. Physikalisches Institut, RWTH Aachen University, D-52056 Aachen, Germany*

*35th International Cosmic Ray Conference — ICRC2017  
10–20 July, 2017  
Bexco, Busan, Korea*

---

<sup>\*</sup>Speaker.

## 1. Introduction

IceCube is a cubic-kilometer neutrino detector with a total of 5160 optical sensors installed in the ice on 86 cable strings at the geographic South Pole [1, 2] between depths of 1450 m and 2450 m. Detector construction finished in 2010. Neutrino reconstruction relies on the optical detection of Cherenkov radiation emitted by secondary particles produced in neutrino interactions in the surrounding ice or the nearby bedrock. During construction, partial detector configurations were taking data with 59 strings from May 2009, and 79 strings from May 2010 on before IceCube became fully operational in May 2011.

In 2013 the IceCube Collaboration reported the observation of a diffuse astrophysical high-energy all-flavor neutrino flux using a sample of starting events [3, 4]. This observation was confirmed by the measurement of a diffuse astrophysical high-energy muon-neutrino flux using the complementary detection channel of through-going muon-neutrinos with interaction vertex in the vicinity of the detector [5, 6, 7]. Those analyses are restricted to the Northern hemisphere to suppress the background of atmospheric muons that arises from cosmic ray air showers. In [6], the diffuse astrophysical high-energy neutrino flux was fitted by a power law with a spectral index of  $2.13 \pm 0.13$  and a flux normalization of  $0.90_{-0.27}^{+0.3} \times 10^{-18} \text{ GeV}^{-1} \text{ cm}^{-2} \text{ s}^{-1} \text{ sr}^{-1}$  at 1 TeV neutrino energy. Until now, no significant source of these high-energy neutrinos could be identified e.g. see [8].

Track-like events from through-going muons are ideal to search for point-like sources. The background for this search are atmospheric neutrinos as well as uncorrelated diffuse astrophysical neutrinos. Atmospheric neutrinos can be distinguished from astrophysical neutrinos on a statistical level, because astrophysical neutrinos are expected to follow a much harder power law than atmospheric neutrinos with  $\sim E^{-3.7}$ .

Here, we present a scan for point-like sources on the Northern hemisphere down to  $-5^\circ$  declination as well as a search based on a list of known candidate objects for the production of high-energy neutrinos. We use a sample of through-going muon neutrinos from 6 years of IceCube data [6] with about 340 000 events from the Northern hemisphere with a known portion of astrophysical events. Despite of smaller live-time, the sensitivity increases by about 20% compared to [8].

## 2. Data Sample

As the data were taken with different partial configurations of IceCube the details of the event selections are different for different seasons. The event selection technique applied here are described in detail in [6]. At final selection level the muon neutrino purity is  $>99.7\%$  where the dominant part is atmospheric muon neutrinos from cosmic ray air showers [6]. These atmospheric neutrinos are an irreducible background and can just be separated on a statistical bases.

In total data with a live-time of 2032 days are analyzed containing about 340 000 events. The event sample for the season from May 2011 to May 2012 has an overlap of about 80% with the selection presented in [8] for the same time range.

At high energies the muon direction is well correlated with the muon-neutrino direction ( $< 0.1^\circ$  above 10 TeV) and the muon is reconstructed with a median angular uncertainty of about  $0.5^\circ$  at 10 TeV. All events have been reconstructed with an improved reconstruction based on the

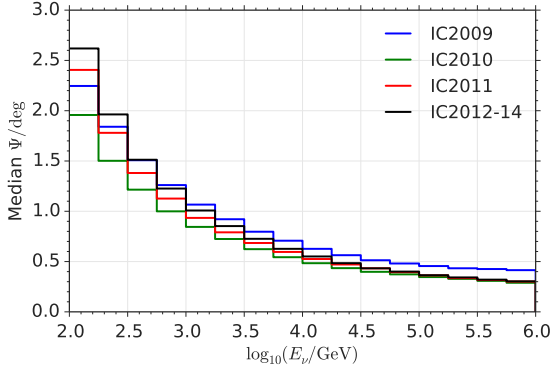


**Figure 1:** Median angular resolution vs  $\log_{10}$  of neutrino energy for the different sub-selections labeled by the year.

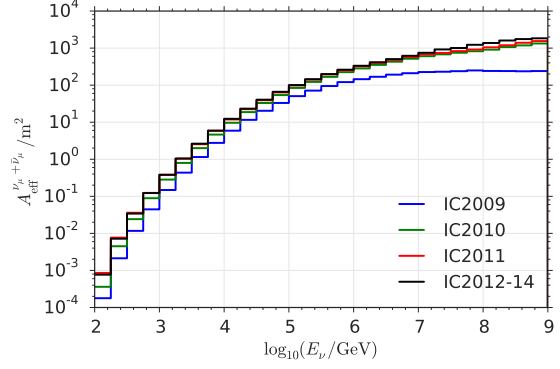


**Figure 2:** Effective area for neutrinos and anti-neutrinos from the Northern hemisphere vs  $\log_{10}$  of neutrino energy for different sub-selections labeled by the year.

reconstruction techniques described in [9, 10]. The median angular resolution  $\Psi$  improves by about 10% compared to the reconstruction used in [8]. The median angular resolution for the different sub-selection labeled by the year of the selection are shown in Fig.1. The effective area for muon neutrino and muon anti-neutrinos for events from the Northern hemisphere of the different sub-selections is shown in Fig.2.

### 3. Unbinned Likelihood Method

The data sample is tested for clustering with an unbinned likelihood method as described in [11]. The likelihood function is given by

$$\mathcal{L} = \prod_j \prod_{i \in j} \left[ \frac{n_s \cdot w_j(\gamma)}{N_j} S_j^{\text{spat}}(\vec{x}_i, \vec{x}_s, \sigma_i) S_j^{\text{ener}}(E_i, \gamma) + \left( 1 - \frac{n_s \cdot w_j(\gamma)}{N_j} \right) B_j^{\text{spat}}(\vec{x}_i) B_j^{\text{ener}}(E_i) \right] \cdot P(\gamma | \gamma_{\text{astro}}) \quad (3.1)$$

where  $i$  is running over all events within a sub-sample  $j$ .  $\vec{x}_i = (\alpha_i, \delta_i)$  is the reconstructed right ascension and declination,  $E_i$  is the reconstructed energy and  $\sigma_i$  is the estimated angular uncertainty on the reconstruction of event  $i$ .  $N_j$  is the total sample size of sub-sample  $j$ .  $n_s$  is the number of signal events from the assumed source position at  $\vec{x}_s$  with a spectral index of  $\gamma$ . The signal and background probability is factorized in a spatial and an energy part. The spatial background probability  $B_j^{\text{spat}}$  is uniform in right ascension due to IceCube's special position at the South Pole. The declination dependence of the spatial background PDF  $B_j^{\text{spat}}$  and the energy background PDF  $B_j^{\text{ener}}$  is estimated using Monte Carlo simulation weighted to the best fit parametrization obtained from [6] including the diffuse atmospheric and astrophysical components, specializing the PDFs for this sample. This allows a better extrapolation to sparse populated regions in the energy, declination plane than using experimental data only. Also the energy signal PDF  $S_j^{\text{ener}}$  and  $w_j$  are estimated using Monte Carlo simulation assuming a power law spectrum of the source with spectral index  $\gamma$ .  $w_j$  is the fraction of signal events that are expected from a specific sub-sample  $j$  that is calculated using the exposure and effective area of the sub-samples. The spatial signal probability  $S_j^{\text{spat}}$  is assumed to be Gaussian with an event individual uncertainty of  $\sigma_i$ .

To focus on those sources that produce the observed spectrum of astrophysical events, we add a Gaussian prior for the spectral index  $P(\gamma|\gamma_{astro} = 2.13 \pm 0.13)$ . The position and the width of the prior are taken from the best fit of [6]. As the source spectrum is not strongly constrained by the few events that contribute to the source the prior has the largest handle on the fit of  $\gamma$  and thus the spectral index is effectively fixed allowing just for a small variation.

For a potential source position, the likelihood is maximized with respect to  $n_s$  and  $\gamma$  with  $n_s \geq 0$  and a likelihood ratio test is performed to compare the best fit likelihood to the null hypothesis of no significant clustering with  $n_s = 0$ . The ratio is the test statistic

$$TS = -2 \cdot \log \left[ \frac{\mathcal{L}(\vec{x}_s, n_s = 0)}{\mathcal{L}(\vec{x}_s, \hat{n}_s, \hat{\gamma})} \right] \quad n_s > 0 \quad (3.2)$$

for  $n_s > 0$  with best fit values  $\hat{n}_s$  and  $\hat{\gamma}$ . Up to 80% of background trials accumulate in a peak at  $\hat{n}_s = 0$  and the sensitivity would be under-estimated if these fits get the same  $TS$ -value. Thus we expand the shape of the  $\log \mathcal{L}$  function at  $n_s = 0$  with a Taylor-expansion of second order to estimate the minimum  $TS$  value for negative  $n_s$  values resolving the peak at  $TS = 0$ .

Due to IceCube's distinguished position at the South Pole, background samples can be generated by scrambling experimental data uniformly in right ascension. It was found that the  $TS$  is slightly declination dependent. Thus the background  $TS$  is generated using background trials for many different declinations. These  $TS$ -distributions are used to calculate a pre-trial p-value.

The sensitivity and discovery potential on the source flux normalization assuming an  $E^{-2}$  power law flux is shown in Fig.5. The sensitivity corresponds to a 90% C.L. averaged upper limit and the discovery potential gives the median source flux resulting in a  $5\sigma$  discovery. The sensitivity and discovery potential are declination dependent. For comparison the sensitivity and discovery potential from [8] are shown. Despite of one year shorter live-time, this analysis outperforms the analysis in [8] by about 10%-20%. This is caused by multiple reasons: 1. the use of an improved angular reconstruction, 2. a slightly better optimized event selection near the horizon, 3. the use of background PDFs in the likelihood that are optimized on the parametrization from [6] which improves sensitivity especially for higher energies, 4. the fact that due to the prior on the spectral index the number of source hypotheses are reduced which results in a steeper falling  $TS$  and 5. the use of negative  $TS$  values which allows not to under-estimate the sensitivity especially near the pole ( $\sin \delta \sim 1$ ) where the background changes strongly. As this search is optimized for hard-spectrum sources it does not outperform the analysis in [8] for soft-spectrum sources, e.g.  $E^{-3}$ .

### 3.1 Unbiased Scan

We perform an unbiased scan of the full Northern hemisphere going down to  $-5^\circ$  declination. The scan is performed on a grid with a typical resolution of about  $0.1^\circ$ . For each grid point the pre-trial p-value is calculated. We select the most significant spot from the scan using the pre-trial p-value. As we test many points in the scan we have to correct for the fact that we choose the most significant point in our scan. Therefore, we repeat the procedure with scrambled background samples. By comparing the pre-trial p-values from the most significant points in the background sample to the experimental pre-trial p-value we can calculate the post-trial p-value. The background pre-trial p-value distribution of the most significant point can be described by

$$p_{\text{pre-trial}} \cdot (1 - p_{\text{pre-trial}})^{N-1} \quad (3.3)$$

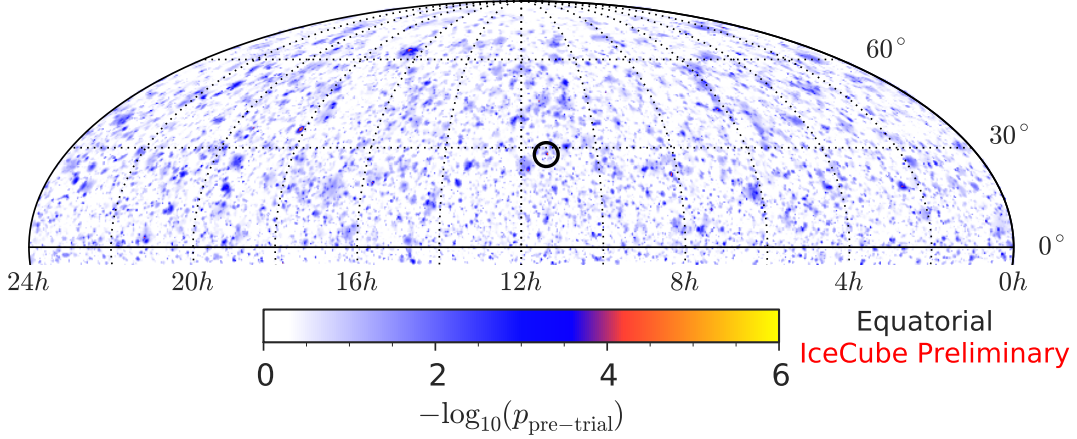


**Figure 3:** Pre-trial p-value sky map of the Northern hemisphere scan in equatorial coordinates down to  $-5^\circ$  declination. The pre-trial p-value is given as  $-\log_{10}(p_{\text{pre-trial}})$ . The position of the hottest spot is indicated by a black circle.

with an effective number of trials  $N$  of about 130 000.

### 3.2 A-Priori Source List

Weak sources suffer from the large number of trials of about 130 000 within the unbiased scan and may appear non-significant after trial correction. However a standard IceCube and ANTARES *a-priori* source list contains 34 promising candidates for high-energy neutrino emission in the Northern hemisphere [8], Tab. 1, reducing the trial factor to about 34. The sources were selected mainly due to their observation in gamma rays. They belong to various categories e.g. Galactic pulsar wind nebulae and supernovae remnants or extra-galactic BL Lacs and FSRQs. We test each source from this list individually. We select the most significant source and apply a trial-correction using background scrambled samples as done for the unbiased scan.

## 4. Results

No significant clustering was found above background expectation. Both the unbiased scan on the Northern hemisphere and the source list are compatible with background only.

The pre-trial p-value map of the unbiased scan is shown in Fig.3. The hottest spot in the scan is indicated by a black circle and is located at right ascension  $\alpha = 170.16^\circ$ , declination  $\delta = 27.91^\circ$ . The Galactic coordinates are  $b_{\text{gal}} = 69.88^\circ$ ,  $l_{\text{gal}} = 205.45^\circ$ . The best fit signal strength is  $n_s = 9.88$  with a fitted spectral index of  $\gamma = 2.118$ . The  $TS$ -value is 17.36 which corresponds to  $p_{\text{pre-trial}} = 10^{-5.14}$ . The post-trial corrected p-value is 90.5% and is thus compatible with background only. A zoom into the pre-trial p-value landscape around the hottest spot position is shown in Fig.4. In addition positions for sources from the Fermi 2FGL, Fermi 3FGL and Fermi 3FHL catalogs are shown [12, 13, 14]. The closest of these sources is 2 degree away.

The  $\mathcal{L}$  fit results for each source of the source list are shown in Tab.1. Sources are sorted by p-value and the best fit  $n_s$  as well as the  $TS$  and the equatorial coordinates are given. The

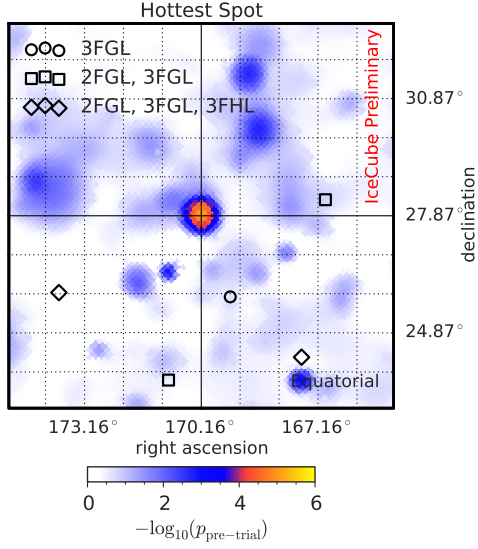


**Figure 4:** Pre-trial p-value landscape centered on the position of hottest spot of the unbiased scan in equatorial coordinates. The pre-trial p-value is given as  $-\log_{10}(p_{\text{pre-trial}})$ . In addition sources of Fermi 2FGL, 3FGL and 3 FHL catalog are indicated by markers [12, 13, 14].

most significant source in the *a-priori* source list is MGRO J1908+06 with a pre-trial p-value of 0.32%. Comparing to the pre-trial p-value distribution of the most significant source from scrambled background samples the post-trial p-value is 10.2%, which is compatible with background. As no significant source was found, we calculate the 90% C.L. Neyman upper limit [15] on the flux normalization  $\Phi_0$  for  $\nu_\mu + \bar{\nu}_\mu$  for each source. The upper limits on the flux normalization are listed in Tab.1 and are shown as blue squares in Fig.5 vs the sine of the declination of the source together with the sensitivity. Note that in case of under-fluctuations the limit was set to the sensitivity level of the analysis. Also note 90% upper limits can exceed the discovery potential as long as the best fit flux is below.

From Table 1 it can be seen that we find four different sources with a pre-trial p-value below 1%. In an *a posteriori* test we have quantified the probability to find such an excess of several small p-values. For this, we have calculated the binomial probability

$$P_{\text{binom}}(k) = \binom{N}{k} p_k^k (1 - p_k)^{N-k} \quad (4.1)$$

to find  $k$  out of  $N = 34$  sources with a pre-trial p-value smaller than  $p_k$ . Here  $p_k$  is the pre-trial p-value of source  $k$ , if sources are sorted by their pre-trial p-value. The maximum significance with almost  $3.8\sigma$  pre-trial is found for  $k = 4$ . Again, we have to correct for the fact that we choose  $k$  which results in the maximal significance. Thus we have repeated this procedure on scrambled background samples, each time selecting the most significant excess of p-values. After trial correction the p-value to find four sources with a pre-trial p-value  $< 0.72\%$  is 0.3% reducing the significance to  $2.75\sigma$ .

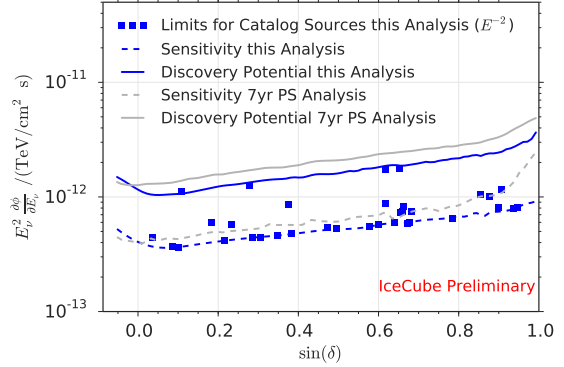


**Figure 5:** Upper limits on the flux normalization at 90% C.L. vs sine of declination of there source in the source list. In addition the sensitivity (dashed) and discovery potential (solid) flux for this analysis (blue) and from [8] (gray) are shown assuming an  $E^{-2}$  source spectrum.

Source	Type	$\alpha$ [deg]	$\delta$ [deg]	p-value	$TS$	$n_s$	$\Phi_0$ [TeV cm <sup>-2</sup> s <sup>-1</sup> ]
MGRO J1908+06	NI	286.99	6.27	0.0032	6.284	3.28	$1.13 \cdot 10^{-12}$
Cyg A	SRG	299.87	40.73	0.0049	6.335	4.30	$1.78 \cdot 10^{-12}$
4C 38.41	FSRQ	248.81	38.13	0.0055	5.686	6.62	$1.72 \cdot 10^{-12}$
3C454.3	FSRQ	343.50	16.15	0.0072	5.503	5.98	$1.26 \cdot 10^{-12}$
Crab Nebula	PWN	83.63	22.01	0.1188	0.709	4.32	$8.65 \cdot 10^{-13}$
Cas A	SNR	350.85	58.81	0.2069	0.033	0.88	$1.05 \cdot 10^{-12}$
1ES 1959+650	BL Lac	300.00	65.15	0.2069	0.124	1.69	$1.17 \cdot 10^{-12}$
PKS 1502+106	FSRQ	226.10	10.52	0.2322	-0.000	0.00	$5.98 \cdot 10^{-13}$
Mrk 421	BL Lac	166.11	38.21	0.2433	0.029	0.48	$8.68 \cdot 10^{-13}$
NGC 1275	SRG	49.95	41.51	0.2582	0.007	0.25	$8.31 \cdot 10^{-13}$
LSI 303	XB/mqso	40.13	61.23	0.2843	0.001	0.17	$1.01 \cdot 10^{-12}$
PKS 0528+134	FSRQ	82.73	13.53	0.2870	-0.002	0.00	$5.74 \cdot 10^{-13}$
Cyg OB2	SFR	308.09	41.23	0.3174	-0.002	0.00	$7.53 \cdot 10^{-13}$
Cyg X-3	XB/mqso	308.11	40.96	0.3230	-0.003	0.00	$7.28 \cdot 10^{-13}$
3C66A	BL Lac	35.67	43.04	0.3306	-0.001	0.00	$7.50 \cdot 10^{-13}$
3C 273	FSRQ	187.28	2.05	0.3807	-0.014	0.00	$4.42 \cdot 10^{-13}$
W Comae	BL Lac	185.38	28.23	0.4420	-0.055	0.00	$5.37 \cdot 10^{-13}$
TYCHO	SNR	6.36	64.18	0.4471	-0.019	0.00	$8.14 \cdot 10^{-13}$
1ES 0229+200	BL Lac	38.20	20.29	0.4762	-0.059	0.00	$4.47 \cdot 10^{-13}$
BL Lac	BL Lac	330.68	42.28	0.5104	-0.028	0.00	$5.58 \cdot 10^{-13}$
Cyg X-1	XB/mqso	299.59	35.20	0.5422	-0.106	0.00	$4.93 \cdot 10^{-13}$
M87	SRG	187.71	12.39	0.6711	-0.256	0.00	$2.85 \cdot 10^{-13}$
Mrk 501	BL Lac	253.47	39.76	0.6847	-0.172	0.00	$3.51 \cdot 10^{-13}$
S5 0716+71	BL Lac	110.47	71.34	0.7230	-0.380	0.00	$3.84 \cdot 10^{-13}$
PKS 0235+164	BL Lac	39.66	16.62	0.7355	-0.400	0.00	$2.04 \cdot 10^{-13}$
H 1426+428	BL Lac	217.14	42.67	0.7890	-0.243	0.00	$1.96 \cdot 10^{-13}$
IC443	SNR	94.18	22.53	0.8153	-0.457	0.00	$1.22 \cdot 10^{-13}$
HESS J0632+057	XB/mqso	98.24	5.81	0.8359	-0.917	0.00	$1.01 \cdot 10^{-13}$
SS433	XB/mqso	287.96	4.98	0.8738	-1.085	0.00	$1.01 \cdot 10^{-13}$
M82	SRG	148.97	69.68	0.8887	-0.888	0.00	$1.83 \cdot 10^{-13}$
3C 123.0	SRG	69.27	29.67	0.9055	-0.747	0.00	$1.30 \cdot 10^{-13}$
1ES 2344+514	BL Lac	356.77	51.70	0.9264	-0.808	0.00	$1.58 \cdot 10^{-13}$
Geminga	PWN	98.48	17.77	0.9754	-2.424	0.00	$1.16 \cdot 10^{-13}$
MGRO J2019+37	PWN	305.22	36.83	0.9884	-3.191	0.00	$1.39 \cdot 10^{-13}$
Hottest spot of the unbiased scan on the Northern hemisphere							
—	—	170.16	27.87	$10^{-5.14}$	17.271	10.28	—

**Table 1:** Results of the *a priori* defined source list search. The fitted spectral index  $\gamma$  is not given as it is effectively fixed by the introduced prior. The most significant source is MGRO J1908+06 with a post-trial p-value of 10.2%. In addition the fit values of the hottest spot of the unbiased sky scan is given.

The four sources are MGRO J1908+06, Cyg A, 3C454.3 and 4C 38.41 that are three extra-galactic and one Galactic source. The type of MGRO J1908+06 is not identified, Cyg A is a FR-II radio galaxy and 3C454.3 and 4C 38.41 are both FSRQ. We note, that we have not found a physical reason to combine these sources belonging to different source classes and that the test for a population of small p-values has been introduced *a posteriori*.

## 5. Conclusions

We have analyzed 6 years of IceCube data for a clustering of through-going muon neutrinos using an improved unbinned likelihood method. No significant source was found in a scan of the Northern hemisphere. Also, the search for significant neutrino emission from objects on a pre-defined list of candidates results in a post-trial p-value of 10.2%, compatible with background. The object on the list with the smallest post-trial p-value is MGRO J1908+06.

With the end of the data taking season 2016 in May 2017, this analysis can be extended to two more years of data. In addition to the analysis presented here, we will also perform a test for a population of sub-threshold sources, similar to the one described in [8]. Currently the event selection is re-optimized to take advantage from the features of the event selection described in [6] and [8].

## References

- [1] **IceCube** Collaboration, A. Achterberg et al., *Astropart. Phys.* **26** (2006) 155 – 173.
- [2] **IceCube** Collaboration, M. Aartsen et al., *JINST* **12** (2017) P03012.
- [3] **IceCube** Collaboration, M. G. Aartsen et al., *Science* **342** (2013).
- [4] **IceCube** Collaboration, [PoS \(ICRC2017\) 981](#) (these proceedings).
- [5] **IceCube** Collaboration, M. G. Aartsen et al., *Phys. Rev. Lett.* **115** (2015) 081102.
- [6] **IceCube** Collaboration, M. G. Aartsen et al., *Astrophys. J.* **833** (2016) 3.
- [7] **IceCube** Collaboration, [PoS \(ICRC2017\) 1005](#) (these proceedings).
- [8] **IceCube** Collaboration, M. G. Aartsen et al., *Astrophys. J.* **835** (2017) 151.
- [9] **AMANDA** Collaboration, J. Ahrens et al., *Nucl. Instrum. Meth. A* **524** (2004) 169 – 194.
- [10] K. Schatto. PhD thesis, Johannes Gutenberg-Universität, 2014.
- [11] J. Braun et al., *Astropart. Phys.* **29** (2008) 299 – 305.
- [12] **Fermi-LAT** Collaboration, P. L. Nolan et al., *Astrophys. J. Suppl. S.* **199** (2012) 31.
- [13] **Fermi-LAT** Collaboration, F. Acero et al., *Astrophys. J. Suppl. S.* **218** (2015) 23.
- [14] **Fermi-LAT** Collaboration, M. Ajello et al., [arXiv:1702.00664](#).
- [15] J. Neyman, *Phil. Trans. R. Soc. A* **236** (1937) 333–380.

## Search for weak neutrino point sources using angular auto-correlation analyses in IceCube

---

### The IceCube Collaboration<sup>†</sup>

<sup>†</sup> [http://icecube.wisc.edu/collaboration/authors/icrc17\\_icecube](http://icecube.wisc.edu/collaboration/authors/icrc17_icecube)

E-mail: [tglauch@icecube.wisc.edu](mailto:tglauch@icecube.wisc.edu), [aturcati@icecube.wisc.edu](mailto:aturcati@icecube.wisc.edu)

The IceCube Neutrino Observatory is a cubic kilometer neutrino telescope located in the Antarctic ice. Recently, IceCube has measured a diffuse all-sky all-flavor astrophysical neutrino flux above 30 TeV. However, the origin and production of these particles still remain unknown. Given the observed flux, the absence of observations of bright point-sources could be explained by a large population of weak sources. This scenario can be tested using autocorrelation methods. We present here the results of two independent analyses on two different neutrino samples based on 6 and 7 years of IceCube data. The first sample is optimized for events coming from the Northern Hemisphere, while the second one is an all-sky sample. Experimental results are obtained by analyzing these samples using a multipole expansion and a two-point angular correlation technique, respectively. In addition, flux upper limits for extended sources and the Cygnus region have been calculated.

**Corresponding authors:** Theo Glauch<sup>1,2</sup>, Andrea Turcati<sup>2</sup>, Kai Krings<sup>2\*</sup>

<sup>1</sup> *III. Physikalisches Institut, RWTH Aachen University, D-52056 Aachen, Germany*

<sup>2</sup> *Physik-department, Technische Universität München, D-85748 Garching, Germany*

*35th International Cosmic Ray Conference -ICRC217-  
10-20 July, 2017  
Bexco, Busan, Korea*

---

\*Speaker.

## 1. Introduction

The origin of charged cosmic rays (CRs), as well as their production mechanisms are one of the most important questions in modern astroparticle physics. In fact, there are reasons to believe that the production of CRs and neutrinos are closely connected. In source environments where protons are accelerated and undergo proton-proton or photonuclear interactions, a cascade of light mesons evolves which subsequently decay into gamma-rays, leptons and (highly-energetic) neutrinos [1]. The latter are the ideal tracer for these processes since they are neither attenuated nor deflected during their travel through the universe and hence point back to their origin. In recent years the multi-messenger approach has been used to derive upper flux limits for various classes of neutrino point-sources [2]. These limits suggest that the observed neutrino flux may originate from the superposition of many weak sources of various types. This motivates our angular correlation approach, searching for a small-scale clustering in the astrophysical neutrino flux coming from a large population of weak neutrino point-sources.

*IceCube* is a neutrino detector designed for the measurement of highly-energetic, i.e. astrophysical neutrinos. The cubic-kilometer detector is installed in the ice at the geographic South Pole between depths of 1450 m and 2450 m [3]. Detector construction started in 2005 and finished in 2010. Neutrino reconstruction relies on the optical detection of Cherenkov radiation emitted by secondary particles produced in neutrino interactions in the surrounding ice or the nearby bedrock [4, 5]. At energies  $E_\nu > 100\text{TeV}$  the mean opening angle between the direction of a secondary muon and the direction of its primary muon-neutrino is less than  $0.03^\circ$  [6]. This motivates the use of through-going muons, which have a median angular reconstruction uncertainty better than  $1^\circ$  at energies above 10 TeV, to search for point-sources [7, 8].

The two analyses presented in this work make use of the direction and energy information of through-going muon measured by the IceCube detector and collected in two different samples. The Multipole Analysis is applied to a data sample of through-going muons with declination  $\delta > -5^\circ$ . The sample was originally developed for the characterization of the diffuse astrophysical neutrino flux in [7]. However, due to its good background rejection (neutrino purity of 99.7%) and good statistics (around 500 astrophysical neutrinos in six years of data) it is also well suited for point-source searches. The 2pt-Autocorrelation Analysis is instead applied to an *all-sky* data sample, consisting of through-going muons coming from both hemispheres during an integrated livetime of seven years. This sample is also used in the Single Point-Source Analysis that provides the best limits so far available [8]. Although mathematically very similar the two analyses follow a different philosophy in their implementations. While the 2pt-Autocorrelation analyses is almost model independent, the Multipole Analysis uses the fitted astrophysical neutrino spectrum from [7] to introduce an optimal energy weighting for the astrophysical flux. The two analyses presented in this paper are closely related to the already published Hotspot Population Search [8] which also searches for a population of weak neutrino point-sources. But while the latter analysis counts the number of neutrino hotspots above a certain flux level, the analyses presented here make use of the angular clustering of the neutrino events, making them more powerful for a high number of sources (also compare results in Figure 2). Stacking Analyses, another extension of point-source analysis only search for a time-integrated flux from a source catalog, while our approach is more generally searching for clustering anywhere in the sky.

## 2. Methods

As stated before, the analyses presented in this paper search for a large population of weak point-sources as opposed to a purely isotropic flux. This can be precisely stated as the following two hypotheses:

- *Background-Hypothesis*: The neutrino flux measured by IceCube consists exclusively of atmospheric neutrinos and an isotropic astrophysical neutrino component.
- *Signal-Hypothesis*: The neutrino flux measured by IceCube consists of an atmospheric and an astrophysical neutrino component. A fraction of the observed diffuse astrophysical flux is clustered in isotropically distributed, equally strong neutrino point-sources.

Apart from the analysis of the Cygnus region, we will always refer to these definitions.

### 2.1 Multipole

The *Multipole Analysis* is one possibility to calculate the two-point autocorrelation of the neutrino flux on a specific angular scale  $\alpha$ . It is based on the expansion of the neutrino skymap into spherical harmonics  $Y_\ell^m(\theta, \varphi)$  according to

$$f(\theta, \varphi) = \sum_{\ell=0}^{\infty} \sum_{m=-\ell}^{\ell} a_\ell^m Y_\ell^m(\theta, \varphi), \quad (2.1)$$

with zenith angle  $\theta$  and azimuth angle  $\varphi$ . The  $a_\ell^m$  coefficients describe structures with an angular size of  $\alpha \sim 180/\ell$ . In order to increase the analysis' sensitivity, neutrino events are not equally weighted, but injected in skymaps with their probability  $\mathcal{P}(\text{astro}|E)$  of being of astrophysical origin

$$\mathcal{P}(\text{astro}|E) = \frac{1}{1 + \frac{\mathcal{E}_B(E)}{\mathcal{E}_S(E)} \cdot \frac{n_{\text{tot}} - n_{\text{astro}}}{n_{\text{astro}}}}, \quad (2.2)$$

with *a-priori* energy distributions  $\mathcal{E}_B(E)$  and  $\mathcal{E}_S(E)$  for atmospheric and astrophysical neutrinos, respectively.  $n_{\text{tot}}$  and  $n_{\text{astro}}$  are the total number of neutrinos and the number of astrophysical neutrinos in the sample, respectively.

In order to quantify the correlation of neutrino events the angular power spectrum  $C_\ell$  is used

$$C_\ell = \frac{1}{2\ell + 1} \sum_{m=-\ell}^{m=\ell} |a_\ell^m|^2. \quad (2.3)$$

In [9], it is shown that this definition gives an unbiased estimator for the two-point autocorrelation of a signal on a sphere. For this work, however, we omit the  $m = 0$  coefficients, since they only include zenith information and therefore coincide with the direction of IceCube's largest detector systematics. Furthermore the angular power spectrum is normalized in order to avoid fake sensitivities caused by fluctuations of the baseline value, which arise when injecting independent Monte Carlo events. Hence, for the following we use the modified angular power spectrum

$$C_\ell^{\text{eff}} \rightarrow \frac{C_\ell^{\text{eff}}}{\sum_{\ell=0}^{\ell_{\text{max}}} C_\ell^{\text{eff}}}. \quad (2.4)$$

Using Monte Carlo generated skymaps the probability density function for each  $C_\ell^{\text{eff}}$  can be shown to be nearly Gaussian in the region of interest. Hence a  $\chi^2$ -inspired test-statistic is used to distinguish background and signal hypothesis

$$TS = \frac{1}{\sum_\ell w_\ell^{\text{eff}}} \cdot \sum_{\ell=1}^{\ell_{\text{max}}} w_\ell^{\text{eff}} \text{sign}_\ell \left( \frac{C_\ell^{\text{eff}} - \langle C_{\ell,\text{bg}}^{\text{eff}} \rangle}{\sigma_{\ell,\text{bg}}} \right)^2. \quad (2.5)$$

Here,  $\langle C_{\ell,\text{bg}}^{\text{eff}} \rangle$  is the background median with standard deviation  $\sigma_{\ell,\text{bg}}$ . The angular weights  $w_\ell^{\text{eff}}$  are a function of  $\ell$  complying with the fact that point-sources are expected to have a typical angular size of around  $1^\circ$  corresponding to the angular reconstruction error of the neutrino events. The weights are deduced from 10'000 Monte Carlo generated skymaps with all astrophysical events clustered in point-sources [10]. Using the median of the resulting signal angular power spectrum  $\langle C_{\ell,\text{sig}}^{\text{eff}} \rangle$  the weights are given by

$$w_\ell^{\text{eff}} = \frac{\langle C_{\ell,\text{sig}}^{\text{eff}} \rangle - \langle C_{\ell,\text{bg}}^{\text{eff}} \rangle}{\sigma_{\ell,\text{bg}}}. \quad (2.6)$$

Finally, the signum function in equation (2.5) ensures that only deviations in the expected direction contribute a positive value to the test-statistic value. Monte Carlo studies show that the test-statistic distributions for all signal strength are well described by a convolution of a Gaussian with an exponential function.

## 2.2 2pt-Autocorrelation

Autocorrelation tests making use of two-point correlation functions are solid statistical methods to evaluate the amount of spatial clustering over different angular scales of a set of events distributed on a skymap. An analysis using a similar method has been performed over earlier versions of IceCube data [11]. The test described here makes use of the distribution of the angular distances between event-pairs  $(i, j)$  to distinguish a potential clustered signal, from the isotropic background hypothesis. The test has been developed to be almost completely data-driven, in the sense that no prior assumptions on the signal model are needed to perform the analysis. The autocorrelation function is defined as the cumulative number of event-pairs having an angular distance  $\Psi_{i,j}$  minor or equal a given angular distance  $\alpha$ ,

$$N(\alpha) = \sum_{i,j>i} \Theta(\alpha - \Psi_{i,j}), \quad (2.7)$$

where  $\Theta$  is the Heaviside step function. The calculation is then repeated in a range of  $\alpha$  that goes from  $0.25^\circ$  to  $5^\circ$  in steps of  $\Delta\alpha = 0.25^\circ$  ( $\Delta\alpha = 0.1^\circ$  for the analysis in the Cygnus Region).

Since astrophysical neutrinos are often expected to have a harder spectrum compared to the atmospheric neutrino background, it is possible to enhance the sensitivity of the analysis by introducing an appropriate weighting system. In a similar way of what is shown in [12], a weighting scheme proportional to the energies  $(E_i, E_j)$  of the neutrinos belonging to each event-pair has been chosen. The weighted cumulative number of pairs takes the following form,

$$N(\alpha) = \sum_{i,j>i} w_i \cdot w_j \cdot \Theta(\alpha - \Psi_{i,j}), \quad (2.8)$$

where  $w_i, w_j$  are the weights assigned to each event. Accordingly to the data-driven purposes of the method, the weights are derived from the normalized energy distribution  $\mathcal{P}(E)$  of the data on the skymap, independent from specific signal models. Each weight is proportional to the logarithm of the probability of observing an event with equal or higher energy in the sample and it is calculated as

$$w_i = w(E_i) = -\log_{10} \left( 1 - \int_0^{E_i} \mathcal{P}(E) dE \right). \quad (2.9)$$

For each angular scale  $\alpha$ , the background distribution is derived by scrambling the data in right ascension to obtain isotropic skymaps. The distribution is then fitted with a Gamma function, that is used to calculate the p-value ( $p(\alpha)$ ) of a given skymap realization. The lowest p-value from the different angular scales is then selected to define the test statistic,

$$TS = -\log_{10}(p(\alpha)_{\text{Best}}). \quad (2.10)$$

As the last step, to correct for the trial factor due to the binning of the angular scales, a large number of realizations of isotropic skymaps has to be analyzed, in order to obtain the  $TS$  p.d.f. The trial corrected p-value then corresponds to the probability of obtaining a  $TS$  at least as large as the one obtained from data.

### 3. Results

#### 3.1 North

The left panel of Figure 1 shows the results of the 2pt-Autocorrelation analysis in the Northern Hemisphere. The trial corrected p-value is 46%, consistent with fluctuations from background expectations. The right panel of the figure shows the angular power spectrum of the neutrino flux from the Northern Hemisphere in black dots. The blue solid and shaded area indicate the median and standard deviation from simulated Monte Carlo skymaps, respectively. The pulls are shown in the bottom panel. There is no obvious structure visible. The test-statistic value is calculated from equation (2.5) and compared to the expectation for the background hypothesis giving a p-value of 31.5%. The non-observation of point-source clustering is used to calculate Neyman upper limits on the flux-per-source for the model of  $N_{Sou}$  equally strong point-sources. The results are shown in Figure 2 for an astrophysical power-law with spectral index  $\gamma = 2.0$ . The intersection of the diffuse flux and the 90% upper limit on the point-source is at around 500 sources with  $E_\nu^2 \partial \Phi / \partial E_\nu \leq 10^{-13} \text{ TeV cm}^{-2} \text{ s}^{-1}$ . In addition to the two analyses presented here, refined upper limit fluxes for the Hotspot Population Analysis are also shown in Figure 2 [8] for comparison.

Considering the various results, there is increasing evidence that the observed flux of astrophysical neutrinos is not produced by a few predominant point-sources in the neutrino sky. Anyway, the results are consistent with the point-source scenario in general. As discussed in the introduction there are many source types that are too abundant to be visible in our analyses. There are, for example,  $\mathcal{O}(10^8)$  Starburst Galaxies in the observable universe, while the presented analyses are only sensitive up to the crossing point of diffuse flux and sensitivity line at  $\sim 700$  sources. One approach to trace such abundant source classes is to include other messenger-particles as cosmic-rays or various kinds of electromagnetic radiation to get a complete view on the origin of cosmic radiation.

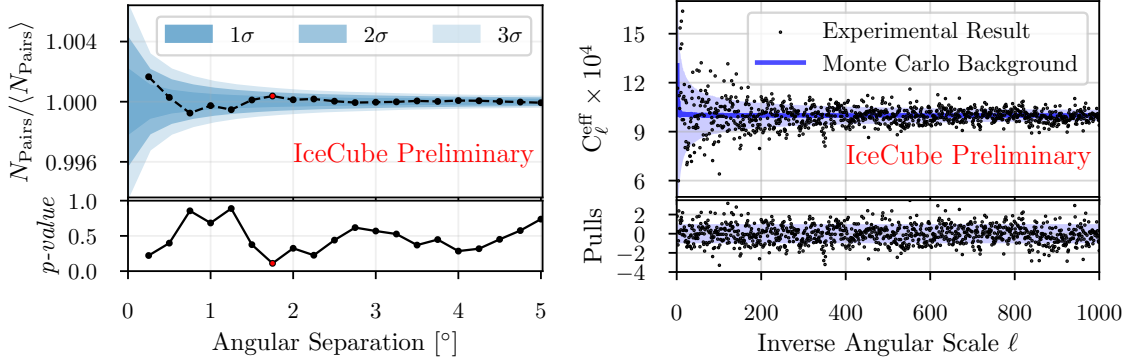


Figure 1: *Left (2pt-Autocorrelation)*: In the top panel is shown the experimental number of pairs divided by the mean number of pairs expected from a pure background hypothesis as a function of the angular scale  $\alpha$ , the shaded areas represent three different sigma bands. The lower panel shows the pre-trial p-value corresponding to each dot. The best clustering scale is marked with a red dot. *Right (Multipole)*: In the top panel the experimental angular power spectrum (black dots) is shown in comparison with the Monte Carlo background expectation as a function of  $\ell$ . The corresponding pulls, i.e. the deviation in Gaussian sigma is shown in the bottom panel.

### 3.2 South

Similar to what has been done for the Northern Hemisphere, the Southern Hemisphere is also studied using the 2pt-Autocorrelation method and yielding a non-observation of any clustering, and hence upper limits are calculated. The left panel of Figure 3 shows the results of the 2pt-Autocorrelation analysis in the Southern Hemisphere. The trial corrected p-value is 60%, which is again consistent with fluctuations from background expectations.

### 3.3 Cygnus

The Cygnus Region is a Galactic region here formally defined as the area of the sky extending between  $72^\circ$  and  $83^\circ$  in galactic longitude and  $-3^\circ$  and  $4^\circ$  in galactic latitude. It has been intensively studied by  $\gamma$ -ray experiments in the GeV and TeV energy ranges [13]. This region has also been considered as a possible location for CR acceleration and neutrino production [14, 15]. For these reasons, the 2pt-Autocorrelation method has been applied on the identified region, considering two different scenarios: point-like sources, as done for the two hemispheres as described above, and extended sources with a Gaussian shape. The right panel of Figure 3 shows the results of the 2pt-Autocorrelation analysis. The trial corrected p-value is 53%, again consistent with fluctuations from background expectations.

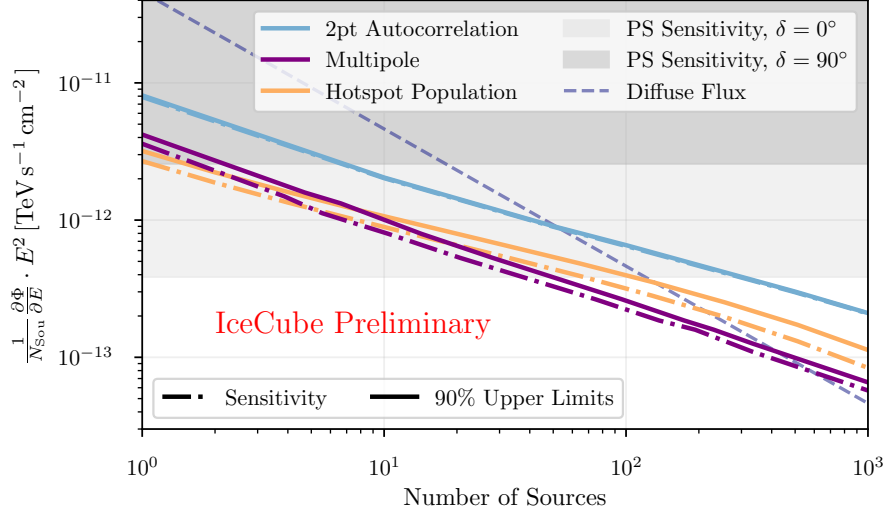


Figure 2: The plot shows the *Northern Hemisphere's* 90% C.L. flux upper limits for equally strong point-sources and draws a comparison to refined results of [8]. The dashed, blue line shows the diffuse astrophysical neutrino flux distributed equally over the number of sources. The gray shaded areas show the sensitivity of the single point-source analysis as in [8]. It can be seen that for a large amount of sources contributing, the flux limits per source of the angular autocorrelation analyses drop under the point-source sensitivity line. At an even higher number of sources, behind the intersection point, these limits are dominated by the constraints from the diffuse astrophysical flux.

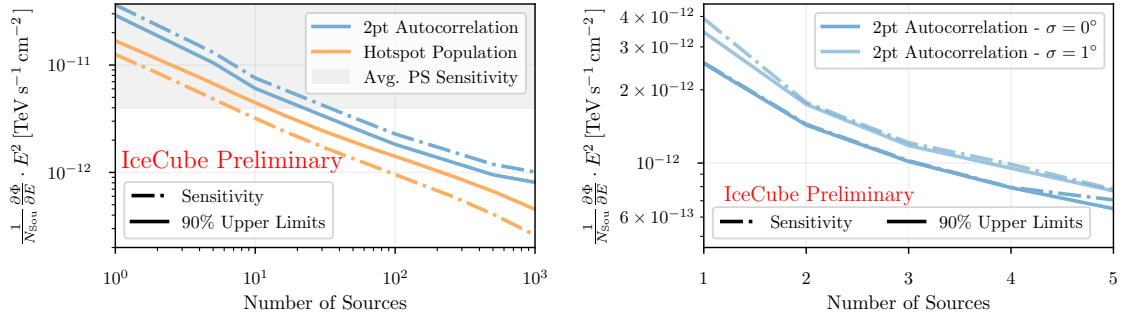


Figure 3: *Left: Southern Hemisphere.* The plot shows the 90% C.L. flux upper limits of the 2pt Autocorrelation analysis and draws a comparison to refined results of a similar analysis described in [8]. The gray shaded area show the average sensitivity of the Single Point-Source Analysis as in [8]. It can be seen that for a large amount of sources contributing, the flux limits per source of the analyses drop under the point-source sensitivity line. *Right: Cygnus Region.* The plot shows the 90% C.L. flux upper limits of the 2pt Autocorrelation analysis for point-like ( $\sigma = 0^\circ$ ) and extended, Gaussian shaped sources ( $\sigma = 1^\circ$ ).

## 4. Conclusions

Two different and complementary analyses focused on the observation of clustering of neutrino events have been presented. The two analyses have been performed on two different neutrino samples with statistics exceeding six years of detector livetime. The Northern Hemisphere, the Southern Hemisphere and the Cygnus Region have been studied separately and the results of the observations are compatible with background expectations. On this basis upper limits have been calculated for all the scenarios, among which the strongest neutrino flux upper limits come from the northern hemisphere.

## References

- [1] S. R. Kelner, F. A. Aharonian, and V. V. Bugayov, *Phys. Rev. D* **74** (Aug, 2006) 034018.
- [2] M. Kowalski, *J. Phys. Conf. Ser.* **632** (2015) 012039.
- [3] **IceCube** Collaboration, M. G. Aartsen et al., *Journal of Instrumentation* **12** (2017) P03012.
- [4] **IceCube** Collaboration, M. G. Aartsen et al., *Journal of Instrumentation* **9** (2014) P03009.
- [5] **AMANDA** Collaboration, J. Ahrens et al., *Nucl. Instrum. Meth.* **A524** (2004) 169–194.
- [6] J. G. Learned and K. Mannheim, *Annual Review of Nuclear and Particle Science* **50** (2000) 679–749.
- [7] **IceCube** Collaboration, M. G. Aartsen et al., *The Astrophysical Journal* **833** (2016) 3.
- [8] **IceCube** Collaboration, M. G. Aartsen et al., *The Astrophysical Journal* **835** (2017) 151.
- [9] C. Copi, D. Huterer, D. Schwarz, and G. Starkman, *Phys. Rev.* **D75** (2007) 023507.
- [10] **IceCube** Collaboration, M. G. Aartsen et al., *Astropart. Phys.* **66** (2015) 39–52.
- [11] **IceCube** Collaboration, M. G. Aartsen et al., *Astropart. Phys.* **66** (2015) 39–52.
- [12] **IceCube** Collaboration, A. Bernhard and S. Odrowski, , in *Proceedings, 33rd International Cosmic Ray Conference (ICRC2013): Rio de Janeiro, Brazil, July 2-9, 2013*, p. 0471.
- [13] A. A. Abdo et al., *Astrophys. J.* **753** (2012) 159.
- [14] T. M. Yoast-Hull, J. S. Gallagher III, F. Halzen, A. Kheirandish, and E. G. Zweibel, [arXiv:1703.02590](https://arxiv.org/abs/1703.02590).
- [15] M. Guenduez, J. Becker Tjus, B. Eichmann, and F. Halzen, [arXiv:1705.08337](https://arxiv.org/abs/1705.08337).

# All-sky search for correlations in the arrival directions of astrophysical neutrino candidates and ultrahigh-energy cosmic rays

The IceCube Collaboration<sup>1</sup>, The Pierre Auger Collaboration<sup>2</sup>, The Telescope Array Collaboration<sup>3</sup>

<sup>1</sup> [http://icecube.wisc.edu/collaboration/authors/icrc17\\_icecube](http://icecube.wisc.edu/collaboration/authors/icrc17_icecube)

<sup>2</sup> [http://www.auger.org/archive/authors\\_icrc\\_2017.html](http://www.auger.org/archive/authors_icrc_2017.html)

<sup>3</sup> <http://www.telescopearray.org/index.php/research/collaborators>

*E-mail:* [imen.alsamarai@icecube.wisc.edu](mailto:imen.alsamarai@icecube.wisc.edu); [golupg@cab.cnea.gov.ar](mailto:golupg@cab.cnea.gov.ar)

High-energy neutrinos, being neutral and weakly interacting particles, are powerful probes of the sites of production and acceleration of cosmic rays. The challenging discovery of cosmic neutrinos by the IceCube Collaboration has moved the field closer to realizing the potential of neutrino astronomy. Meanwhile, ground-based cosmic ray detectors like the Pierre Auger Observatory and the Telescope Array have reached an unprecedented accuracy in the determination of the features of the cosmic rays at the highest energies. We report on a collaborative effort between IceCube, the Pierre Auger Observatory and Telescope Array to identify directional correlations between the arrival directions of the highest-energy cosmic rays from both hemispheres and of the most probable cosmic neutrino events detected by IceCube. We describe the updated results of two independent searches using seven years of IceCube neutrino data and the most energetic cosmic-ray events detected by the Pierre Auger Observatory and the Telescope Array. The directional correlation found between UHECRs and neutrinos is reported with a significance of  $\sim 2\sigma$ .

**Corresponding authors:** G. Golup<sup>4</sup>, I. Al Samarai<sup>\*5</sup>, L. Caccianiga<sup>6</sup>, A. Christov<sup>5</sup>, P.L. Ghia<sup>7</sup>, U. Giaccari<sup>8</sup>, T. Montaruli<sup>5</sup>, H. Sagawa<sup>9</sup>, L. Schumacher<sup>10</sup>, P. Tinyakov<sup>11</sup>.

<sup>4</sup> *Centro Atómico Bariloche, S.C de Bariloche, Argentina*

<sup>5</sup> *Département de physique nucléaire et corpusculaire, Université de Genève, Genève, Switzerland.*

<sup>6</sup> *Università di Milano, Dipartimento di Fisica, Italy*

<sup>7</sup> *Institut de Physique Nucléaire d'Orsay (IPNO), Université Paris-Sud, Univ. Paris/Saclay, CNRS-IN2P3, France*

<sup>8</sup> *Universidade Federal do Rio de Janeiro, Instituto de Física, Rio de Janeiro, Brazil*

<sup>9</sup> *Institute for Cosmic Ray Research, University of Tokyo, Kashiwa, Chiba, Japan.*

<sup>10</sup> *RWTH Aachen University, III. Physikalisches Institut B, Aachen, Germany.*

<sup>11</sup> *Service de Physique Théorique, Université Libre de Bruxelles, Ixelles, Belgium.*

*35th International Cosmic Ray Conference ICRC 2017-  
10-20 July, 2017  
Bexco, Busan, Korea*

---

\*Speaker.

## Introduction

The determination of the origin of cosmic rays (CRs) is a difficult task since CRs are deflected during propagation. The extent of this angular deflection is still poorly constrained. Neutrinos produced during hadronic interactions of CR primaries propagate unaffected from their sources to us. They can therefore deliver potentially valuable information on the most energetic CR sources of the Universe. Neither of the observatories of neutrinos or ultrahigh-energy cosmic rays (UHECRs) dedicated to unravel the quest of the CR origin have delivered evidence for specific cosmic sources. This search for a common origin of UHECRs and neutrinos results from a joint collaboration between the IceCube Neutrino Observatory, the Pierre Auger Observatory and the Telescope Array (TA). Previous results of this work [1] provided a potentially interesting connection between neutrino and UHECR directions at the  $3\sigma$  level. We update that work here including two additional years of neutrino data from IceCube and one more year of TA data.

### 1. The observatories and the data sets

#### The IceCube South Pole Neutrino Observatory

IceCube [2] is a cubic-kilometer high-energy neutrino detector (energy threshold  $>\sim 100$  GeV) located at the geographic South Pole at about 1.5 to 2.5 km beneath the ice sheet surface. It is composed of 86 strings instrumented by 5160 photomultiplier tubes housed in pressure resistant spheres. Since 2005, data have been taken with partially completed configurations (9, 22, 40, 59 and 79 strings) until its final completion in December 2010. In 2013, a neutrino flux compatible with astrophysical neutrino expectations was reported [3, 4, 5]. Cumulating four years of data, the hypothesis of a pure atmospheric origin has been rejected at  $\sim 6.5\sigma$  level. These detected neutrinos are of all flavors interacting inside the detection volume (starting events) with deposited energies ranging from 60 TeV up to 2 PeV. They compose the HESE dataset ('High-Energy Starting Events'). They are mostly composed of shower-like events (cascades) characterized by an angular resolution of  $\sim 15^\circ$  above 100 TeV. The track-like events are induced by muons and have a better angular resolution of  $\lesssim 1^\circ$ . The resolution of the deposited energy for tracks and cascades is around 15% [6] but cascades have a better resolution for the reconstructed neutrino energy since most of the energy is deposited in the detector, which is not the case for tracks.

In this analysis, we present results on the published updated sample of 39 HESE cascades and 7 HESE tracks [1] with two additional years of data composed of 19 cascades and 8 tracks, giving a total of 58 cascades and 15 tracks constituting the six-year HESE dataset [7].

A complementary dataset of through-going muons induced by charged current interactions of candidate  $\nu_\mu$  from the Northern sky [8] is also added to the track dataset. It has been reported that events giving this set of tracks do have a spectrum that is inconsistent with the hypothesis of atmospheric neutrino origin at the level of  $5.6\sigma$ . The events considered here are 35 tracks corresponding to seven years of data from the eight-year data sample presented in [9]. Only events with 'signalness'  $> 50\%$  are considered, where the signalness is defined as the ratio of the astrophysical expectation over the sum of the atmospheric and astrophysical expectations for a given energy proxy and best-fit neutrino spectral index of 2.16. This requirement of 'signalness'  $> 50\%$

translates to a selection of events with a lower energy threshold of  $\sim 200$  TeV of the muon energy proxy [8].

The events from the HESE sample and that from the complementary dataset from the Northern sky only confirm the picture of an isotropic neutrino emission, but measured differences in the energy spectrum may suggest a mixed origin of the events detected in IceCube. Nonetheless, no astrophysical counterpart has so far been supported by the current observational data.

### The Pierre Auger Observatory

The Pierre Auger Observatory [10] is a hybrid high-energy cosmic-ray detector, covering an area of about  $3000 \text{ km}^2$ , located in Argentina. It combines a large surface detector array (SD) composed of 1660 water-Cherenkov detectors with an atmospheric fluorescence detector (FD) made of 27 fluorescence telescopes. The dataset used for this analysis is composed of 231 cosmic rays with energies  $E_{CR} \geq 52 \text{ EeV}$  recorded with the SD array from January 2004 to March 2014. The cut on the zenith angle  $\theta \leq 80^\circ$  allows for a field-of-view ranging from  $-90^\circ$  to  $+45^\circ$  in declination. The angular resolution, defined as the 68<sup>th</sup> percentile of the distribution of the opening angles between the true and reconstructed directions of simulated events, is better than  $0.9^\circ$  [11].

### Telescope Array

Telescope Array (TA) is a  $700 \text{ km}^2$  cosmic-ray surface array detector located in the United States [12]. It is composed of 507 plastic scintillators distributed on a square grid with 1.2 km spacing overlooked by three fluorescence detector stations housing 38 telescopes. The selected events have an energy  $E_{CR} \geq 57 \text{ EeV}$  and zenith angles smaller than  $55^\circ$ . The angular resolution of these events is about  $1.5^\circ$ . In addition to the 87 events detected from May 2008 to May 2014 and used in [1], 22 additional events collected in an additional year of data were used, reaching a total of 109 UHECRs from TA.

In both UHECR observatories, the absolute energy scale is given by fluorescence calibrations, using ‘hybrid’ events which are detected simultaneously by the SD array and the FD. For these events, it is possible to take advantage of the quasi-calorimetric energy determination from the FD technique. For the Pierre Auger Observatory, the systematic uncertainty on the energy scale is 14% and the statistical energy uncertainty is smaller than 12% [13]. For TA, the energy resolution is  $\sim 20\%$ , while the systematic uncertainty on the energy scale is 22% [14]. In accordance with the TA and Auger Energy Spectrum Working Group, and as presented in [1], the energy measured by TA is downshifted by 13%, so that the measured Auger and TA energy spectra coincide at 10 EeV.

The directions of the neutrinos detected by IceCube and the UHECRs detected by the Pierre Auger Observatory and Telescope Array used in this work are shown in Figure 1 in Equatorial coordinates. The complementary field-of-views of the UHECR observatories allow for an all-sky search for correlations with neutrinos of all-flavors detected by IceCube.

## 2. The methods

The search for correlations in the arrival directions of UHECRs and neutrinos relies on two in-

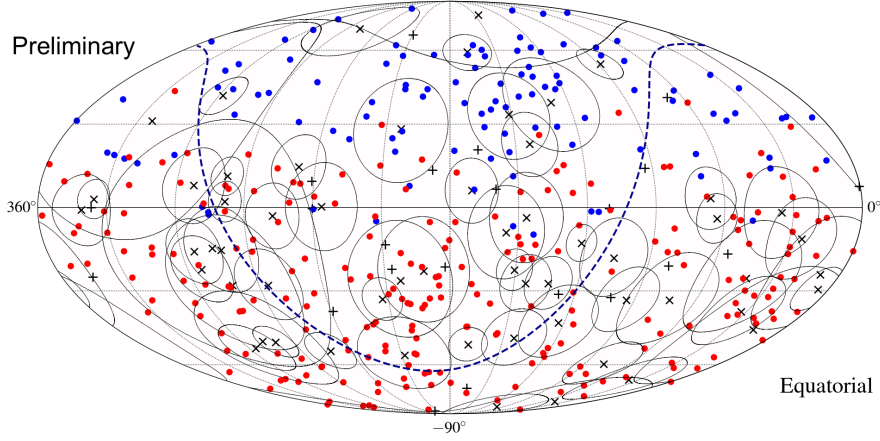


**Figure 1:** Directions of the UHECR events detected by Telescope Array (blue points) and the Pierre Auger Observatory (red points). The directions of the shower-like neutrino events detected by IceCube are shown in black crosses surrounded by the angular uncertainties shown in black circles. The track-like events are shown with ‘plus’ signs. The Galactic plane is represented by the dashed blue line.

dependent methods adapted for this analysis [1]: the unbinned-likelihood and the cross-correlation method.

### Cross-correlation method

The cross-correlation method consists in computing the relative excess in the number of neutrino-UHECR pairs as a function of their angular separation over the expectation of isotropically distributed CR arrival directions, keeping the arrival directions of the neutrinos fixed. The isotropic distribution of the arrival directions of UHECRs is simulated according to the corresponding geometric exposures of the observatories. We also compare the number of pairs to an isotropic distribution of neutrinos, keeping the arrival directions of the UHECRs fixed and thus preserving the degree of anisotropy in the arrival directions of CRs. The isotropic flux of neutrinos is simulated by producing random right ascensions and keeping their declination fixed to account for the declination dependence in the IceCube acceptance. The angular separation in this study ranges from  $1^\circ$  to  $30^\circ$  with steps of  $1^\circ$ . This angular scan does not require one to make an assumption on the deflection of CRs while they propagate from their (supposedly) common source with neutrinos.

### The unbinned-likelihood method

The second test is a stacking likelihood test assuming that the stacked sources are the neutrino directions. This test requires a hypothesis on the CR deflections. We have nonetheless made a scan on different values of the deflections also to account for the uncertainty on the composition of the CRs.

We considered a few models of cosmic ray deflections, which are based on backtracking simulations of UHECRs in the Galactic magnetic field models of Pshirkov et al. [15] and Jansson and Farrar [16]. Assuming a pure proton composition with an energy  $E_{\text{CR}}=100$  EeV, we obtained a median angular deflection of  $2.7^\circ$  due to the Galactic magnetic field. In this work, the assumed

angular deflections in the CR directions are thus taken as  $3^\circ \times 100 \text{ EeV}/E_{\text{CR}}$ . To account for a possible heavier composition or larger contribution of the intervening magnetic fields, additional test values of  $6^\circ \times 100 \text{ EeV}/E_{\text{CR}}$  and  $9^\circ \times 100 \text{ EeV}/E_{\text{CR}}$  were considered. It is to be noted that the likelihood test is less optimal but not insensitive if the ‘true’ deflection of CRs is slightly different than foreseen by models. The expression of the log-likelihood is defined as:

$$\ln \mathcal{L}(n_s) = \sum_{i=1}^{N_{\text{Auger}}} \ln \left( \frac{n_s}{N_{\text{CR}}} S_{\text{Auger}}^i + \frac{N_{\text{CR}} - n_s}{N_{\text{CR}}} B_{\text{Auger}}^i \right) + \sum_{i=1}^{N_{\text{TA}}} \ln \left( \frac{n_s}{N_{\text{CR}}} S_{\text{TA}}^i + \frac{N_{\text{CR}} - n_s}{N_{\text{CR}}} B_{\text{TA}}^i \right),$$

where  $n_s$ , the number of signal events, is the only free parameter,  $N_{\text{CR}} = N_{\text{Auger}} + N_{\text{TA}}$  is the total number of UHECR events (340),  $S_{\text{Auger}}^i$  and  $S_{\text{TA}}^i$  are the signal PDFs (Probability Distribution Functions) for Auger and for TA, respectively, and  $B_{\text{Auger}}^i$  and  $B_{\text{TA}}^i$  are the corresponding background PDFs. The signal PDFs, in which the different neutrino positions are stacked, take into account the exposure and angular resolution of the CR observatories, the assumed CR magnetic deflections and the likelihood maps for the reconstruction of the  $\nu$  arrival directions (Figure 2). Thus, for each CR  $i$  at a given direction  $\vec{r}_i$  and energy  $E_i$ , the signal PDF is expressed as:

$$S_{\text{CR observatory}}^i(\vec{r}_i, E_i) = R_{\text{CR observatory}}(\delta_i) \cdot \sum_{j=1}^{N_{\text{src}}} S_j(\vec{r}_i, \sigma(E_i)) \quad (2.1)$$

$R_{\text{CR observatory}}(\delta_i)$  is the relative exposure for a given event declination and  $N_{\text{src}}$  is the number of stacked sources, 58 for the cascades and 49 for the tracks. The last term,  $S_j(\vec{r}_i, \sigma(E_i))$ , is the value of the normalized directional likelihood map for the  $j^{\text{th}}$  source (i.e neutrino) taken at  $\vec{r}_i$  and smeared with a Gaussian with standard deviation  $\sigma(E_i)$ . The Gaussian smearing takes into account the energy-dependent magnetic deflections imprint on the CR directions  $\sigma(E_i) = \sqrt{\sigma_{\text{CR observatory}}^2 + \sigma_{\text{MD}}^2}$ , where  $\sigma_{\text{CR observatory}}$  is the angular resolution of the CR observatory ( $0.9^\circ$  for Auger and  $1.5^\circ$  for TA) and  $\sigma_{\text{MD}} = D \times 100 \text{ EeV}/E_{\text{CR}}$ . Figure 2 represents the directional likelihood maps of the stacked neutrinos for shower-like and track-like topologies before smearing and convolved with the exposure of each CR observatory. The background PDFs are obtained from the normalized (by the total number of detected events by each observatory) exposures of the CR observatories. The test statistic  $TS$  is defined as:  $TS = -2 \ln \frac{\mathcal{L}(n_s)}{\mathcal{L}(n_s=0)}$  and follows a distribution close to  $\chi^2$  with one degree of freedom.

### 3. Results

#### Cross-correlation results

Applying the cross-correlation method to the data, it is found that the maximum departure from the expectation for an isotropic CR flux, keeping the arrival directions of the neutrinos fixed, occurs at an angular distance of  $1^\circ$  for tracks and  $22^\circ$  for cascades, with post-trial  $p$ -values of 0.48 and  $5.4 \times 10^{-3}$ , respectively. In Figure 3, the relative excess of neutrino-UHECR pairs found in the data,  $[n_p(\alpha)/\langle n_p^{\text{iso}}(\alpha) \rangle] - 1$ , as a function of the scanned separation angles is shown with respect to the expectations of an isotropic flux of CRs. Evaluating the significance under the hypothesis of an isotropic flux of neutrinos, keeping the arrival directions of the CRs fixed, we find that for the high-energy cascades the maximum departure from isotropic expectations is at  $16^\circ$ , with a post-trial  $p$ -value of  $1.0 \times 10^{-2}$ .

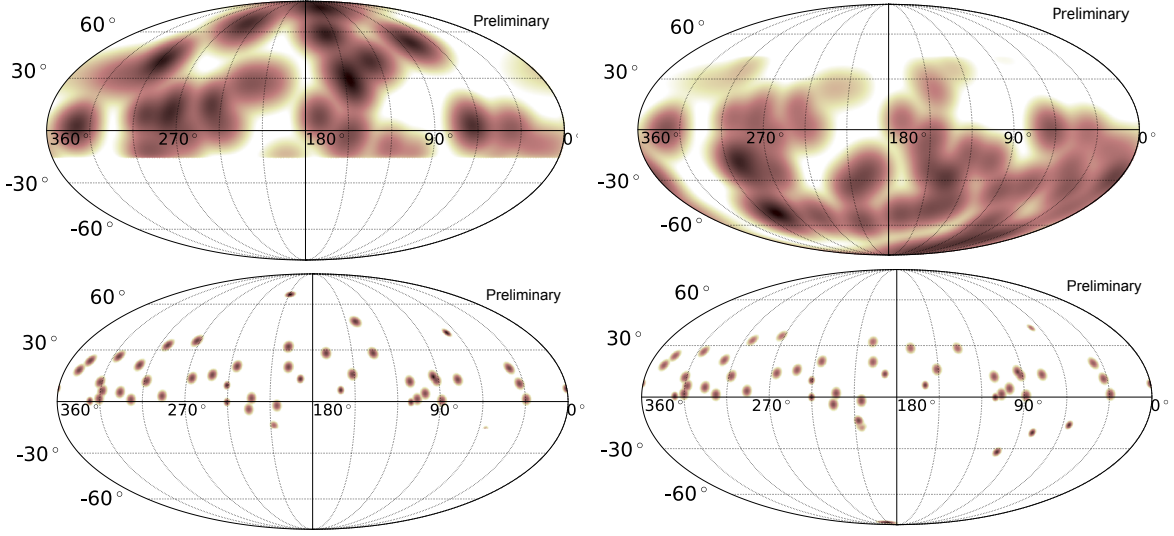


**Figure 2:** The signal PDFs before the Gaussian smearing in equatorial coordinates. The upper plots are for the high-energy cascades, while the lower ones are for the high-energy tracks. The declination-dependent exposure is applied for Auger in the right-hand plots and for TA in the left-hand plots.

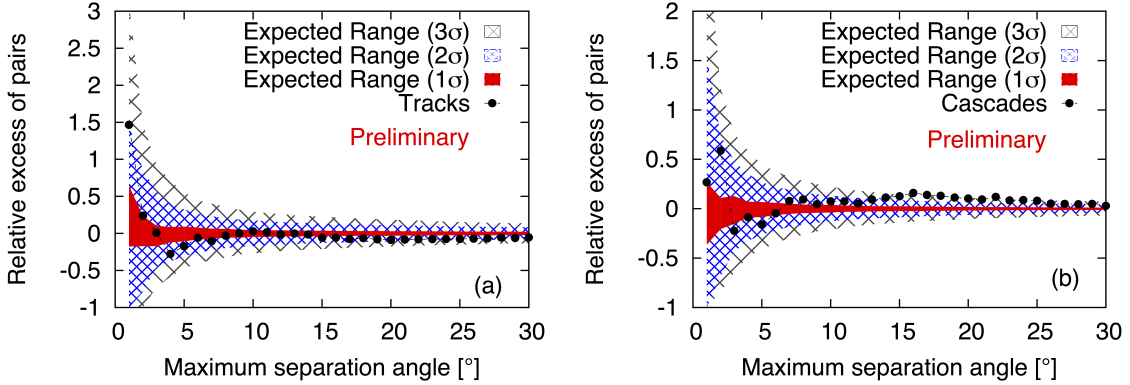


**Figure 3:** Relative excess of pairs,  $[n_p(\alpha)/\langle n_p^{iso}(\alpha) \rangle] - 1$ , as a function of the maximum angular separation between the neutrino and UHECR pairs, for the analysis done with the high-energy tracks (left) and with the high-energy cascades (right). The  $1\sigma$ ,  $2\sigma$  and  $3\sigma$  fluctuations expected from an isotropic distribution of arrival directions of CRs, keeping the arrival directions of the neutrinos fixed, are shown in red, blue and grey, respectively.

### Unbinned likelihood method results

The results for the stacking method are shown in Table 1. The most significant deviation from an isotropic flux of CRs occurs for the magnetic deflection parameter  $D = 6^\circ$  with the high-energy cascades. The observed pre-trial  $p$ -value of  $1.0 \times 10^{-2}$  corresponds to  $2.2 \times 10^{-2}$  post-trial, by considering 1000 realizations of randomly distributed CRs with  $6^\circ \times 100 \text{ EeV}/E_{CR}$  deviation from the neutrino source positions. The test maintaining the CR directions fixed while simulating an

$D$	High-energy tracks		High-energy cascades	
	$n_s$	pre-trial $p$ -value	$n_s$	pre-trial $p$ -value
$3^\circ$	0.9	0.44	45.5	$2.7 \times 10^{-2}$
$6^\circ$	-	underfluctuation	71.5	$1.0 \times 10^{-2}$
$9^\circ$	-	underfluctuation	84.7	$1.5 \times 10^{-2}$

**Table 1:** Results for the stacking analyses with the sample of high-energy tracks and high-energy cascades assuming an isotropic flux of CRs.

isotropic flux of neutrinos results in a post-trial  $p$ -value of  $1.7 \times 10^{-2}$  for shower-like events.

#### 4. Discussion

In [1], post-trial  $p$ -values of  $2.7 \times 10^{-4}$  and  $5 \times 10^{-4}$  with respect to an isotropic flux of UHECRs were found using the unbinned likelihood method and the cross-correlation method, respectively. With the addition of two years of HESE shower-like events, the updated  $p$ -values do not strengthen the hint of a possible anisotropic distribution of UHECRs and neutrinos previously found. Similarly, the computation of the  $p$ -values, assuming an isotropic flux of neutrinos while keeping the UHECR directions fixed, resulted in  $p$ -values which are less significant than those found in [1]. To illustrate the results found in this update, the UHECRs weights assuming  $D = 6^\circ$  and contributing to the signal PDF derived from equation 2.1 are shown in Figure 4 on top the neutrino directional maps in the exposures of the Auger Observatory and TA. Local clustering in the directions illustrate the  $\sim 2.3\sigma$  level correlation found.

It is noteworthy that this result can be explained by many facts. First, the not-yet-exhaustive knowledge of the CRs composition at such high energies and the poor knowledge of the Galactic magnetic field are the main limitations to the determination of the cosmic-ray sources using UHECRs. As already noted in [1], UHECRs can reach us from sources within the GZK horizon, meaning order of 10-100 Mpc. On the other hand, neutrinos can reach us from cosmological distances, so that if sources were stationary and uniformly distributed, only a few percent of neutrinos would be expected from the emitters of the detected UHECRs.

Many speculations on the possible sources of the four-year HESE sample still have not yet reached the significance of an evidence. The addition of two more years requires further correlation tests with various hypotheses of source candidates. It is also possible that there could be a contribution from galactic sources to the observed cosmic neutrino flux which would not be UHECR sources.

The future evolution of this search will concern the treatment of the magnetic deflection with updated models, the addition of updated data samples from the Pierre Auger Observatory and the cross-correlation with a sample of neutrinos of lower energy by IceCube and ANTARES.

#### References

- [1] The **IceCube**, **Pierre Auger** and **Telescope Array** Collaborations, *JCAP* **1601** (2016) 037.
- [2] **IceCube** Collaboration, *Astropart. Phys.* **26** (2006) 155.

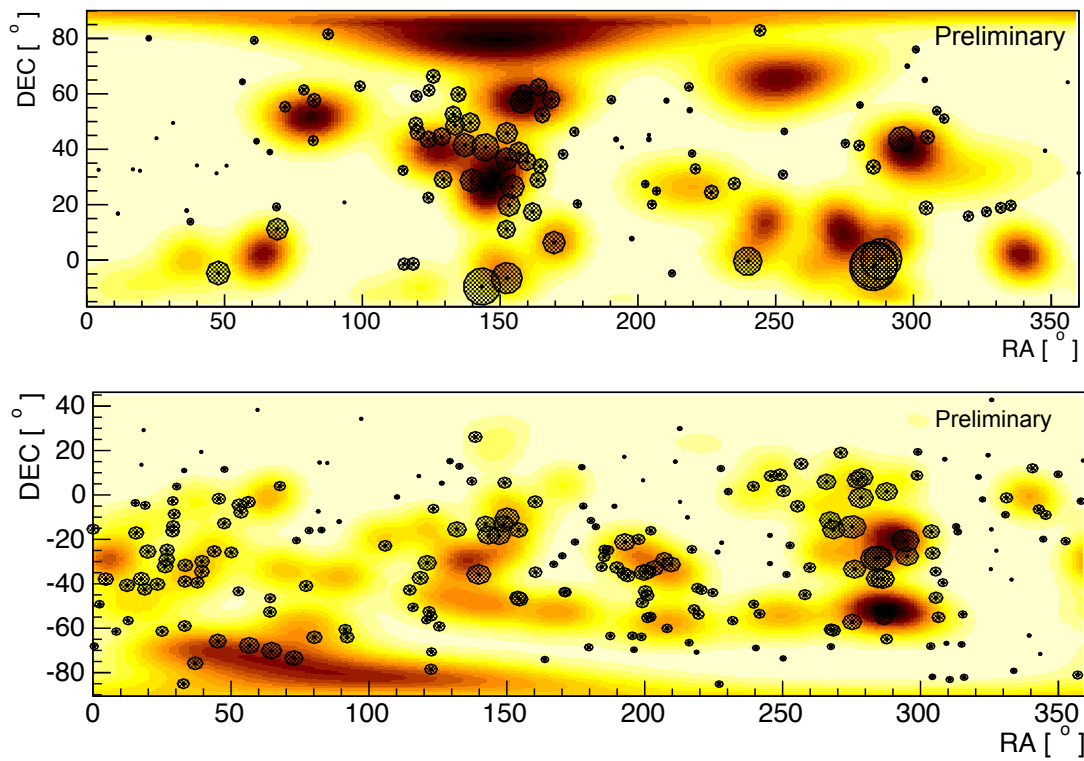


**Figure 4:** Neutrino signal PDF in the Telescope Array (top) and the Pierre Auger Observatory (bottom) exposures. The black dots represent the UHECRs directions. The black dashed circles radii are proportional to the weight assigned to each UHECR.

- [3] **IceCube** Collaboration, *Science* **342** (2013) 1242856.
- [4] **IceCube** Collaboration, *Phys. Rev. Lett.* **113** (2014) 101101.
- [5] **IceCube** Collaboration, *PoS (ICRC2015)* 1099 (2016).
- [6] **IceCube** Collaboration, *JINST* **9** (2014) P03009.
- [7] **IceCube** Collaboration, *PoS (ICRC2017)* 981 (these proceedings).
- [8] **IceCube** Collaboration, *Astrophys. J.* **833** (2016) 3.
- [9] **IceCube** Collaboration, *PoS (ICRC2017)* 1005 (these proceedings).
- [10] The **Pierre Auger** Collaboration, *Nucl. Instrum. Meth. A* **A798** (2015) 172.
- [11] C. Bonifazi for the **Pierre Auger** Collaboration, *Nucl. Phys. B (Proc. Suppl.)* **190** (2009) 20.
- [12] The **Telescope Array** Collaboration, *Nucl. Instrum. Meth. A* **689** (2012) 87 and *Nucl. Instrum. Meth. A* **676** (2012) 54.
- [13] The **Pierre Auger** Collaboration, *JCAP* **8** (2014) 19; R. Pesce for the **Pierre Auger** Collaboration, *Proc. 32nd ICRC*, Beijing, China, 2 (2011) 214 [arXiv:1107.4809].
- [14] The **Telescope Array** Collaboration, *Astrophys. J.* **768** (2013) L1.
- [15] M. S. Pshirkov, P. G. Tinyakov, P. P. Kronberg, K. J. Newton-McGee, *Astrophys. J.* **738** (2011) 192.
- [16] R. Jansson and G. R. Farrar, *Astrophys. J.* **757** (2012) 14.

## Results of IceCube searches for neutrinos from blazars using seven years of through-going muon data

---

### The IceCube Collaboration<sup>†</sup>

<sup>†</sup> [http://icecube.wisc.edu/collaboration/authors/icrc17\\_icecube](http://icecube.wisc.edu/collaboration/authors/icrc17_icecube)

E-mail: [mhuber@icecube.wisc.edu](mailto:mhuber@icecube.wisc.edu)

Located at the South Pole, the IceCube Neutrino Observatory is the world largest neutrino telescope, instrumenting one cubic kilometre of Antarctic ice at a depth between 1450 m to 2450 m. In 2013 IceCube reported the first observations of a diffuse astrophysical high-energy neutrino flux. Although in the meantime the collaboration has detected more than 50 high energy neutrino events, the origin of these neutrinos is still not identified. Blazars, a subclass of Active Galactic Nuclei and one of the most powerful classes of objects in the universe, have long been considered plausible sources of high energy neutrinos. This scenario can be examined using stacking methods testing the correlation between IceCube neutrinos and catalogs of hypothesized sources. Here the results of stacking analyses using three different blazar catalogs will be presented. The analyses are performed on 7 years of through-going muon data, recorded by IceCube between 2008 and 2015.

**Corresponding authors:** Matthias Huber<sup>\*1</sup>, Kai Krings<sup>1</sup>

<sup>1</sup> Technische Universität München, Physik-Departement, James-Franck-Str. 1, 85748 Garching

*35th International Cosmic Ray Conference - ICRC217-  
10-20 July, 2017  
Bexco, Busan, Korea*

---

\*Speaker.

## 1. Introduction

With the first discovery of an astrophysical neutrino flux at PeV energies the IceCube collaboration marked the beginning of a new era of study not only in high energy neutrino astronomy but more generally in the study of the high energy universe [1]. Due to their neutral charge and their very low interaction cross sections neutrinos are neither deflected by magnetic fields nor significantly absorbed in the interstellar medium. Consequently neutrinos carry unique information about their site of production. They are not only ideal messengers for the directional origin of the most powerful objects in the Universe but can also give insight in the acceleration mechanisms within these objects at the highest energies.

Blazars, a subclass of Active Galactic Nuclei (AGNs) hosting a jet of highly relativistic particles pointing towards the Earth, are among the most luminous objects in the entire universe [5]. Depending on the conditions for particle acceleration at the site of these objects, they can be regarded as potential extragalactic sources for the emission of high energy neutrinos [7].

In the following the neutrino signal from three different samples of blazars is tested with a stacking method using seven years of data from the IceCube Neutrino Observatory [2]. The IceCube Observatory is the world's largest neutrino telescope, instrumenting one cubic kilometre of Antarctic ice at a depth between 1450 m to 2450 m. The detection principle relies on the observation of Cherenkov light emitted from secondary particles created in interactions of neutrinos within the Antarctic ice or the nearby bedrock. Muons, which produce a long luminous track within the detector, are most suitable to get an accurate pointing towards the origin of the events. Above energies of 10 TeV the direction of muon events in IceCube can be reconstructed with a median angular resolution of less than  $1^\circ$  [3]. Hence the results of this analysis are based on a sample of approximately 700 000 through-going muon events from the whole sky integrated over a livetime of seven years.

## 2. Blazar populations

Among the most luminous objects in the universe, blazars generate photons over a broad emission band ranging from radio to TeV energies. In general the spectral energy distribution (SED) of blazars is composed of two broad humps. While the low energy peak between infrared and x-ray energies can be associated with synchrotron radiation from relativistic electrons, different potential scenarios exist for the generation of the second hump at gamma-ray energies.

Based on different properties in the spectral energy distribution, blazars can be further classified into flat-spectrum radio quasars (FSRQs) and BL Lacertae objects (BL Lacs). While the latter only show weak emission lines in the optical spectrum, strong and broad emission lines are visible in the SED of FSRQs [5]. A second complementary classification is based on the non-thermal emission of blazars. It makes use of the rest frame value of the frequency of the synchrotron peak  $\nu_{peak}^S$ , reflecting the maximum energy of the accelerated electrons within the relativistic jets. According to the position of the synchrotron peak blazars are categorized as low and intermediate synchrotron peaked (LSP and ISP) if  $\nu_{peak}^S < 10^{15}$  Hz ( $\sim 4$  eV) and high synchrotron peaked (HSP) if  $\nu_{peak}^S > 10^{15}$  Hz. In particular HSP BL Lacs (HBL), a rare class of blazars, are very powerful

gamma-ray emitters. Hence these objects are of special interest in the investigation of the generation processes of ultra high energy cosmic rays and the related high energy neutrinos [6, 7].

Following theoretical model explanations, neutrinos could be produced via the decay of charged pions from photo-hadronic interactions of high energy protons with ambient photons or with gas within the jets. This neutrino flux would be accompanied by a flux of very high energy (VHE) gamma-rays from the decay of neutral pions.

The existence of the highest energy IceCube neutrinos ( $\sim$  PeV) implies the generation of a  $\gamma$ -ray flux in the  $\geq$  TeV range [13]. Hence in general blazars with higher gamma-ray flux are assumed to emit more high-energy neutrinos. Yet this conclusion has to be treated carefully. Since VHE gamma-rays are strongly attenuated by extragalactic background light (EBL) or reabsorbed at the source, the photon-neutrino connection on a source by source basis might be diluted. Given that for the theoretical description of the low energy synchrotron hump the existence of relativistic electrons is inevitable, it seems reasonable to assume that also the acceleration of hadrons is possible within the jets of blazars. Nevertheless, it has not yet been possible to determine the fraction of the hadronic component to the high energy hump of blazars nor to disprove purely leptonic models. The detection of neutrinos from blazar populations would directly prove the existence of this hadronic component.

By studying a list of VHE IceCube neutrinos in [7], a possible association between eight HBLs and neutrinos from the tested sample was suggested. In a following study [8], the authors tested the correlation between different blazar catalogs and a list of high energy starting events (HESE) from IceCube, always finding the most significant correlation for the HBLs within each catalog.

Motivated by these observations three different blazar catalogs are analyzed in this paper. These are the second WISE<sup>1</sup> High Synchrotron Peaked catalog (2WHSP) [9, 10], the HBLs from the second catalog of Hard Fermi-LAT<sup>2</sup> sources (2FHL) [11] and the FSRQs from the third catalog of AGN detected by Fermi-LAT (3LAC) [12]. The locations of the blazars from each of these catalogs are illustrated in Figure 1. Since the goal of this analysis is the detection of extragalactic neutrino point sources only blazars with galactic latitude  $|b_{ll}| > 10^\circ$  are selected to avoid any bias from the Galactic Plane.

## 2.1 2WHSP

The 2WHSP catalog is currently the largest and most complete list of HSP blazars, consisting of 1681 sources [10]. The catalog is built up by correlating data from different multi-wavelength surveys and applying selection criteria based on spectral features in the radio to infra-red (IR) and IR to X-ray region that are known to be specific to blazar SEDs [9, 10]. Since the selection procedure of the 2WHSP catalog does not rely on gamma-ray observations this sample of blazars is not limited by the sensitivity constraints of currently available gamma-ray surveys. Hence also the effect of attenuation of very high energy photons due to extragalactic background light is negligible. All 2WHSP objects are supposed to radiate up to highest gamma-ray energies. Nevertheless only a few sources are confirmed GeV or even TeV photon emitters. To account for this lack of information the 2WHSP catalog provides every source with a quantitative measure of its potential

<sup>1</sup>WISE:Wide-field Infrared Survey Explorer

<sup>2</sup>Large Area Telescope

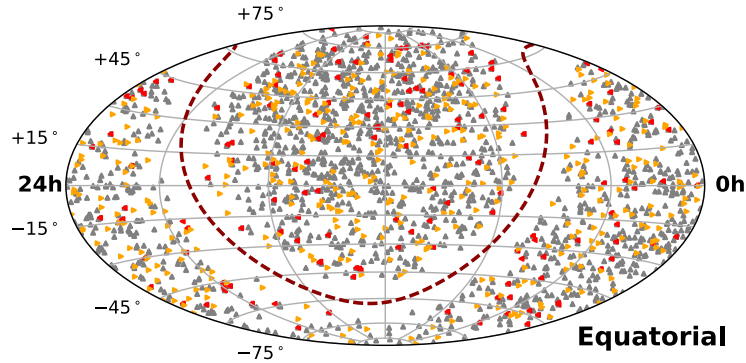


Figure 1: Skymap showing the source positions of the 2WHSP catalog (grey), the 2FHL HBLs (red) and the 3LAC FSRQs (orange). The dotted line (dark red) indicates the location of the galactic plane, with no sources selected in the region with  $|b_{II}| > 10^\circ$ .

visibility in TeV range. This property, called figure of merit (FOM), is defined as the ratio of the flux of the synchrotron peak of the blazar in question to the flux of the synchrotron peak of the faintest blazar that was already detected in the TeV band [9]. Blazars that are powerful enough to generate TeV gamma-rays might also be potential sources for astrophysical neutrinos.

## 2.2 2FHL HBLs

The 2FHL catalog consists of  $\sim 360$  extragalactic sources detected by the Fermi LAT during  $\sim 6$  years of run time [11]. All sources in this catalog are detected at energies above 50 GeV. Since the focus of this paper is only on the connection between blazars and neutrinos, only HBLs are extracted from the catalog yielding a total population of 149 HBLs with galactic latitude  $|b_{II}| > 10^\circ$ .

## 2.3 3LAC FSRQs

Since not only HBLs but also FSRQs are promising candidates for high-energy neutrino emitters, the last blazar sample that is tested in this paper is a population of FSRQs from the 3LAC catalog established by Fermi-LAT [12]. The 3LAC catalog consists of 1591 AGNs detected between 100 MeV and 300 GeV, with most of the AGNs being blazars. The subsample of the 3LAC that is used in this analysis consists of 414 confirmed FSRQs at  $|b_{II}| > 10^\circ$ .

## 3. Analysis method

### 3.1 Unbinned likelihood stacking approach

The through-going muon data set used for this analysis is vastly dominated by track-like events arising from atmospheric muons and neutrinos. Hence in order to find a significant indication of neutrino point sources it is essential to separate any astrophysical neutrino signal from this much larger atmospheric background. The statistical method that is used here to test the connection between the populations of blazars and the IceCube data is based on an unbinned likelihood ratio

maximization using the likelihood

$$\mathcal{L}(n_s, \gamma | \delta) = \prod_j^{N_{\text{sample}}} \prod_{i \in j} \left[ \frac{n_s^j}{N_{\text{tot}}^j} \mathcal{F}_i^j(\vec{x}_i, \vec{x}_s, \sigma_i, E_i, \gamma) + \left(1 - \frac{n_s^j}{N_{\text{tot}}^j}\right) \vec{\mathcal{B}}_i^j(\vec{x}_s, E_i) \right], \quad (3.1)$$

with  $j$  indexing the samples  $j \in \{\text{IC40, IC59, IC79, IC86 I-IV}\}$  and  $i$  the respective event index. This likelihood is defined as a function of the spectral index  $\gamma$  and the number of expected signal events  $n_s$ , where  $n_s^j$  describes the portion of expected signal events coming from sample  $j$ . The separation power between background and signal likeliness of a specific scenario in Equation (3.1) is mainly based on two event criteria. These criteria are the direction  $\vec{x}_i$  and the energy  $E_i$  of the events. Neutrino signal events from point sources are expected to be distributed close to the direction of their origin assuming a Gaussian-distributed spatial signal likelihood  $\mathcal{F}_i^j(\vec{x}_i, \vec{x}_s, \sigma_i, E_i, \gamma)$  for each event position  $\vec{x}_i$  around the source location  $\vec{x}_s$  with angular uncertainty  $\sigma_i$ . On the other hand events resulting from atmospheric background are locally spread uniformly in space, in the sense that the frequency of their appearance only depends on the declination angle. Hence the background probability  $\vec{\mathcal{B}}_i^j(\vec{x}_s)$  for each event  $i$  can be obtained from experimental data scrambled in right ascension.

In addition to the event position relative to the source the respective energy information  $E_i$  can be used to discriminate sources with a  $E^{-\gamma}$  spectrum from the atmospheric background, which follows a very soft  $E^{-3.7}$  spectrum.

Using the likelihood from Equation (3.1) the test statistic  $\Lambda$  is defined as

$$\Lambda = -2 \log \left[ \frac{\mathcal{L}(n_s = 0)}{\mathcal{L}(n_s = \hat{n}_s, \gamma = \hat{\gamma})} \right]. \quad (3.2)$$

By maximizing this likelihood ratio with respect to the number of expected signal events  $\hat{n}_s$  and a globally fixed spectral index  $\hat{\gamma}$  the validity of the point source hypothesis can be examined.

In case of a stacking analysis not only one point source but multiple point sources are assumed to generate a cumulative astrophysical neutrino signal inside the detector. In order to test such a scenario the signal PDF in Equation (3.1) has to be extended to the more general case of  $M$  source candidates

$$\vec{\mathcal{F}}_i \rightarrow \vec{\mathcal{F}}_i^{\text{Stack}} = \frac{\sum_{k=1}^M W^k R^k(\delta_k, \gamma) \cdot \vec{\mathcal{F}}_i^j(\vec{x}_i, \vec{x}_s^k, \sigma_i, E_i, \gamma)}{\sum_{k=1}^M W^k R^k(\delta_k, \gamma)}, \quad (3.3)$$

with  $\vec{x}_s^k = (\alpha_k, \delta_k)$  indicating the position of source  $k$ . This extended signal PDF can be regarded as superposition of the signal PDFs from the individual sources, with each source weighted with a detector specific weight  $R^k(\delta_k, \gamma)$  accounting for the declination and energy dependent detection efficiency of IceCube and a theoretical weight  $W^k$  accounting for theoretically predicted parameters of the individual sources.

### 3.2 Catalog scans

For the statistical analysis method in this paper all blazars in the respective catalog are assumed to emit neutrinos with the same strength, yielding  $W^k = \frac{1}{M}$ . Nevertheless for all three catalogs in this paper a correlation between the VHE gamma-ray flux and the neutrino flux is taken into

Table 1: Pre trial-corrected results of the 10 cumulative subsamples of the 2WHSP catalog.

# Sources	10	17	26	38	60	136	252	516	1099	1681
FOM ( $\geq$ )	4.00	4.00	2.55	2.00	1.60	1.00	0.50	0.25	0.10	0.00
$\gamma$	3.2	3.3	3.2	3.1	3.2	3.2	3.0	2.7	2.7	2.6
p-value	0.013	0.212	0.341	0.161	0.236	0.432	0.531	0.058	0.065	0.224

account indirectly on the whole sample scale. The two Fermi-LAT catalogs are partitioned into cumulative subsets, starting with the subset of blazars with the highest integrated gamma-ray fluxes and adding up this set with blazars having the next higher fluxes. Since the individual sources in each subsample are still weighted equally within the stacking method ( $W^k = \frac{1}{M_{\text{sub}}}$ , with  $M_{\text{sub}}$  being the number of blazars in the respective subsample), the analyses do not strongly depend on the correlation assumption. Since for the 2WHSP catalog no complete gamma-ray observations are available, the FOM (refer to section 2.1) is used instead of the flux for the partitioning. The exact partitioning is chosen according to the binning in [8].

For each of the subsamples of each catalog the p-value is evaluated. The final post-trial p-value of each catalog is then the trial corrected best p-value from the respective subsamples, yielding in total three final p-values from this analysis.

#### 4. Results

None of the three blazar catalogs tested showed any significant evidence for a neutrino signal above background expectations. The pre-trial corrected results of all catalogs are listed in Table 1 and 2. For the 2WHSP catalog the best pre-trial p-value results from the subsample including the 10 blazars with the highest FOM values in the catalog, yielding a post-trial p-value of 7.6%<sup>3</sup>.

Scanning the 2FHL HBL sample yields a most significant pre-trial p-value of 8.7% arising from the subsample including 127 blazars. The final post-trial p-value of the 2FHL HBL catalog is 24.8%. Similar to the 2WHSP catalog the best pre-trial p-value of FSRQ population from the 3LAC sample is received from smallest subsample, yielding a post-trial p-value of 46%.

All the outcomes from the three catalog stacking analyses are fully compatible with background fluctuations. Moreover looking at the catalog scans (shown in Tables 1 and 2) there is no obvious correlation visible between the integrated gamma-ray flux (or FOM respectively) and the neutrino p-values.

#### 5. Conclusions

Since no significant evidence for neutrino emission from the blazar samples analyzed was found, upper limits on the  $\nu_\mu$  flux from these blazar samples were calculated. The astrophysical muon neutrino flux observed by the IceCube collaboration yields a spectrum compatible with a single unbroken power law and spectral index of  $\gamma = 2.13 \pm 0.13$  between 194 TeV and 7.8 PeV [4]. Using a similar power law for the blazar sample, the maximum contribution from that population

<sup>3</sup>Overlaps of the catalogs are not taken into account in the trial correction.

Table 2: Pre-trial corrected results of the 2FHL HBL (**left**) and 3LAC FSRQ catalog (**right**). For the 2FHL HBL catalog the flux parameter corresponds to the integrated gamma-ray flux above 50 GeV. For the 3LAC FSRQs the flux corresponds to the integrated flux above 100 MeV.

# Sources	flux <sub>2FHL</sub>	$\gamma$	p-value	# Sources	flux <sub>3LAC</sub>	$\gamma$	p-value
12	$\geq 10^{-10.00}$	3.1	0.103	13	$\geq 1.0 \cdot 10^{-8}$	2.3	0.148
36	$\geq 10^{-10.45}$	4.0	> 0.66	20	$\geq 7.0 \cdot 10^{-9}$	2.4	0.352
42	$\geq 10^{-10.50}$	3.5	0.620	29	$\geq 5.6 \cdot 10^{-9}$	2.4	0.454
61	$\geq 10^{-10.60}$	3.4	0.500	40	$\geq 4.9 \cdot 10^{-9}$	2.8	0.205
92	$\geq 10^{-10.75}$	2.4	0.149	59	$\geq 3.1 \cdot 10^{-9}$	4.0	> 0.5
127	$\geq 10^{-10.90}$	3.0	0.087	102	$\geq 1.9 \cdot 10^{-9}$	2.9	0.532
143	$\geq 10^{-11.00}$	3.1	0.092	172	$\geq 1.0 \cdot 10^{-9}$	3.1	0.222
149	$\geq 10^{-11.13}$	3.0	0.289	353	$\geq 3.1 \cdot 10^{-10}$	3.0	0.256
				414	$\geq 1.0 \cdot 10^{-10}$	3.0	0.290

to the diffuse flux can be evaluated. The 90 % C.L. upper limit for the 2FHL HBLs following a  $\gamma = 2.13$  power law is illustrated in Figure 2. Assuming this unbroken power law the 2FHL HBLs can explain at most 4.5 % to 5.7 % of the diffuse flux at 90 % C.L.. Instead, when assuming that the neutrino emission strength of the individual blazars is directly proportional to their gamma-ray flux, the 2FHL HBLs can only describe 3.8 % of the diffuse  $\nu_\mu$  flux.

Since there is no indication for the blazar populations to follow a single unbroken power law, other scenarios are also tested. Several theoretical models allow blazars to follow a very hard spectrum [14]. In case of such a hard spectrum an energy cut off is expected once the hadronic acceleration of protons at the source breaks off. In the right part of Figure 2 the flux upper limits for  $\gamma = 1.5$  and  $\gamma = 1.0$  with different cut off energies are shown. In case of a spectral index  $\gamma = 1.5$  with an exponential cut off at 1 PeV, the 2FHL HBLs can contribute at most  $\sim 12\%$  to the diffuse muon neutrino flux between 0.2 PeV and 1.2 PeV. When assuming an even harder spectral index of  $\gamma = 1.0$  with the same cut off at 1 PeV, the 2FHL HBLs might still be able to explain up to  $\sim 21\%$  of the diffuse flux between 0.4 PeV and 1.7 PeV.

In [14] the shape of the SED of several HBLs was modeled with a leptohadronic emission model, automatically yielding a prediction for the neutrino emission. For Mrk 421 the prediction was found to be in good agreement with the neutrino flux implied by a cascade-like IceCube event (ID 9) located in the vicinity of Mrk 421 [14, 7]. Using this neutrino emission shape from Mrk 421 for all of the 2FHL HBLs, this blazar population could still account for no more than  $\sim 27\%$  of the diffuse flux within 1.3 PeV and 3.8 PeV.

Consequently one can find that the population of the 149 HBLs from the 2FHL catalog does not account for the majority of the diffuse muon neutrino flux at 90 % C.L.. Nevertheless depending on the spectral shape of the neutrino emission of the blazar sample they could still explain up to 27 % of the diffuse flux within certain energy ranges.

Adding more IceCube data to this analysis will improve our sensitivity towards a significant signal detection in the next years. Nevertheless assuming for instance that the actual neutrino flux of the 2FHL HBLs corresponds to the upper limit flux of the model from [14] one would still need

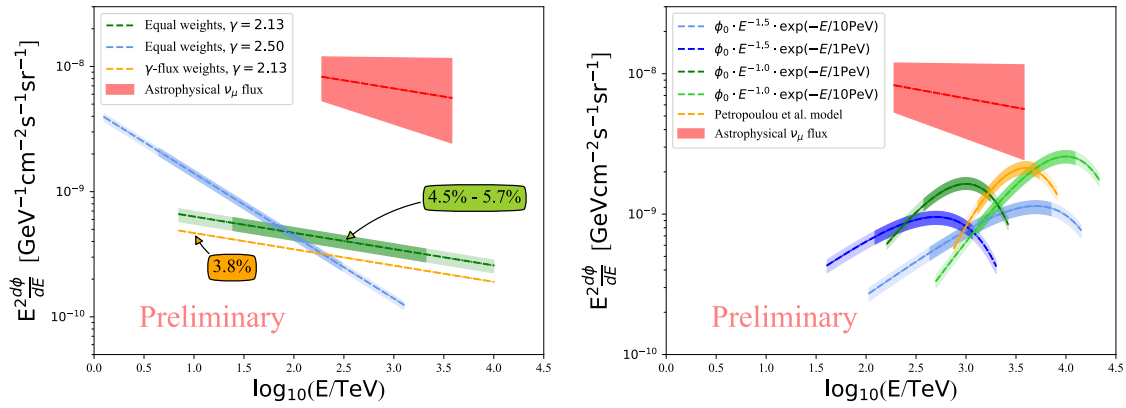


Figure 2: 90 % C.L. upper limits of the 2FHL HBL catalog using different assumptions on the spectral shape of the blazars. All fluxes are given in intensity units. The dark-shaded bands illustrate the  $1\sigma$  energy regions where IceCube has the highest exclusion power for the particular model, the light shaded bands the 90 % region. The best fit to the astrophysical diffuse muon neutrino flux  $\phi_{\nu_\mu + \bar{\nu}_\mu}^{\text{astro}}$  from [4] including the 68 % C.L. contours is displayed in red. **Left:** Equal and gamma-ray flux weighted limits for single unbroken power laws. The numbers illustrate the maximal contribution to the diffuse  $\nu_\mu$ -flux. **Right:** Limits for single power laws with different energy cut offs and the limit using the theoretical model from [14].

at least  $\sim 10$  more years of data from the current IceCube detector to get a  $5\sigma$  discovery. Hence in the future, the analysis can also be extended to larger HBL samples, such as 3FHL catalog, being an extension of the 2FHL catalog.

## References

- [1] **IceCube** Collaboration, M. Aartsen et al., *Science* **342** (2013) 1242856.
- [2] **IceCube** Collaboration, M. Aartsen et al., *JINST* **12** (2017) P03012.
- [3] **IceCube** Collaboration, M. Aartsen et al., *Astrophys. J.* **835** (2017) 2.
- [4] **IceCube** Collaboration, M. Aartsen et al., *Astrophys. J.* **833** (2016) 1.
- [5] C. Urry and P. Padovani, *Publ. Astron. Soc. Pac.* **107** (1995).
- [6] P. Padovani et al., *Astrophys. J.* **444** (1995).
- [7] P. Padovani et al., *Mon. Not. Roy. Astron. Soc.* **443** (2014) 1.
- [8] P. Padovani et al., *Mon. Not. Roy. Astron. Soc.* **457** (2016) 4.
- [9] B. Arsioli et al., *Astron. Astrophys.* **579** (2015) A34.
- [10] B. Arsioli et al., *Astron. Astrophys.* **598** (2017) A17.
- [11] Fermi-LAT Collaboration, M. Ackermann et al., *Astrophys. J. Suppl.* **222** (2016) 1.
- [12] Fermi-LAT Collaboration, M. Ackermann et al., *Astrophys. J.* **810** (2015) 1.
- [13] Kelner, S. R. et al., *Phys. Rev.* **D78** (2008) .
- [14] M. Petropoulou et al., *Mon. Not. Roy. Astron. Soc.* **448** (2015) 3, 2412-2429.

## IceCube Search for Neutrinos from 1ES 1959+650: Completing the Picture

---

### The IceCube<sup>1</sup>, FACT<sup>2</sup> and MAGIC<sup>3</sup> Collaborations

<sup>1</sup> [http://icecube.wisc.edu/collaboration/authors/icrc17\\_icecube](http://icecube.wisc.edu/collaboration/authors/icrc17_icecube)

<sup>2</sup> [http://fact-project.org/collaboration/icrc2017\\_authorlist.html](http://fact-project.org/collaboration/icrc2017_authorlist.html)

*E-mail:* [thomas.kintscher@desy.de](mailto:thomas.kintscher@desy.de), [kai.krings@tum.de](mailto:kai.krings@tum.de),  
[dorner@astro.uni-wuerzburg.de](mailto:dorner@astro.uni-wuerzburg.de),  
[wrijupan.bhattacharyya@desy.de](mailto:wrijupan.bhattacharyya@desy.de), [takhsm@icrr.u-tokyo.ac.jp](mailto:takhsm@icrr.u-tokyo.ac.jp)

The IceCube neutrino observatory is a 1 km<sup>3</sup> detector deployed in the ice at the South Pole. While it has observed an astrophysical flux of neutrinos, individual sources have yet to be identified and the high-peaked BL Lac object 1ES 1959+650 is an intriguing candidate. It exhibited an “orphan flare” in 2002: a TeV gamma ray flare without a simultaneous X-ray flare, behavior that is hard to accommodate in leptonic synchrotron self-compton models. This suggests that it is a potential site of hadronic acceleration and thus a prime source candidate for neutrinos. A recently observed increase in gamma ray activity from 1ES 1959+650 between May and July of 2016 has provided a new opportunity, prompting a dedicated search in IceCube data for neutrinos correlated with the flaring states during this period. We present results based on two model-independent approaches which look only for an excess of neutrinos from the source, as well as a more targeted search for a direct time correlation between neutrino events observed by IceCube and gamma ray emission observed with the FACT and MAGIC telescopes.

**Corresponding authors:** Thomas Kintscher<sup>\*1a</sup>, Kai Krings<sup>1b</sup>, Daniela Dorner<sup>23c</sup>, Wrijupan Bhattacharyya<sup>3a</sup>, Mitsunari Takahashi<sup>3d</sup>

<sup>a</sup> *Deutsches Elektronen-Synchrotron (DESY), 15738 Zeuthen, Germany*

<sup>b</sup> *Technische Universität München, 85748 Garching, Germany*

<sup>c</sup> *Universität Würzburg, 97074 Würzburg, Germany*

<sup>d</sup> *Institute for Cosmic Ray Research, University of Tokyo, Japan*

*35th International Cosmic Ray Conference – ICRC2017 –  
10-20 July, 2017  
Bexco, Busan, Korea*

---

\*Speaker.

## 1. Introduction

Ever since the discovery of cosmic rays more than 100 years ago, the field of astroparticle physics strives to locate and understand their sources. In the pursuit of this goal, this work focuses on two cosmic messengers: gamma rays and neutrinos. The former are subject to intergalactic absorption effects [1], while the latter may also be detected from sources at high redshifts. Both particles' uncharged nature leaves them undeflected by (inter-)galactic magnetic fields, enabling observers to point back at their origin and provide a complementary picture of the sources.

1ES 1959+650, at a redshift of  $z = 0.047$  [2], belongs to the class of high-frequency peaked BL Lac objects (HBL), i.e. active galactic nuclei with jets pointed towards the observer and a spectral energy distribution characterized by two broad humps in the UV–X-ray and GeV–TeV energy ranges without emission lines. It was established as a very high energy (VHE,  $E > 100$  GeV) gamma ray emitter [3, 4]. The most notable VHE flaring episode was recorded on June 4th, 2002 by Whipple, when a gamma ray flare without a simultaneous increase in X-ray emission was detected from this source [3, 5, 6]. Several emission models were proposed to describe this “orphan” gamma ray flare. A simple Synchrotron Self Compton (SSC) one [5] was found to underpredict the observed radio and optical fluxes. Alternatively, hadronic models, such as the “mirror model” [7] were also developed for this event and predict a correlated neutrino flux.

A search for neutrino events correlated with the VHE flare was performed on the data from AMANDA [8, 9]. Three neutrino events were found to arrive during the flaring episode, including one simultaneous with the peak of the “orphan” flare. Yet, no reliable estimate of the significance could be determined as the analysis was not performed in a blind fashion.

Since 2002 1ES1959+650 has remained in a quiescent state in gamma rays [10, 11]. Also, no signal was detected from this source on top of the background in a dedicated search on 7 years of IceCube data [12].

More recently, increased gamma ray activity of 1ES 1959+650 with gamma ray flux levels of the order of the 2002 flare, has been observed between April and July 2016 [13]. This new flare provides another, rare opportunity to investigate a direct connection between the neutrino and VHE gamma ray emission in 1ES 1959+650.

## 2. Observatories

**IceCube** is a neutrino observatory at the geographic South Pole [14] consisting of over 5000 digital optical modules (DOMs) buried at depths between 1450 and 2450 meters in the Antarctic glacier. Cherenkov radiation from charged particles, produced in interactions of neutrinos in the ice or the nearby bedrock, is detected and used to reconstruct the direction, energy and to some extent the flavor of the neutrinos.

Of particular interest to this analysis are charged-current interactions of muon neutrinos. The resulting muon traverses the ice and its track-like signature allows for a reconstruction of the direction. The source is located in the Northern sky, allowing for an analysis with a selection of upgoing tracks in the detector, which significantly reduces the the background from atmospheric muons.

Several available event selection methods have been compared. Eventually, the one described in [15] was chosen as it provides the best discovery potential at this particular declination. It

relies on boosted decision trees (BDTs) to suppress the backgrounds from both misreconstructed downgoing muons as well as electron neutrino and neutral-current muon neutrino interactions.

**FACT**, the First G-APD Cherenkov Telescope, located next to the two MAGIC telescopes at 2200 m a.s.l. on the Canary Island of La Palma, is equipped with a camera using novel silicon photomultipliers (SiPM; also Geiger-mode Avalanche Photo Diodes, G-APDs) providing an excellent performance [16]. As SiPMs do not degrade when exposed to bright light, the duty cycle of the instrument is maximized and the gaps in the light curves around full moon are minimized. Monitoring blazars at TeV energies, FACT provides an unprecedented dense and unbiased data sample [17], which is ideally suited to constrain the neutrino flux from gamma ray light curves.

**MAGIC** is a system of two 17 m Cherenkov telescopes, combining a large mirror area, allowing for observations of gamma rays with energies as low as 50 GeV, with the stereoscopic technique providing strong hadronic background rejection. The integral sensitivity achieved in the energy range  $> 220$  GeV is at the level of 0.66% of the Crab Nebula flux in 50 h of observations, when considering point-like sources with Crab Nebula-like spectrum [18]. The angular resolution at those energies is  $\leq 0.07^\circ$ . As detailed in [19], MAGIC can also observe under moonlight conditions. The MAGIC telescopes performed the observations of 1ES 1959+650 in April–July during moonless nights and moon time, with zenith angles in the range of 35 to 52 degrees. The collected data were analyzed in the MARS analysis framework by means of the standard stereoscopic analysis routines [20].

### 3. Analysis Methods

The IceCube analyses are based on an unbinned maximum-likelihood method [21], considering each event's individual properties, such as the direction and its uncertainty, an energy proxy, and the arrival time of the neutrino. The exact formulation of the likelihood varies between the three analyses, and will be described in the following sections.

#### 3.1 Time-Integrated Likelihood Analysis with IceCube

This analysis makes the least amount of assumptions about the time structure of a potential signal. As the total time window is short compared to previous IceCube point source searches [12], the formulation of the test statistic  $\Lambda$  is modified with respect to the original one from [21] assuming the average background event rate  $\langle n_b \rangle$  is known: [22]:

$$\Lambda(n_s, \gamma) = -n_s + \sum_i^{\text{events}} \log \left[ \frac{n_s}{\langle n_b \rangle} \frac{S_i(\gamma)}{B_i} \right] \quad \text{with} \quad \frac{S_i}{B_i} = \frac{\mathcal{S}_{\text{sig}}(\alpha_i, \delta_i, \sigma_i) \mathcal{E}_{\text{sig}}(E_i, \delta_i | \gamma)}{\mathcal{S}_{\text{bkg}}(\delta_i) \mathcal{E}_{\text{bkg}}(E_i, \delta_i)}. \quad (3.1)$$

The amount of signal  $n_s$  and its spectral index  $\gamma$  are free parameters in the fit. The probability densities  $S_i$  and  $B_i$  for an event to belong to the signal or background, respectively, consider the spatial and energy information, where  $\alpha$  and  $\delta$  are the reconstructed right ascension and declination,  $\sigma$  is the estimated, circularized uncertainty on the direction, and  $E$  is a proxy for the muon energy at the detector.

The spatial term  $\mathcal{S}_{\text{sig}}$  assumes a two-dimensional Gaussian distribution of the signal with a width of  $\sigma$  around the fixed location of the source, compared to a uniform distribution  $\mathcal{S}_{\text{bkg}}$  of

background events. The energy term  $\mathcal{E}_{\text{sig}}$  considers the probability for a certain observation  $E$  given a spectral index of  $\gamma$  of the signal versus the energy spectrum of the atmospheric background  $\mathcal{E}_{\text{bkg}}$ . In order to minimize the influence of a potential signal, the background event rate  $\langle n_b \rangle$  and its energy spectrum are derived using the off-time data recorded between May 2015 and April 2016, i.e. before the flaring activity of the source.

Eventually, the test statistic is maximized with respect to  $n_s$  and  $\gamma$ . The spectral index is bound to  $\gamma \in [-4, -1]$ , and the signal strength must be non-negative ( $n_s \geq 0$ ). Thus the test statistic can take values of  $\Lambda \geq 0$ .

The distribution of the test statistic in the absence of a signal is obtained from trials on off-time data, scrambled in right ascension: The arrival times of the neutrinos are shuffled and the transformation from detector coordinates into equatorial coordinates is repeated. While any potential spatial clustering is destroyed, detector effects and correlations between the other variables used in the analysis are retained.

### 3.2 Time-Clustering Analysis with IceCube

In this approach, it is assumed that a potential burst of neutrinos is clustered in time, superimposed on a uniform distribution of background events.

The so-called “time-clustering” algorithm defines subsets of events (clusters) in time and maximizes the likelihood for each subset. Afterwards, the cluster with the highest test statistic is chosen and its significance is evaluated.

As the number of possible clusters grows rapidly, it is useful to limit the trials to the promising ones, which contain events close to the source or of very energetic nature. Therefore, the events fulfilling  $S_i/B_i > 1$  mark the boundaries of clusters, which are tested using the likelihood formulation from [21]

$$\mathcal{L} = \prod_{i=1}^N \left[ \frac{n_s}{N} S_i + \left( 1 - \frac{n_s}{N} \right) B_i \right], \quad (3.2)$$

with  $N$  being the number of events in the candidate cluster. Comparing the sensitivity of this analysis to that of the aforementioned time-integrated analysis, only time windows no longer than 21 days ( $T_{\text{max}}$ ) need to be tested.

The likelihood maximization yields the best fit values of  $\hat{n}_s$  and  $\hat{\gamma}$ . More short time windows than long time windows can be defined, and a bias towards short time windows needs to be avoided. A marginalization term [23] in the test statistic corrects for the number of trials with a duration  $T_{\text{sig}}$ :

$$\Lambda = -2 \log \left( \frac{\mathcal{L}(\hat{n}_s, \hat{\gamma}) T_{\text{sig}}}{\mathcal{L}(0, -) T_{\text{max}}} \right). \quad (3.3)$$

As before, the background distribution of the test statistic is derived from trials on scrambled off-time data. An example is shown in Fig. 1.

### 3.3 Correlation between Neutrinos and Gamma Rays

Whereas the previous analyses have focused solely on neutrinos, the third analysis combines the data from the IceCube experiment with the observations of the FACT and MAGIC telescopes. Once the flaring state of the source became evident, it has been observed by the MAGIC telescopes

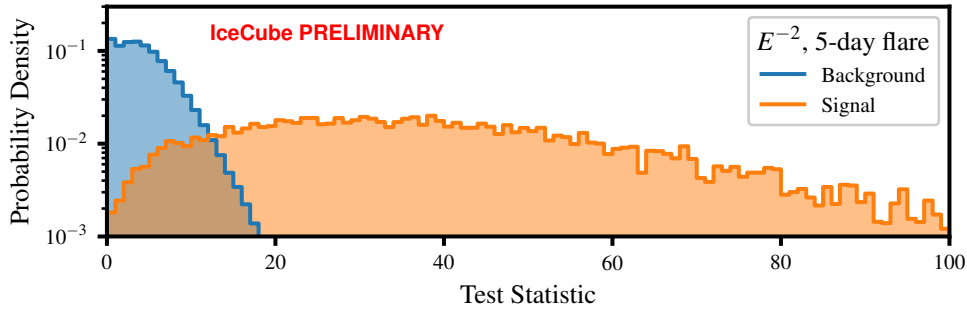


**Figure 1:** Test statistic ( $\Lambda$ ) distribution of the time-clustering search. The background distribution (blue) is derived from scrambled, off-time data. The distribution shifts (yellow) as simulated signal events are injected, here drawn with a Poisson mean of 6.02 events in 5 days from an  $E^{-2}$  spectrum.

on a regular basis. For 45 out of the 89 nights considered here, the telescopes were able to provide precise measurements of the flux in VHE gamma rays [13]. There are gaps in between the observations, which are largely caused by poor visibility conditions or strong moonlight. Due to the technical design of the FACT camera, it is able to operate in conditions of ambient light and can thus provide measurements for 80 nights [17], adding 36 (MAGIC has one night not included in FACT data) nights of coverage next to the MAGIC observations. Thus, the data from both experiments has been combined to fully utilize their respective strengths and obtain the largest possible coverage of the source behavior over time.

This analysis tests for a direct correlation between the gamma ray and neutrino emission by extending Eqn. 3.1 with an additional PDF in the time domain. In order to construct this time PDF, the telescopes have provided measurements of the integrated gamma ray flux above 750 GeV. If on a given night the source has only been observed by one instrument, that measurement is used. On nights where both instruments did provide data, the measured fluxes have been averaged, weighted by their respective errors. As the observations are only possible for a few hours at night-time, the lightcurve has been binned in one day intervals lasting from noon on one day to noon on the next day. This approach strives to balance a conservative extrapolation of the gamma ray flux with a possible time delay between the arrival of neutrinos and gamma rays. In case that no observations were taken on a given night, the surrounding bin is excluded from the analysis. On such nights, no statements on the activity of the source can be made in good conscience, as the strong flaring typically occurs on the timescale of a day. In any case, both a significant flare of neutrinos on an excluded day, as well as a large time delay between the emission of gamma rays and multiple neutrinos would be covered by the two previous analyses, which rely only on the neutrino data.

Figure 2 compares the discovery potential for the three analyses. In general, if single flares in neutrinos with a duration of less than 30 days could be resolved, the time-clustering analysis would be the most sensitive one, whereas for longer time-scales the time-integrated test is more sensitive. The correlation test is very sensitive, if the neutrinos were to follow the gamma ray light curve. Thus, the analyses are complementary as they test different time scales and emission scenarios.

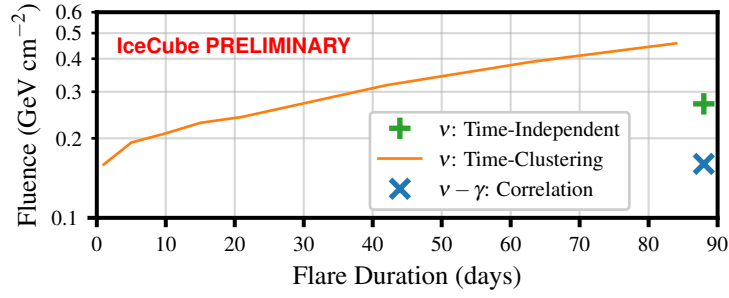


**Figure 2:** Discovery potential of the three analyses. The time-integrated test is independent of the arrival times of the neutrinos. The sensitivity of the time-clustering method depends on the length of the most-significant flare. The time-correlation test assumes a signal distributed according to the gamma ray lightcurve, yet it is shown in this plot for comparison.

#### 4. Results

The analyses have been applied to the 89-day time window from April 29th to July 26th, 2016. Figure 3 shows the location of events, which might contribute to the likelihood analyses due to their proximity to the source. Three events are spatially compatible with the location of 1ES 1959+650 within their  $1\sigma$  error circles, yet they are poorly localized with an uncertainty larger than two degrees.

As the majority of events is well compatible with the background expectation, a test statistic of zero was obtained from the time-integrated test at the position of the source. The right panel of Fig. 3 shows a scan of the test statistic in the vicinity of the source. No spatial clustering is visible near the source.

Figure 4 shows the arrival times and energy proxy of the neutrinos (less than  $5\sigma$  away from the source) as a function of time. The time-clustering test is bound to decide on one most signal-like cluster. It selected a time window of 3.3 hours around the most-energetic event in the sample. There are two events in this time window and the fit results yield a signal strength of  $n_s = 2$  and a spectral index of  $\gamma = -1.4$ . Such an outcome is expected from background with a  $p$ -value of 37%.

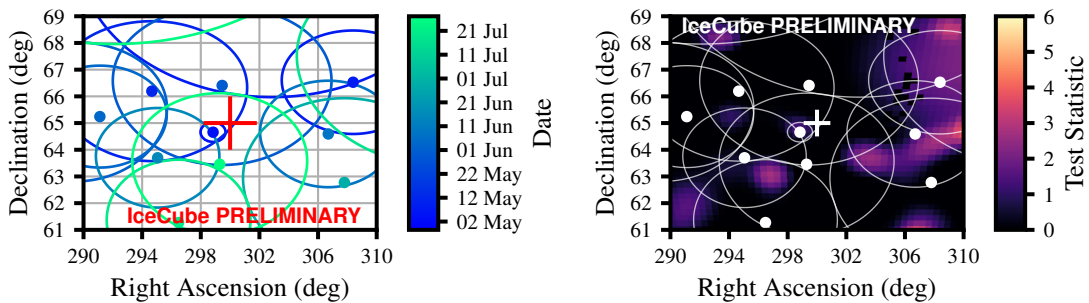


**Figure 3:** Skymap of the events closer than  $2\sigma$  to the source in equatorial coordinates (J2000). The event locations are shown with a dot; and the circles indicate the  $1\sigma$  uncertainty. Left: The color scale indicates the arrival time. Right: A scan of the test statistic of the time-integrated analysis is shown in the background.

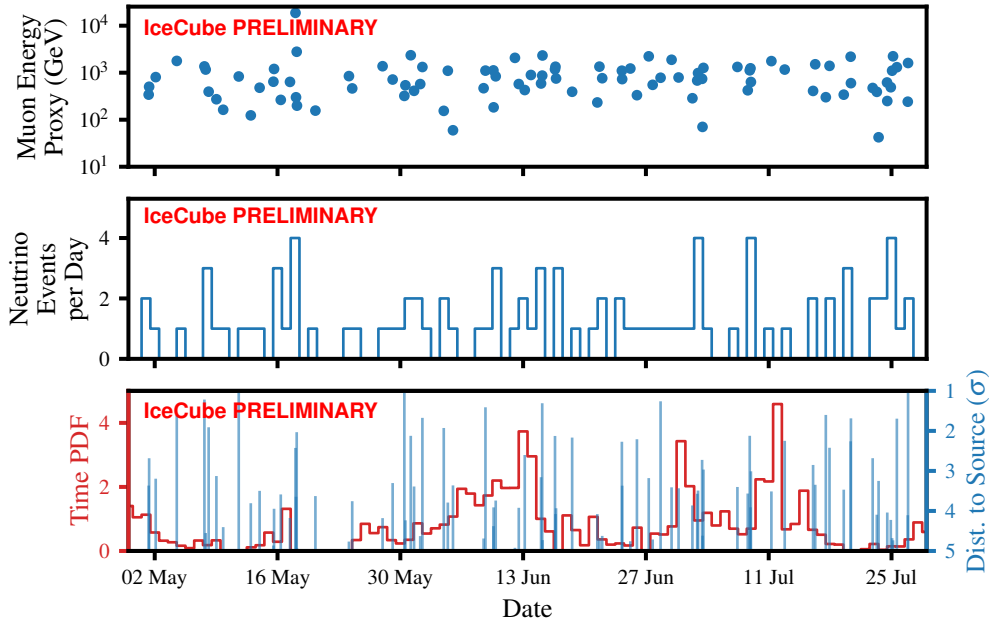


**Figure 4:** Properties of events compatible with the source location within  $5\sigma$  of their estimated uncertainty, as a function of time. Each event’s proxy for the muon energy at the detector [24] is shown in the top plot. The center plot and the red line in the bottom plot show the number of neutrinos and the state in gamma rays (Sec. 3.3), respectively, using the same binning. In the lower plot, the neutrinos’ arrival time and distance to the source is overlaid. The most-significant cluster consists of two events observed on May 18th, however it is well compatible with the background expectation.

Additionally, the state of the source in gamma rays is unknown; no observations are available for this particular day.

Finally, due to the absence of signal-like events the final neutrino–gamma correlation test also yields a test statistic of zero and is therefore most-compatible with background.

## 5. Summary

The high-peaked BL Lac object 1ES 1959+650 exhibited major flares in VHE gamma rays in the spring of 2016. A search for neutrinos coincident with the flares has been performed. No significant excess has been observed, neither by integrating over the whole flaring episode, nor by testing for clusters on shorter time scales. Also, no indication for a neutrino flux correlated with the gamma ray flux was found. During the previous episode of strong gamma ray flares from this source in 2002, a neutrino was observed arriving from the location of the source within a few hours of the gamma ray observations [8]. However, back then it was found to be an orphan flare, while for the time considered here, the available X-ray data [25] do not confirm an orphan behavior<sup>1</sup>.

For both the 2002 flare and the recent one, several models attempt to predict possible neutrino fluxes in the light of strong VHE gamma-ray flares: Yet, even with an IceCube-sized detector, a stacking of 40 hours of similar, known orphan flares is required for a detection in the mirror

<sup>1</sup>It cannot be excluded during the highest gamma ray emission (June 13th) due to lack of concurrent X-ray data.

model [7, 26]. Similarly, the recent spine-sheath model [27] predicts only 0.04 additional neutrino events on the days of the brightest flares, where the gamma ray flux levels reach 10-15 times that of the low state [11].

Further observations in all wavelengths of this and similar objects are necessary to properly constrain acceleration scenarios. In the context of IceCube's realtime alert program, continued monitoring for potential neutrinos from this source and subsequent, timely alerts to follow-up partner observatories [28] may help to create a larger dataset of simultaneous multi-messenger observations in the future.

## References

- [1] F. W. Stecker, O. C. De Jager, and M. H. Salamon, *Astrophys. J.* **473** (1996) L75–L78.
- [2] J. F. Schachter et al., *Astrophys. J.* **412** (1993) 541–549.
- [3] VERITAS Collaboration, J. Holder et al., *Astrophys. J.* **583** (2003) L9–L12.
- [4] T. Nishiyama, *ICRC1999* **3** 370.
- [5] H. Krawczynski et al., *Astrophys. J.* **601** (2004) 151–164.
- [6] VERITAS Collaboration, M. K. Daniel et al., *Astrophys. J.* **621** (2005) 181.
- [7] M. Böttcher, *Astrophys. J.* **621** (2005) 176–180. [Erratum: *Astrophys. J.* 641,1233(2006)].
- [8] IceCube Collaboration, M. Ackermann et al., *ICRC2005* **5** 1.
- [9] F. Halzen and D. Hooper, *Astropart. Phys.* **23** (2005) 537–542.
- [10] VERITAS Collaboration, E. Aliu et al., *Astrophys. J.* **775** (2013) 3.
- [11] MAGIC Collaboration, K. Satalecka et al., *AIP Conf. Proc.* **1112** (2009) 223–232.
- [12] IceCube Collaboration, M. G. Aartsen et al., *Astrophys. J.* **835** (2017) 151.
- [13] *The Astronomer's Telegram* **9010, 9139, 9148, 9203, 9239** (2016).
- [14] IceCube Collaboration, M. G. Aartsen et al., *JINST* **12** (2017) P03012.
- [15] IceCube Collaboration, M. G. Aartsen et al., *Astrophys. J.* **833** (2016) 3.
- [16] A. Biland et al., *JINST* **9** (2014) P10012.
- [17] FACT Collaboration, D. Dorner, *POS (ICRC2017)* 868 (these proceedings).
- [18] J. Aleksić et al., *Astropart. Phys.* **72** (2016) 76–94.
- [19] MAGIC Collaboration, M. L. Ahnen et al., [arXiv:1704.00906](https://arxiv.org/abs/1704.00906).
- [20] MAGIC Collaboration, R. Zanin et al., *Braz. J. Phys.* **ICRC2013** 773.
- [21] J. Braun et al., *Astropart. Phys.* **29** (2008) 299–305.
- [22] IceCube Collaboration, M. G. Aartsen et al., *Astrophys. J.* **805** (2015) L5.
- [23] R. Abbasi et al., *Astrophys. J.* **744** (2012) 1.
- [24] IceCube Collaboration, M. G. Aartsen et al., *JINST* **9** (2014) P03009.
- [25] M. C. Stroh and A. D. Falcone, *Astrophys. J. Suppl.* **207** (2013) 28.
- [26] A. Reimer, M. Böttcher, and S. Postnikov, *Astrophys. J.* **630** (2005) 186–190.
- [27] C. Righi, F. Tavecchio, and D. Guetta, *Astron. Astrophys.* **598** (2017) A36.
- [28] IceCube, MAGIC, VERITAS Collaboration, M. G. Aartsen et al., *JINST* **11** (2016) P11009.

## Using all-flavor and all-sky event selections by IceCube to search for neutrino emission from the Galactic plane

---

### The IceCube Collaboration<sup>†</sup>

<sup>†</sup> [http://icecube.wisc.edu/collaboration/authors/icrc17\\_icecube](http://icecube.wisc.edu/collaboration/authors/icrc17_icecube)

E-mail: [kai.krings@icecube.wisc.edu](mailto:kai.krings@icecube.wisc.edu)

The IceCube Neutrino Telescope has observed a diffuse all-flavor astrophysical neutrino flux above 30 TeV. The neutrino flux is currently compatible with an isotropic distribution; no astronomical counterparts have been identified yet. Here, we propose a binned forward-folding likelihood fit of the available neutrino data to search for integrated emission in the Galactic plane. We use two independent neutrino samples, one consisting of all-sky all-flavor events with deposited energies larger than 1 TeV whose interaction vertex is contained in the detector's fiducial volume, the other of up-going muon neutrinos; both samples are integrated over a time period of six years. By performing a joint analysis of through-going and starting events, degeneracies between Galactic and extra-galactic neutrinos can be resolved and uncertainties in the atmospheric neutrino fluxes are better controlled. We present preliminary sensitivities for different models of neutrino emission from the Galactic plane.

**Corresponding authors:** Kai Krings<sup>\*1</sup>

<sup>1</sup> *Physik-Department, Technische Universität München, James-Franck-Str. 1, D-85748 Garching, Germany*

*35th International Cosmic Ray Conference — ICRC2017  
10–20 July, 2017  
Bexco, Busan, Korea*

---

\*Speaker.

## 1. Introduction

IceCube has observed neutrinos of extra-terrestrial origin using two independent detection channels: high-energy cascade and track-like events whose interaction vertices are contained inside the detector's fiducial volume and through-going muon tracks entering the detector from below. Cascade-like events are induced by neutrinos of all flavors: the measured light from the evolving cascade of secondary particles leaves a spherical imprint in the detector due to photon scattering, which challenges the reconstruction of the incoming neutrino's direction; current algorithms achieve a median angular resolution of about  $15^\circ$ . On the other hand, track-like events are primarily produced in charge-current muon neutrino interactions and the emitted light along the trajectory of the outgoing muon functions as a lever arm that allows reconstruction of the incoming neutrino detection with an uncertainty of better than  $2^\circ$ . Due to their containment in the detector, the energy resolution of starting events is on the order of 20%; through-going muon tracks in contrast deposit only part of the initial neutrino energy in the detector, which gives a lower limit on the neutrino energy itself. Starting cascade and track-like events are selected from all directions based on a veto-driven event selection, while through-going muon tracks are only selected from the northern sky; the latter are free of background from atmospheric muons, after application of all selection criteria; see section 4.

The two independent measurements of the astrophysical neutrino flux are in agreement above 200 TeV with a single isotropic power-law flux, which has a spectral index close to 2 [1]. Our current interpretation is that this part of the neutrino energy spectrum is of extra-galactic origin. Assuming the power-law to be unbroken over the entire energy range, the individual best-fit spectral shapes are in tension at the  $2\sigma$  level [1]. We will follow the assumption that IceCube is measuring the superposition of a hard extra-galactic neutrino flux and a softer second astrophysical flux component of Galactic origin, which motivates the search presented here for an integrated neutrino flux along the Galactic plane, using a binned forward-folding likelihood template fit.

Galactic neutrinos are expected from the decay of light mesons produced in interactions of cosmic-rays with the matter in the Galaxy or they could be produced in the direct vicinity of potential Galactic cosmic-ray accelerators. A search for a Galactic neutrino flux has already been performed using 7 years of through-going muon track data only [2]. Because of the good angular resolution, through-going muon tracks can easily probe the northern sky for an anisotropy in the arrival direction of neutrinos due to the Galactic plane. Moreover, they give a precise measurement of the extra-galactic part of the astrophysical neutrino flux at higher energies and constrain the conventional and prompt (not observed yet) atmospheric neutrino fluxes at lower energies. A discovery with this detection channel alone is however not feasible due to the limited sky coverage of the analysis and the overwhelming background of atmospheric neutrinos below 100 TeV. That said, a joint analysis with the starting event selection is the obvious next step, taking advantage of the positive features of both detection channels: good angular resolution and large statistics in through-going muon tracks to constrain the extra-galactic and atmospheric neutrino fluxes, and good energy resolution, full-sky coverage, and low energy threshold of starting events to disentangle Galactic and extra-galactic neutrino flux.

## 2. Analysis method

The binned forward-folding likelihood template fit is based on a simple Poisson likelihood<sup>1</sup>,

$$-\log(\mathcal{L}) = \sum_i \mu_i(\vec{\theta}, \vec{\xi}) - d_i \log(\mu_i(\vec{\theta}, \vec{\xi})) + \dots + \sum_k f(\xi_k), \quad (2.1)$$

which is summed over the bins  $i$  of the binned experimental data  $d_i$  and the sum  $\mu_i$  of all binned Monte Carlo (MC) flux templates listed in Table 1. Each template describes the number of lepton

Lepton flux template	Lepton flux model
Atmospheric muons	GaisserH4a [3]
Conventional atmospheric neutrinos	HKKM06 [4]
Prompt atmospheric neutrinos	ERS [5]
Extra-galactic neutrinos	isotropic, unbroken power-law
Galactic plane neutrinos	<i>Fermi</i> -LAT, KRA- $\gamma$

**Table 1:** Lepton flux templates that enter the forward-folding likelihood template fit. For more details about the Galactic plane models, see section 3. The conventional atmospheric neutrino flux model is re-weighted with respect to the cosmic-ray knee.

events expected from the modeled lepton fluxes of atmospheric or astrophysical origin that describe the experimental data. The log-likelihood function is minimized numerically with respect to the physics parameters  $\vec{\theta}$  and nuisance parameters  $\vec{\xi}$  upon which the MC templates depend. The physics parameters we are interested in are the Galactic and extra-galactic flux normalizations and spectral indices. The nuisance parameters include all other flux normalizations, the primary cosmic-ray (CR) spectral index relative to the model prediction, which enters both atmospheric neutrino flux components, and the relative contribution of neutrinos from kaon decays to the conventional atmospheric neutrino flux. The primary CR spectral index and the kaon fraction affect the energy spectrum of atmospheric neutrinos; additionally, the kaon fraction changes the ratio of electron to muon neutrinos and thus the ratio of cascade to track-like events. They are both implemented in a way that they do not change the total numbers of expected conventional and prompt neutrino events in order to avoid degeneracies with the atmospheric flux normalizations. Gaussian penalty terms,

$$f(\xi) = \frac{(\xi - \xi_0)^2}{2\sigma_\xi^2}, \quad (2.2)$$

are incorporated in the log-likelihood function to arbitrarily increase the negative log-likelihood when the nuisance parameter  $\xi$  differs too much from its mean expectation  $\xi_0$  relative to its uncertainty  $\sigma_\xi$ . For the primary CR spectral index and the kaon fraction, we assume uncertainties of 0.05 and 10 %, respectively; all other nuisance parameters are completely free to float. In a later stage, we will also include detector-related nuisance parameters like the optical efficiency of the digital optical modules and the optical properties of the South Pole ice.

Experimental data and MC flux templates are binned in estimated energy, declination, and right ascension. Starting events are also separated into cascade and track-like subsets.

<sup>1</sup>Constant terms are not shown.

### 3. Galactic plane models

In this analysis, we focus on the predicted diffuse neutrino flux from the decay of light mesons produced in interactions of cosmic rays with the matter in the Galaxy. Two models are taken into account that are described in the following.

#### 3.1 *Fermi*-LAT model

This is our more generic benchmark model based on *Fermi*-LAT's observation of diffuse gamma-ray emission from the Galaxy [6]. We take the  $\pi^0$ -component of the fit to the gamma-ray data as a tracer for the intensity of neutrino emission along the Galactic plane and normalize it to construct a spatial probability density function for our neutrino flux model. For the energy part, we assume an unbroken power-law. Figure 1 shows the expected differential neutrino flux at 10 TeV for an spectral index of 2.5.

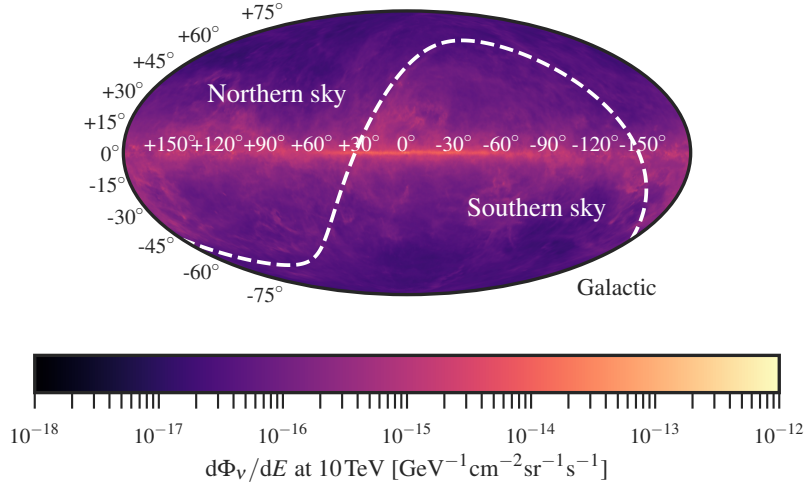


**Figure 1:** *Fermi*-LAT model for a spectral index of 2.5: differential all-flavor neutrino flux in Galactic coordinates, assuming a neutrino flavor ratio of 1:1:1. The model is normalized with respect to the KRA- $\gamma$  model.

#### 3.2 KRA- $\gamma$ model

This model is based on the work of Gaggero et al. and was developed to describe the large gamma-ray flux observed by Milagro at TeV energies and the measured *Fermi*-LAT gamma-ray flux from the inner Galaxy that is systematically underestimated by the conventional diffuse gamma-ray emission models [7]. The predicted differential neutrino flux defines our best-case scenario. As shown in Fig. 2, the expected neutrino flux is more concentrated towards the inner Galaxy and the Galactic Center than the benchmark *Fermi*-LAT model. The KRA- $\gamma$  model incorporates the observed hardening of the cosmic-ray spectral slope above 250 GeV per nucleon, which leads to the neutrino spectral slope presented in Fig. 5.

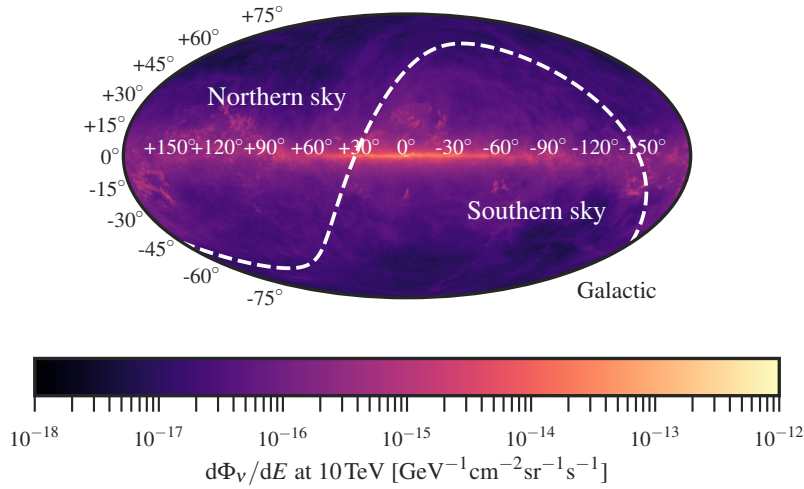


**Figure 2:** KRA- $\gamma$  model for an exponential high-energy cosmic-ray cutoff at 50 PeV per nucleon: differential all-flavor neutrino flux in Galactic coordinates, assuming a neutrino flavor ratio of 1:1:1.

#### 4. IceCube event selections

As motivated in section 1, two types of event topologies will be used in this analysis: all-sky and all-flavor starting events and through-going muon tracks originating from the northern sky. Both samples are integrated over a livetime of 6 years, starting from the 2010 detector run in its 79 string configuration.

##### 4.1 Starting events

The selection of cascade and track-like events starting inside the detector described in [8] is the updated version of the one published in [9]. It is completely based on straight cuts, using the outer layers of IceCube as an active veto against incoming atmospheric muons. In comparison to the high-energy starting event selection, which is a subsample of this selection, the low-energy threshold is lowered down to about 1–10 TeV. The muon veto acts also as a veto against atmospheric neutrinos that accompany the incoming muon. We differentiate between correlated and uncorrelated veto where muon and neutrino either do or do not originate from the same interaction vertex in the atmospheric air shower. A refined estimation of the veto probability is still under study; at this stage, we are using the parametrization obtained in [10] with veto threshold energies for both conventional and prompt atmospheric neutrinos of 100 and 1250 GeV below and above a total deposited charge in the detector of 6000 photoelectrons, respectively.

##### 4.2 Through-going muon tracks

Well-reconstructed through-going muon tracks are selected based on *Boosted Decision Trees*, as described in [11]; the background of mis-reconstructed atmospheric muons is efficiently removed and a neutrino purity of 99.7% is achieved. The experimental data, which was taken between 2008 and 2014, consists of about 350000 neutrino-induced events; it is dominated by conventional atmospheric neutrinos, but sensitive to neutrinos of astrophysical origin above 200 TeV.

The best-fit isotropic astrophysical neutrino flux per flavor is

$$\frac{d\Phi_{\nu+\bar{\nu}}}{dE_\nu} = 0.9_{-0.27}^{+0.30} \times 10^{-18} \text{ GeV}^{-1} \text{ cm}^{-2} \text{ s}^{-1} \text{ sr}^{-1} \left( \frac{E_\nu}{100 \text{ TeV}} \right)^{-2.13 \pm 0.13}, \quad (4.1)$$

and no prompt atmospheric neutrinos were observed, yielding an upper limit of 1.06 times the flux prediction by Enberg et al. These results are used as the seed values for the extra-galactic and prompt atmospheric neutrino flux fit components in our analysis and as the input for the calculation of sensitivities and discovery potentials.

## 5. Sensitivities and discovery potentials

In the following we will focus only on starting events; through-going muon tracks are not included in the analysis framework yet.

Figure 3 shows the number of expected starting cascade and track-like events of extra-galactic and Galactic origin binned in reconstructed declination and right ascension, assuming the flux in Eq. (4.1) and the KRA- $\gamma$  model, respectively. Reconstruction algorithms dedicated to the individual event topologies are used and the binning corresponds to the one used in the likelihood fit. The bin size has been chosen according to the angular resolution. In total, we expect about 94 events of extra-galactic origin, 36 events of Galactic origin, and twice as many cascade as track-like events in 6 years of data; the latter are mostly up-going. The most Galactic neutrinos are expected in the bins containing the Galactic center.

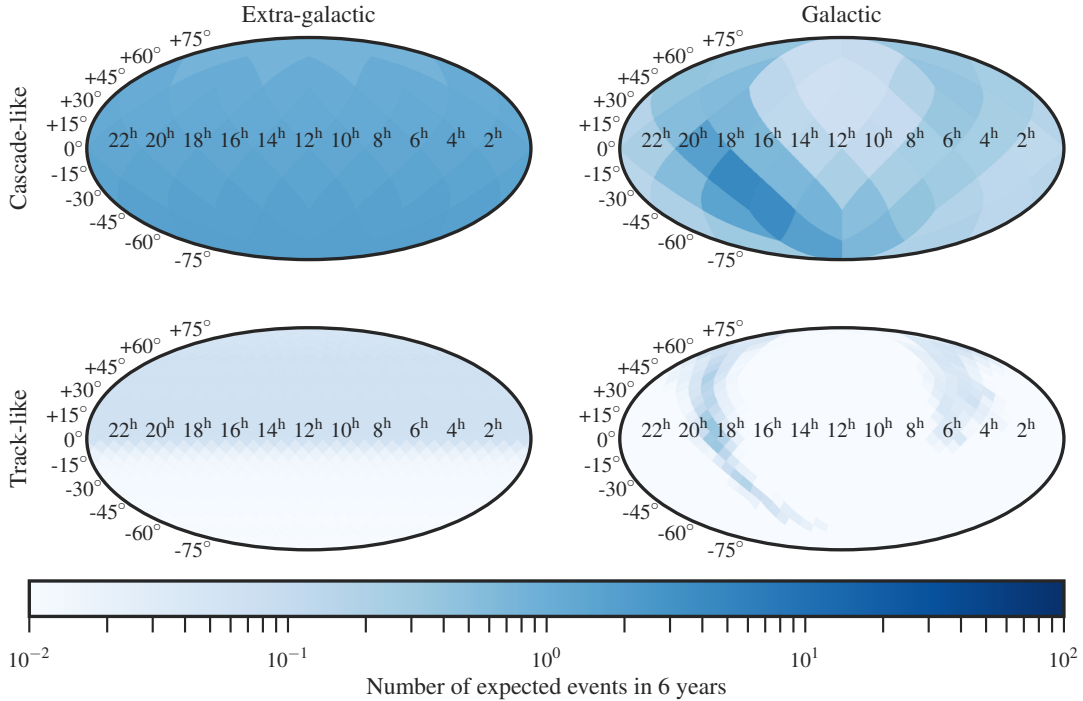


**Figure 3:** Expectation for extra-galactic and Galactic (KRA- $\gamma$ ) neutrinos in equatorial coordinates. The pixels have a resolution of about 30° and 7° for starting cascade and track-like events, respectively.

Taking the negative log-likelihood function (2.1), we define the test statistic

$$t = -2 \times \log \left( \frac{\mathcal{L}(\hat{c}_{\text{GP}}, \hat{\gamma}_{\text{GP}}, \dots)}{\mathcal{L}(c_{\text{GP}} = 0, \dots)} \right) \quad (5.1)$$

in order to test the extra-galactic plus Galactic neutrino flux hypothesis against the single isotropic astrophysical flux hypothesis (null-hypothesis). The test statistic depends on the best-fit Galactic flux normalization  $\hat{c}_{\text{GP}}$ , the spectral index  $\hat{\gamma}_{\text{GP}}$ , and the nuisance parameters described in section 2. For the sensitivity and discovery potential estimation, we assume the null-hypothesis, create an *Asimov dataset* [12], and scan the Galactic flux normalization until we can exclude the null-hypothesis at 90% and  $3\sigma$  confidence level (CL), respectively, using a  $\chi^2$ -distribution with 1 degree of freedom for the background test statistic distribution.

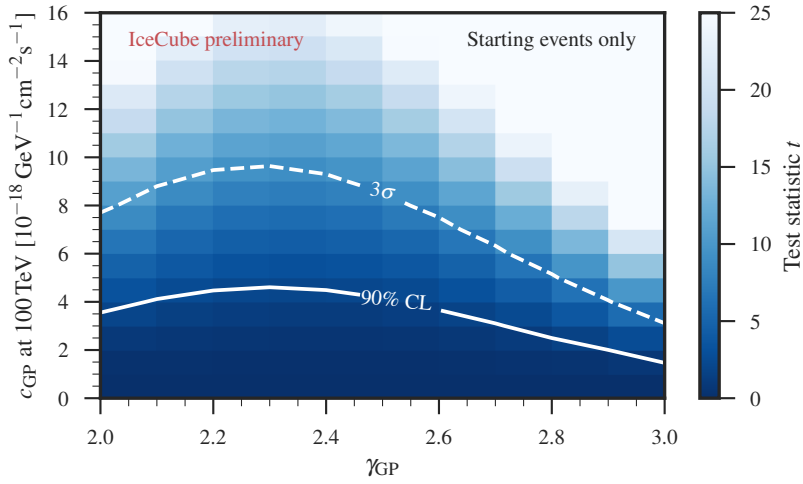


**Figure 4:** Sensitivity and  $3\sigma$  discovery potential differential neutrino flux ( $\nu + \bar{\nu}$ ) per flavor assuming *Fermi*-LAT benchmark models of different Galactic spectral indices; color-coded is the underlying test statistic.

Figure 4 shows the sensitivity and  $3\sigma$  discovery potential for the *Fermi*-LAT benchmark model. At the reference Galactic spectral index of 2.5, the sensitivity on the flux normalization is  $4.2 \times 10^{-18} \text{ GeV}^{-1} \text{ cm}^{-2} \text{ s}^{-1}$ , which is of the same order of magnitude but worse than the values obtained in [2]. We expect the sensitivity to improve significantly once the through-going muon track selection is included in this analysis, because they will help to remove the degeneracy between the fitted extra-galactic and Galactic neutrino fluxes. For the KRA- $\gamma$  model with a high-energy cosmic-ray cutoff of 50 PeV, we obtain 0.7 and 1.6 times the model prediction for sensitivity and  $3\sigma$  discovery potential, respectively; compare Fig. 5. The sensitivity is slightly better than the one presented in [2]. We benefit from the concentration of the KRA- $\gamma$  model towards the inner Galaxy and the Galactic Center; thus, more neutrinos are expected to arrive from the southern sky.

## 6. Conclusions

We presented the first steps towards a combined Galactic plane neutrino search using multiple IceCube event selections that follows the assumption that IceCube is measuring the superposition

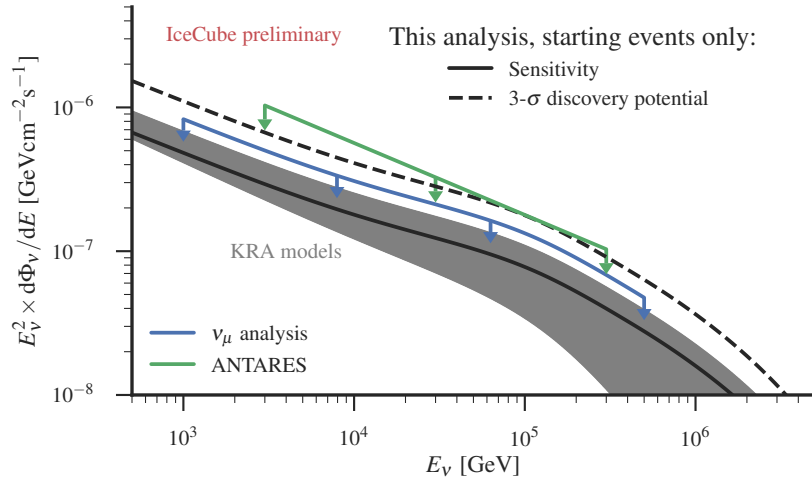


**Figure 5:** Sensitivity and  $3\sigma$  discovery potential differential all-flavor neutrino flux assuming the KRA- $\gamma$  model with a cosmic-ray high-energy cutoff of 50 PeV and a neutrino flavor ratio of 1:1:1, compared to the IceCube [2] and ANTARES [13] upper limits. The gray band shows the envelope of the different realizations of the KRA model presented in [7].

of a hard isotropic neutrino flux of extra-galactic origin and a softer Galactic neutrino flux. Using six years of starting events, we obtain preliminary sensitivities for the *Fermi*-LAT and KRA- $\gamma$  Galactic plane models comparable to the search with through-going muon tracks in the northern sky. The next steps include the incorporation of detector-related systematic uncertainties, including a refined estimation of the atmospheric neutrino self-veto probabilities, and through-going muon tracks into the analysis.

## References

- [1] **IceCube** Collaboration, [PoS \(ICRC2017\) 981](#) (these proceedings).
- [2] **IceCube** Collaboration, [PoS \(ICRC2017\) 1011](#) (these proceedings).
- [3] T. K. Gaisser, *Astropart. Phys.* **35** (2012) 801–806.
- [4] M. Honda et al., *Phys. Rev.* **D83** (2011) 123001.
- [5] R. Enberg et al., *Phys. Rev.* **D78** (2008) 043005.
- [6] **Fermi-LAT** Collaboration, M. Ackermann et al., *Astrophys. J.* **750** (2012) 3.
- [7] D. Gaggero et al., [PoS \(ICRC2015\) 489](#) (2016).
- [8] **IceCube** Collaboration, [PoS \(ICRC2017\) 976](#) (these proceedings).
- [9] **IceCube** Collaboration, M. G. Aartsen et al., *Phys. Rev.* **D91** (2015) 022001.
- [10] T. K. Gaisser et al., *Phys. Rev.* **D90** (2014) 023009.
- [11] **IceCube** Collaboration, M. G. Aartsen et al., *Astrophys. J.* **833** (2016) 3.
- [12] G. Cowan et al., *Eur. Phys. J.* **C71** (2011) 1554.
- [13] **ANTARES** Collaboration, S. Adrian-Martinez et al., *Phys. Lett.* **B760** (2016) 143–148.

## Constraints on diffuse neutrino emission from the Galactic Plane with 7 years of IceCube data

---

**The IceCube Collaboration<sup>†</sup>,**

<sup>†</sup> [http://icecube.wisc.edu/collaboration/authors/icrc17\\_icecube](http://icecube.wisc.edu/collaboration/authors/icrc17_icecube)

E-mail: [analysis@icecube.wisc.edu](mailto:analysis@icecube.wisc.edu)

The origins of high-energy astrophysical neutrinos measured by the IceCube Neutrino Observatory remain a mystery despite extensive searches for multimessenger correlations. In particular, no point sources have been identified so far. However, a likely source for diffuse neutrino emission are cosmic-ray interactions in the Galactic plane. Due to the excellent pointing of their track-like signature, muon-neutrino-induced muons are an excellent channel for measuring spatial correlations. Two methods were developed to test for a spatially extended flux from the entire Galactic plane. Both methods are maximum likelihood fits, one binned and the other unbinned, and using different background estimation methods. We consider two templates for Galactic neutrino emission based primarily on gamma-ray observations and models that cover a wide range of possibilities. We present constraints from seven years of IceCube Neutrino Observatory muon data on the neutrino flux coming from the Galactic plane.

**Corresponding authors:** Christian Haack<sup>\*1</sup>, Jon Dumm<sup>2</sup>

<sup>1</sup>*III. Physikalisches Institut B, RWTH Aachen University*

<sup>2</sup>*Oskar Klein Centre and Dept. of Physics, Stockholm University*

*35th International Cosmic Ray Conference - ICRC2017-  
10-20 July, 2017  
Bexco, Busan, Korea*

---

<sup>\*</sup>Speaker.

## 1. Introduction

The high-energy gamma-ray sky is dominated by diffuse emission from our Galaxy, being the first discovered steady source of astrophysical gamma rays [1]. Cosmic-ray interactions with ambient interstellar gas are the dominant production mechanism for high-energy gamma rays in the plane of the Galaxy via the decay of neutral pions. Diffuse neutrinos from the plane of the Galaxy are expected from these same interactions via decay of charged pions. We perform searches for diffuse neutrino emission based on models constructed from gamma-ray observations.

The IceCube collaboration has reported the detection of a flux of high-energy ( $>10$  TeV) astrophysical neutrinos [2, 3, 4]. In a combined fit to multiple data sets, the flux was characterized from 25 TeV to 2.8 PeV as a power law with spectral index  $2.50 \pm 0.09$  [5]. A recent analysis of only muon neutrinos in the northern sky, with a higher energy threshold of 191 TeV and sensitive up to 8.3 PeV, yields a harder spectral index of  $2.13 \pm 0.13$  [4]. This difference could indicate either anisotropy or a spectral break. Both explanations are consistent with the existence of a relatively soft Galactic contribution dominating in the southern sky in addition to a harder, isotropic extragalactic component. The astrophysical neutrino signal is so far compatible with isotropy despite searches for anisotropy including point sources (e.g. [6]).

In the three-year sample of IceCube high-energy starting events (HESE), some correlation with the Galactic plane was observed with a chance probability of 2.8% [3]. In [7], the authors explore the addition of an energy cut in the public HESE data<sup>1</sup> and report a  $> 3\sigma$  a posteriori correlation with the Galactic plane in the HESE arrival distribution for an energy cut  $>100$  TeV.

Additionally, the ANTARES neutrino detector has performed a search for muon neutrinos in the region of the Galactic ridge. For the case of a neutrino flux that extends into the GeV energy range as an  $E^{-2.5}$  power law, they set a per-flavor flux normalization (at 100 GeV) upper limit of  $1.9 \times 10^{-17} \text{ GeV}^{-1} \text{ cm}^{-2} \text{ s}^{-1} \text{ sr}^{-1}$  in the region Galactic longitude  $|l| < 40^\circ$  and Galactic latitude  $|b| < 3^\circ$  (encompassing 0.145 sr). [8].

Using IceCube muon samples, we search for diffuse Galactic neutrino emission using two parallel maximum likelihood methods sensitive primarily in the outer Galactic plane region (the northern sky). The first method, denoted as the *unbinned method*, is an extension of a commonly used point-source analysis. It employs an unbinned maximum likelihood method to search for an anisotropic pattern in the neutrino arrival directions. The second method, denoted as the *binned method*, is an extension of the diffuse astrophysical neutrino measurement [4]. It is based on binned multi-dimensional templates of all contributing flux components from atmospheric and astrophysical neutrinos. This method inherently includes systematic uncertainties but requires higher purity with respect to atmospheric muon background and is thus restricted to the northern hemisphere.

## 2. Models of Galactic Neutrino Emission

Models for diffuse gamma-ray production are driven by current gamma-ray observations. Thanks to the high-precision measurements of the *Fermi*-LAT satellite (see [9] for a summary), accurate models of the gamma-ray diffuse emission are available. From the pionic component of these models neutrino predictions can also be made. We discuss two spatial models used in our

<sup>1</sup><https://icecube.wisc.edu/science/data>

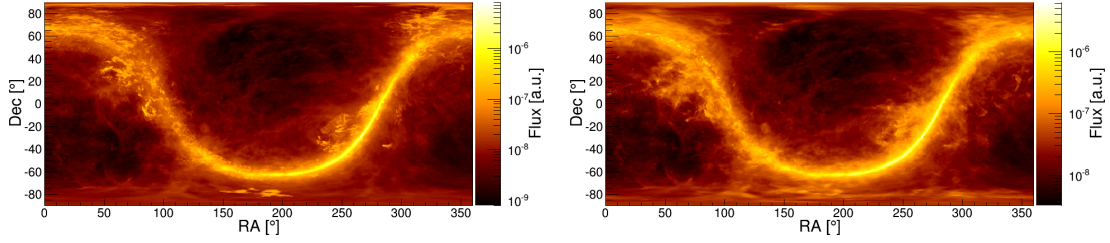


**Figure 1:** Two models for diffuse Galactic neutrino production described in section 2 are shown: (a) KRA- $\gamma$  (50 PeV cutoff), and (b) *Fermi*-LAT  $\pi^0$ -decay map.

analysis that span a robust range of possibilities for Galactic neutrino emission: the *Fermi*-LAT pion-decay template [9] and the KRA- $\gamma$  (50 PeV cutoff) model<sup>2</sup> [11]. The *Fermi*-LAT pion-decay template is taken from the reference Galactic model in [9]. We extract just the pion-decay component of this model and use it as a template for neutrino emission. We do not convert the gamma-ray flux into an absolute prediction of the number of neutrinos but only consider the spatial distribution of the emission. The *Fermi*-LAT energy range where the model is validated is substantially lower than the energies of the neutrinos to which we are sensitive. A hardening in the spectrum of the cosmic rays could substantially increase the neutrino predictions.

In [11] the authors noticed that the model above does, in fact, under-predict the flux of gamma rays above a few GeV in the Galaxy, especially for higher-energy observations of the H.E.S.S and Milagro collaborations. The same authors were able to explain this residual flux by allowing the diffusion coefficient to vary depending on the Galactic radius. The result of this study is the KRA- $\gamma$  model, which matches the gamma-ray data quite closely. Since the KRA- $\gamma$  model is based on the same underlying model of the interstellar medium (ISM) as the *Fermi*-LAT pion-decay template, the spatial features are very similar between the two models, with KRA- $\gamma$  being brighter at the Galactic center.

### 3. Analysis Methods

#### 3.1 Unbinned Maximum Likelihood Spatial Template Analysis

The *unbinned method* used in this work is a modification of the unbinned maximum likelihood analysis commonly employed in IceCube point-source searches [12, 6]. The first modification is to account for the extension of the source by mapping the changing detector acceptance and convolving the extended source hypothesis (in contrast with the delta-function source hypothesis used in point-source searches) with the PSF of the events. The other modification relates to the estimate of the background using data. In a point-source analysis, a hypothetical source has a very small contribution to its declination band and is treated as negligible for determining the background. For the Galactic plane, the signal may extend over the entire sky and is no longer negligible and so a different likelihood formalism is needed. The signal-subtracted likelihood acknowledges this contribution by making a small correction to the method as introduced in [13]:

<sup>2</sup>The conventional KRA diffusion model is defined in [10]

$$L(n_s, \gamma) = \prod_{i=1}^N \left( \frac{n_s}{N} S_i(\mathbf{x}_i, \sigma_i, E_i; \gamma) + \tilde{D}_i(\delta_i, E_i) - \frac{n_s}{N} \tilde{S}_i(\delta_i, E_i) \right), \quad (3.1)$$

where  $n_s$  is the number of signal events for a flux following spectral index  $\gamma$ ;  $N$  is the total number of events in the sample;  $S_i(\mathbf{x}_i, \sigma_i, E_i; \gamma)$  is the signal probability distribution function (PDF) for event  $i$  at equatorial coordinates  $\mathbf{x}_i = (\alpha_i, \delta_i)$  with Gaussian PSF of width  $\sigma_i$  and energy estimator  $E_i$ ;  $\tilde{D}_i$  is defined as:

$$\tilde{D}_i(\delta_i, E_i) = \frac{n_s}{N} \tilde{S}_i(\delta_i, E_i) + \left(1 - \frac{n_s}{N}\right) B_i(\delta_i, E_i), \quad (3.2)$$

where  $\tilde{S}_i$  is constructed by integrating  $S_i$  in a small declination bin ( $\sim 1^\circ$ ) over right ascension;  $B_i$  is the background PDF.

The  $S_i$  terms, which encode information about both the raw signal expectation and the detector performance, are obtained by convolving the neutrino flux model with the effective area obtained from detailed simulations (cf. [4]). The resulting map is finally convolved with the PSF for each event, modeled by a Gaussian distribution of width  $\sigma_i$  estimated for each event and ranging from  $0.1^\circ$  to  $3.0^\circ$ .

A nested log-likelihood ratio between the best-fit signal strength and the null hypothesis (no Galactic component) is used to construct a test statistic. Under the null hypothesis and in the large sample limit, the test statistic follows a half- $\chi^2$ -distribution as expected from [14]. Final upper limits, sensitivities (given as median upper limits) and significances, such as the p-value of the observed test statistic, are always calculated using background trials obtained from scrambled data. We use a 90% Neyman upper limit construction.

The data sample for this analysis is described in [6]. It is an all-sky sample that spans seven years with a total live time of 2431 days and 730130 events. The sensitivity comes primarily from the northern sky, where IceCube sees a wide energy range of muons induced by neutrinos. Though the sample extends into the southern sky, the sensitivity there is limited to very high energies since energy selection and veto techniques are used that reject the softer background of down-going muons from cosmic-ray air showers.

### 3.2 Binned Maximum Likelihood Spatial Template Analysis

The binned maximum likelihood analysis is an extension of the analysis presented in [4]. In this analysis, the contributions from conventional atmospheric neutrinos [15], prompt atmospheric neutrinos [16] and isotropic astrophysical neutrinos with a power-law energy spectrum are fitted to experimental data. The events are binned according to the reconstructed zenith angle and an energy estimator. The resulting histograms are analyzed using a maximum-likelihood approach. Each bin is modeled by a Poisson likelihood function:

$$L_i(\theta, \xi) = e^{-\mu_i(\theta, \xi)} \cdot \frac{\mu_i^k}{k!}, \quad (3.3)$$

where  $\theta = \theta(\Phi_{\text{astro}}, \gamma_{\text{astro}}, \dots)$  describes the signal parameters (i.e. properties of the astrophysical fluxes) and  $\xi$  describe the nuisance parameters. The expected number of events in bin  $i$ ,  $\mu_i$ , is given by the sum of the four flux expectations for the conventional, prompt, isotropic astrophysical and

Galactic flux:

$$\begin{aligned} \mu_i(\theta, \xi) = & \mu_i^{\text{conv}}(\xi_{\text{conv}}, \xi_{\text{det}}) + \mu_i^{\text{astro}}(\Phi_{\text{astro}}, \gamma_{\text{astro}}, \xi_{\text{det}}) \\ & + \mu_i^{\text{prompt}}(\xi_{\text{prompt}}, \xi_{\text{det}}) + \mu_i^{\text{Galactic}}(\Phi_{\text{Galactic}}, \xi_{\text{det}}), \end{aligned} \quad (3.4)$$

where  $\xi_{\text{conv}}$  and  $\xi_{\text{prompt}}$  refer to nuisance parameters taking into account the theoretical uncertainties on the respective fluxes and  $\xi_{\text{det}}$  refers to nuisance parameters taking into account detector uncertainties. For more information on these parameters we refer to [4]. The final, global likelihood is the product of all per-bin likelihoods  $L = \prod_i L_i$ .

Compared to [4], this analysis is extended by including the reconstructed right ascension, thus changing the histograms from two to three dimensions. Additionally, a template for the Galactic contribution,  $\mu^{\text{Galactic}}$ , is added to the fit. Note that for the *Fermi*-LAT  $\pi^0$ -decay template the Galactic spectral index is an additional signal parameter free to float in the fit. In contrast to the method described in the previous section, this method models the expected contributions of every flux component using Monte Carlo simulations. This allows us to see how the isotropic component changes with the best-fit Galactic component. The test statistic is defined as a log-likelihood ratio in the same fashion as the previous method, with the same limit and significance calculations.

The data sample for this is described in [4]. Compared to the previous method, the sample has a significantly higher muon neutrino purity of  $>99.7\%$  with comparable effective area and a slightly improved PSF. The sample is, however, limited to the northern hemisphere where the high neutrino purity standards can be achieved. The time period is somewhat smaller as this selection does not apply to the time period when IceCube had just 40 of the final 86 strings deployed. The data set spans six calendar years with a total live time of 2060 days and 354792 events.

## 4. Results

### 4.1 Constraints on Diffuse Emission in the Plane

The sensitivities and results of spatial template analyses are summarized in Table 1. Some excess from the Galaxy is observed in all cases, though it is not statistically significant. Because of the somewhat better sensitivity, the *unbinned method* was assigned, in advance of unblinding the data, to be the main result, with the *binned method* acting as a cross check. The upper limit for the KRA- $\gamma$  test is shown in Figure 2 in comparison to the ANTARES upper limit, the KRA family of predictions, and the isotropic diffuse neutrino flux.

**Table 1:** Summary of results for both Galactic plane analysis methods. The sensitivities and upper limits for KRA- $\gamma$  are given in units of the model prediction. For the *Fermi*  $\pi^0$ -decay template they are given in units of a  $(E_{\text{nu}}/100\text{TeV})^{-2.5} \nu_{\mu} + \bar{\nu}_{\mu}$  flux.

Spatial Template	p-value	unbinned method		binned method (cross check)		
		Sens. $\phi_{90\%}$	U.L. $\phi_{90\%}$	p-value	Sens. $\phi_{90\%}$	U.L. $\phi_{90\%}$
$\pi^0$ -decay, $E^{-2.5}$	37%	$2.97 \times 10^{-18}$	$3.83 \times 10^{-18}$	7.0%	$3.16 \times 10^{-18}$	$6.13 \times 10^{-18}$
KRA- $\gamma$ (50 PeV)	29%	79%	120%	6.9%	95%	170%

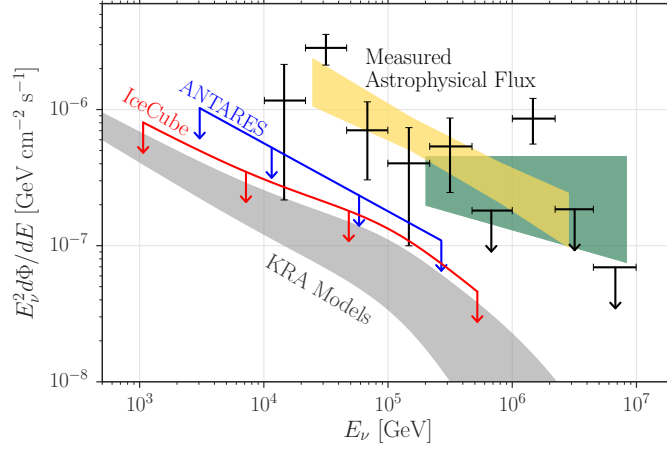


**Figure 2:** Upper limits on the three-flavor (1:1:1 flavor ratio assumption) neutrino flux from the Galaxy with respect to KRA model predictions and the measured astrophysical neutrino flux. The limit for the KRA- $\gamma$  (50 PeV) model test is shown in red. The energy range of validity is from 1 TeV to 500 TeV. This range is calculated by finding the high and low energy thresholds where removing simulated signal events outside these values decreases the sensitivity by 5% each. The ANTARES limit is shown in blue [8]. The range of predictions for all KRA models [11] is shown as the gray band. For comparison, measurements of the all-sky diffuse flux are shown: a differential unfolding (black points) and a power-law unfolding (yellow band) of combined IceCube data sets from [5] as well as a measurement based only on northern sky muon data (green band) from [4].

The Galactic excesses are somewhat larger and more significant for the cross check, and this difference was investigated carefully for the benchmark *Fermi* pion decay template. Part of the difference comes from the additional year of data used by the *unbinned method*. If we restrict this method to the same time period, the p-value drops from 37% to 22%. Running the *unbinned method* on the alternative sample yields a p-value of 21%. Due to the purity requirement for modeling the background with simulation, the check of the *binned method* on the alternative data set is not possible.

#### 4.2 2D Likelihood Scan and Implications for the Isotropic Astrophysical Flux

Using the *binned method* a two-dimensional profile likelihood scan of the Galactic normalization and Galactic spectral index is performed for the benchmark *Fermi*-LAT pion-decay template. The results of this scan are shown in Figure 3 (left). The best-fit spectral index is  $\gamma_{\text{Galactic}} = 2.07$ , and the best-fit normalization at 100 TeV is  $\Phi_{\text{Galactic}} = 3.13 \cdot 10^{-18} \text{GeV}^{-1} \text{cm}^{-2} \text{s}^{-1}$  (the same units and reference energy are used in Table 1). The confidence contours have been estimated using Wilks' Theorem [17], which has been cross-checked at several points in the parameter space with Monte Carlo pseudo-experiments. The best-fit spectral index is harder than expected from a naive extrapolation of the pion template. However, it is consistent with an index of 2.5 at the  $1.65\sigma$  level.

Since the *binned method* is an extension of the method used to characterize the isotropic astrophysical flux in [4], we can analyze the impact of allowing an additional Galactic component in the fit on the isotropic flux parameters. For this we performed a profile-likelihood scan of the isotropic flux normalization and spectral index while allowing the Galactic flux parameters to float

freely at every scan point. Figure 3 (right) shows the resulting likelihood contours in comparison to the contours obtained by restricting the Galactic flux to zero. The color scale shows the best-fit Galactic plane spectral index at each point in the scan. Although the additional freedom given by the Galactic flux nuisance causes the isotropic normalization to decrease, the size of the contour grows only marginally. The hypothesis of zero isotropic flux is still excluded with  $> 3\sigma$  significance. This shows that the observation of an isotropic astrophysical signal is robust against a signal from the Galactic plane and that the latter can only contribute a sub-dominant fraction to the total observed astrophysical flux.

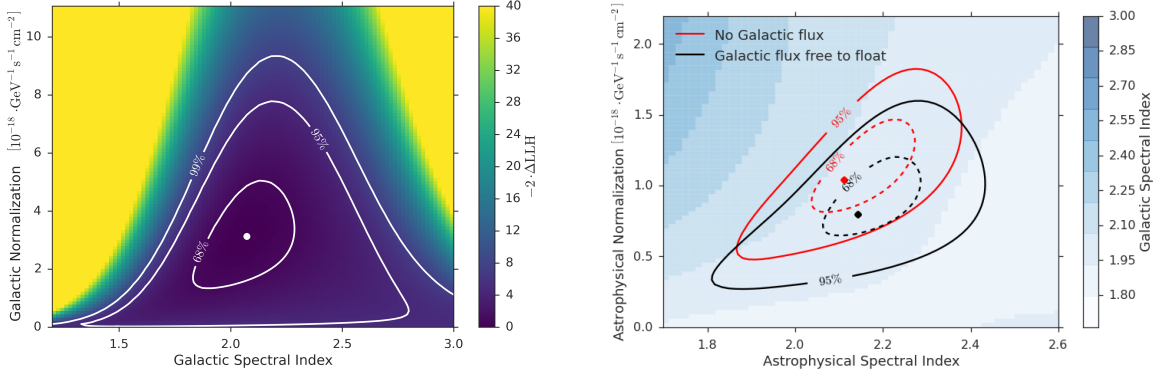


**Figure 3:** Left: 2D likelihood scan of Galactic flux normalization and Galactic spectral index. Right: Contours of isotropic astrophysical flux normalization and spectral index with and without Galactic flux.

## 5. Conclusions

We have presented searches for neutrino signals associated with the Galactic plane using seven years of IceCube muon neutrino data, focusing on diffuse emission from interactions of cosmic rays with the ISM. We are able to exclude that more than 14% of the diffuse neutrino flux as measured in [5] comes from the Galactic plane for the case of the *Fermi*-LAT template and an  $E^{-2.5}$  power law.

Our measurement is primarily sensitive in the northern hemisphere, where IceCube has a high efficiency for a wide energy range of muons induced by neutrinos. Our limits are quoted assuming various all-sky spatial models of neutrino emission. The most optimistic, KRA- $\gamma$  with a 50 PeV cosmic-ray cutoff, concentrates the most flux towards the Galactic center. Even though a higher fraction of the flux is in the southern sky, our limits are just 20% higher than this model prediction.

The ANTARES detector also sets relevant constraints measured directly in the region surrounding the Galactic center ( $-40^\circ < l < 40^\circ$  and  $-3^\circ < b < 3^\circ$ ). They limit the neutrino flux to be less than 60% higher than the KRA- $\gamma$  model at 100 TeV [8].

While our flux constraints focus on the plane of the Galaxy, there are still possibilities for the flux to originate in or very near the Galaxy. The possibility of cosmic-ray interactions with a gas halo extending out to  $\sim 100$  kpc is still actively explored [18, 19, 20]. Another possibility would be the annihilation [13] or decay [21] of dark matter particles in the Galactic halo. For these hypotheses, the emission is much more isotropic than the Galactic emission templates that we tested.

There are possibilities to improve the sensitivity for Galactic neutrino searches. A search for point sources in the southern hemisphere using cascade-like events in IceCube has been shown to have a sensitivity comparable to ANTARES [22]. A joint analysis that includes both the track and cascade channels will offer promising improvements. Additionally, a joint Galactic plane analysis between IceCube and ANTARES, similar to the joint point-source analysis that produced excellent limits in the southern sky [23], would provide the strongest constraints on neutrinos from the Milky Way with all available data.

## References

- [1] G. W. Clark, G. P. Garmire, and W. L. Kraushaar, *ApJL* **153** (1968) L203.
- [2] **IceCube** Collaboration, M. G. Aartsen et al., *Science* **342** (2013) 1242856.
- [3] **IceCube** Collaboration, M. G. Aartsen et al., *Phys. Rev. Lett.* **113** (2014) 101101.
- [4] **IceCube** Collaboration, M. G. Aartsen et al., *Astrophys. J.* **833** (2016) 3.
- [5] **IceCube** Collaboration, M. G. Aartsen et al., *Astrophys. J.* **809** (2015) 98.
- [6] **IceCube** Collaboration, M. G. Aartsen et al., *Astrophys. J.* **835** (2017) 151.
- [7] A. Neronov and D. Semikoz, *Phys. Rev.* **D93** (2016) 123002.
- [8] S. Adrián-Martínez et al., *Physics Letters B* **760** (2016) 143–148.
- [9] M. Ackerman et al., *ApJ* **750** (2012) 3.
- [10] C. Evoli et al., *Phys. Rev.* **D85** (2012) 123511.
- [11] D. Gaggero et al., *ApJL* **815** (2015) L25.
- [12] J. Braun et al., *Astroparticle Physics* **29** (2008) 299–305.
- [13] **IceCube** Collaboration, M. G. Aartsen et al., *Eur. Phys. J.* **C75** (2015) 492.
- [14] G. Cowan et al., *Eur. Phys. J.* **C71** (2011) 1554. [Erratum: *Eur. Phys. J.*C73,2501(2013)].
- [15] M. Honda et al., *Phys. Rev. D* **75** (2007) 043006.
- [16] R. Enberg, M. H. Reno, and I. Sarcevic, *Phys. Rev. D* **78** (2008) 043005.
- [17] S. S. Wilks, *Ann. Math. Statist.* **9** (1938) 60–62.
- [18] R. Feldmann, D. Hooper, and N. Y. Gnedin, *ApJ* **763** (2013) 21.
- [19] A. M. Taylor, S. Gabici, and F. Aharonian, *PhRvD* **89** (2014) 103003.
- [20] O. Kalashev and S. Troitsky, *PhRvD* **94** (2016) 063013.
- [21] K. Murase, R. Laha, S. Ando, and M. Ahlers, *PhRvL* **115** (2015) 071301.
- [22] **IceCube** Collaboration, M. G. Aartsen et al., [arXiv:1705.02383](https://arxiv.org/abs/1705.02383).
- [23] S. Adrian-Martinez et al., *Astrophys. J.* **823** (2016) 65.

## Search for extended sources of neutrino emission with 7 years of IceCube data

---

### The IceCube Collaboration<sup>†</sup>

<sup>†</sup> [http://icecube.wisc.edu/collaboration/authors/icrc17\\_icecube](http://icecube.wisc.edu/collaboration/authors/icrc17_icecube)

E-mail: [epinat@icecube.wisc.edu](mailto:epinat@icecube.wisc.edu), [juaguila@ulb.ac.be](mailto:juaguila@ulb.ac.be)

The IceCube Neutrino Observatory has demonstrated the existence of an astrophysical high-energy neutrino flux with a significance exceeding  $7\sigma$ . Nevertheless, the observed astrophysical neutrino flux shows no clear association with any known source class so far. The most recent searches for point sources using seven years of data from IceCube have found no significant clustering of neutrino events nor correlation with preselected sources. However not all potential neutrino sources would appear point-like, and it is therefore important to widen the search to different source topologies. The high-energy gamma-ray and cosmic-ray skies show clear indications of extended structures. In the case of cosmic-ray interactions in these environments, both gamma-ray and neutrino emission are expected, and the detection of this neutrino flux would represent unambiguous proof of the hadronic nature of the sources. In addition, an extended source search could improve sensitivity to several point sources located close together in space, for example the Cygnus region, even if the individual fluxes are too low to be detected separately. Here we present the results of an extended source analysis with seven years of IceCube data. Because the extensions of potential sources are not always known *a priori*, five different extensions have been considered, from  $1^\circ$  to  $5^\circ$ . All the five maps are consistent with the background-only hypothesis.

**Corresponding authors:** Elisa Pinat and Juan Antonio Aguilar\*

*Université Libre de Bruxelles, Science Faculty CP230, B-1050 Brussels, Belgium*

*35th International Cosmic Ray Conference — ICRC2017  
10–20 July, 2017  
Bexco, Busan, Korea*

---

\*Speaker.

## 1. Introduction

The IceCube Neutrino Observatory is a neutrino detector located at the South Pole, encompassing a cubic kilometer of Antarctic ice between depths of 1450 m and 2450 m [1]. Completed in 2011, it is the largest neutrino detector built to date. During the construction period data was collected in four different string configurations, until the final 86 string configuration was reached. Similarly to other neutrino detectors, IceCube exploits the fact that charged particles, resulting from neutrino interactions, move faster than the phase velocity of light in the ice and emit Cherenkov radiation.

Neutrinos are ideal messengers, and their use in astronomy was imagined already in the 1960s. Stars, Active Galactic Nuclei (AGNs) and astrophysical engines are opaque to photons, while neutrinos can easily escape, preserving directional information and carrying information from the densest regions of the Universe. Astrophysical neutrinos are also tracers of hadronic interactions, and the identification of their sources may help to clarify cosmic ray acceleration processes.

The detection of a diffuse high-energy astrophysical neutrino flux made in 2013 by the IceCube collaboration is now established at more than  $7\sigma$  confidence level with both events starting within the detector (all flavor) [2] and events traversing through the Earth ( $\nu_\mu$  charged-current) [3]. However, the sources of this neutrino flux have not been identified yet [4]. Finding neutrino point sources in the sky requires locating an excess of events from a particular direction over the background of atmospheric neutrinos and muons. Together with the spatial component, also the energy distribution of events is used as discriminator between the signal and the background hypotheses. Since point source searches have been unfruitful so far, it is important to widen the search to different source topologies to maximize the discovery potential. A different topology are extended sources that are motivated by clear indications of extended structures seen in the high-energy gamma-ray and cosmic-ray skies.

In these proceedings we present the result of the search of spatially extended sources with seven years of IceCube data from three years of operation in partial levels of completion (IC-40, IC-59 and IC-79) and the first four years of the completed 86 string detector (IC86-I, IC86-II, IC86-III and IC86-IV). Data have been collected from May 2008 to May 2015, for a total of 713752 events after event selection for through-going muon neutrinos (see [4]) in 2426.2 days of livetime. The previous extended source analysis was limited to four years, using samples from IC40 to IC86-I, and the results are shown in [5]. The likelihood method has been improved by accounting for signal contamination in the background estimation. With this new method, sensitivities and discovery potentials have been calculated, and five significance skymaps have been produced, testing extensions from  $1^\circ$  to  $5^\circ$ .

## 2. Physics case

Motivations for searching for extended sources are manifold. Extended sources have been detected in the  $\gamma$ -sky. For example, the H.E.S.S. survey of the inner part of the Galactic Plane [6] revealed a number of bright extended  $\gamma$ -ray sources. If the observed  $\gamma$ -rays are produced by cosmic-ray interactions, a very-high-energy neutrino flux should be associated as well. If detected, this would represent an unambiguous proof of the hadronic nature of the sources. Despite many

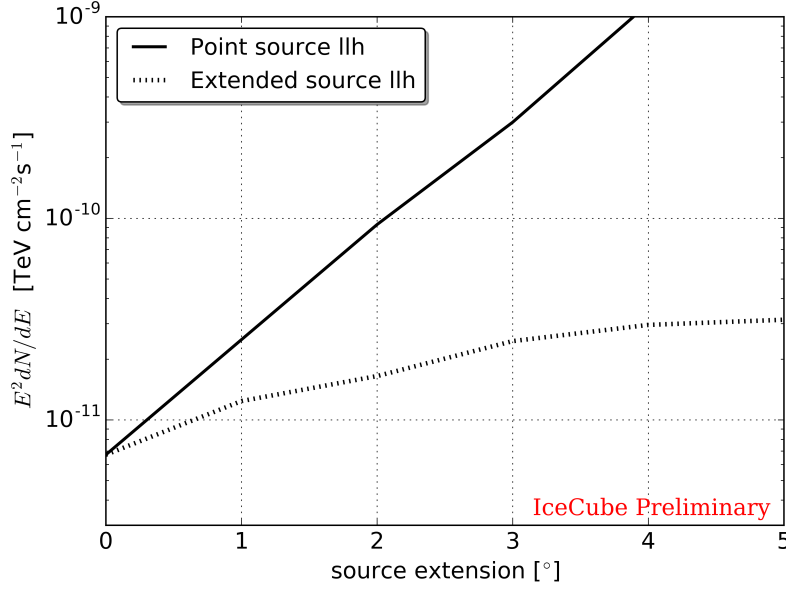


Figure 1: Discovery potential for an  $E^{-2}$  flux from an extended source at a declination of  $16^\circ$  for one year of IC86 data with no trial factor correction. The regular point source analysis (solid line) is compared to the discovery potential of the extended source analysis (dotted line), where the latter employs the known source extension.

$\gamma$ -ray sources show an extension of about  $0.3^\circ - 0.4^\circ$ , which is below IceCube’s median angular resolution of about  $1^\circ$  at 1 TeV, some sources show even larger extension, thus providing a strong motivation to look for extended sources.

The high-energy cosmic-ray sky shows also clear indications for extended structures: although being at larger scales and higher energies, the Telescope Array has observed a  $5.1\sigma$  excess in cosmic rays with energies above 57 EeV in a region centered on coordinates  $146.7^\circ$  RA,  $43.2^\circ$  DEC [7], hotspot larger than the extension expected by propagation effects. In addition, the Cascade Grande experiment has observed at  $5.5\sigma$  significance a  $1^\circ$  extended 300 TeV cosmic-ray hotspot in a mainly isotropic sky [8].

Finally, motivation in favor of a dedicated extended source analysis can also be found in Figure 1. Assuming the presence of extended sources and modeling the signal injection according to their extension, this plot shows the discovery potential for an  $E^{-2}$  flux of the regular point source analysis method that relies on an unbinned likelihood maximization, compared to the one calculated with our extended source analysis, with the spatial extension properly accounted for. In this case, the same value used to simulate the spatial extension enters the likelihood calculation, showing that, when the correct source extension is used, the improvement can be substantial. A point source analysis risks to be blind in the presence of an hypothetical extended source.

### 3. Analysis Method

To calculate the significance of a possible excess of neutrino events for a given direction in the sky over the background of atmospheric muons and neutrinos, this analysis uses an unbinned

maximum likelihood method similar to the one described in [9]. The method exploits the fact that not only signal events from a neutrino source are expected to cluster in space, but also their energy spectrum is different from those of the backgrounds. Signal events follow a harder spectrum than atmospheric muons and neutrinos [10], and it has been demonstrated that the introduction of the energy term performs better than the simple spatial approach [9]. The likelihood expression adopted in standard point source searches is defined as:

$$L(n_s, \gamma) = \prod_{i=1}^N \left( \frac{n_s}{N} S(\vec{x}_s, \vec{x}_i, \sigma_i, E_i; \gamma) + \left(1 - \frac{n_s}{N}\right) B(\delta_i, E_i) \right) \quad , \quad (3.1)$$

where  $S$  and  $B$  are the signal and background probability density functions respectively,  $n_s$  is the unknown number of signal events for a flux following a spectral index  $\gamma$  and  $N$  total number of events in the data sample under evaluation. The error associated to the reconstructed direction is represented by  $\sigma_i$ ,  $E_i$  is the reconstructed energy. Both the signal and background PDFs contain a spatial and an energy term,  $S = S_{space} \times S_{energy}$  and  $B = B_{space} \times B_{energy}$ . The two parameters maximized in the likelihood are the number of signal events  $n_s$  and the spectral index of the extended source assumed to be located at  $\vec{x}_s$  where the likelihood is being evaluated.

The first modification with respect to the standard point source searches affects the term  $S_{space}$ . The signal spatial probability density function is assumed to be Gaussian but the point spread function, instead of depending only on the error on the reconstructed direction  $\sigma_i$ , is now convoluted with the source extension  $\sigma_{src}$ , resulting in:

$$S_{space} = \frac{1}{2\pi(\sigma_i^2 + \sigma_{src}^2)} \exp\left(-\frac{|\vec{x}_i - \vec{x}_s|^2}{2(\sigma_i^2 + \sigma_{src}^2)}\right) \quad (3.2)$$

where  $\sigma_{src}$  is fixed to one of the several discrete values from  $1^\circ$  to  $5^\circ$  and  $|\vec{x}_i - \vec{x}_s|$  is the angular distance to the source.

The second modification is related to the estimate of the background using data, whose energy and spatial distribution are  $B_{space}$  and  $B_{energy}$ . The spatial background PDF  $B_{space}$  depends only on declination, and is right ascension independent due to Earth's rotation. In a point source analysis, any hypothetical point source has a very small contribution in the declination band of interest, and is treated as negligible when building background PDFs using spatial and energy distribution of the data. In contrast, the contribution of an *extended* source within its declination band is not negligible anymore, and a small correction needs to be applied. To account for this contribution, a third PDF, called *scrambled signal*  $\tilde{S}(\delta_i, E_i; \gamma)$ , is needed. The term is self explanatory, as the scrambled signal represents how a signal contribution looks like when scrambled in right ascension. The background derived from data is expressed in term of a mixture of this scrambled signal and the pure background  $B(\delta_i, E_i)$ :

$$\tilde{D}(\delta_i, E_i) = \frac{n_s}{N} \tilde{S}(\delta_i, E_i; \gamma) + \left(1 - \frac{n_s}{N}\right) B(\delta_i, E_i) \quad . \quad (3.3)$$

The new signal-subtracted likelihood is finally expressed as:

$$L(n_s, \gamma) = \prod_{i=1}^N \left( \frac{n_s}{N} S(x_i, \sigma_i, E_i; \gamma) + \tilde{D}(\delta_i, E_i) - \frac{n_s}{N} \tilde{S}(\delta_i, E_i; \gamma) \right) \quad . \quad (3.4)$$

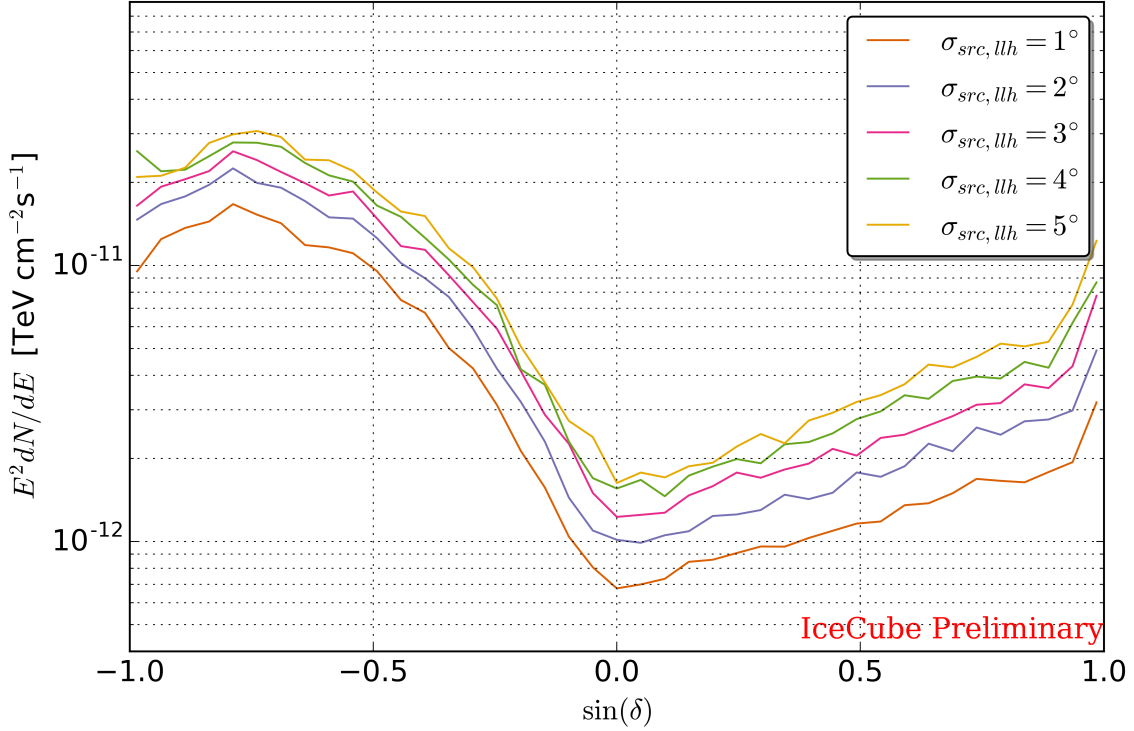


Figure 2: Sensitivity at 90% confidence level for the five extensions considered and an  $E^{-2}$  power law spectrum. The best case scenario is assumed, that is when the simulated source extension ( $\sigma_{src}$ ) matches exactly the extension of the likelihood scan ( $\sigma_{llh}$ ).

The scrambled signal PDF has an energy and a spatial term,  $\tilde{S} = \tilde{S}_{space} \times \tilde{S}_{energy}$ . In this analysis, as in standard point-source ones, the signal energy term  $S_{energy}$  is described by a power law, and the same power law is used to describe  $\tilde{S}_{energy}$ . The spatial part,  $\tilde{S}_{space}$ , depends on the description adopted for the signal spatial PDF  $S_{space}$ . In our case the signal spatial PDF is modeled as 2D Gaussian, and therefore the scrambled signal spatial PDF is described as a 1D Gaussian with the sole dependence on the declination, divided by the cosine of the declination.

#### 4. Performance

This analysis is sensitive to TeV-PeV neutrino sources in the Northern Hemisphere, and to PeV-EeV sources in the Southern Hemisphere, due to an energy constraint imposed by the need to reject the atmospheric muon background. The difference in the background rates for the Northern and Southern Hemispheres affects the shape of the two figures of merit of the analysis, the sensitivity and the discovery potential. The sensitivity, shown in Figure 2, represents the 90% confidence level upper limit that is set 50% of the time assuming the absence of a source. The discovery potential represents instead the flux required to have a  $5\sigma$  discovery, knowing this will be detected only 50% of the time. Curves have been produced assuming the best case scenario, that is when the source extension in the injector matches the extension of the likelihood scan, and considering an  $E^{-2}$  power law. The Southern Sky performance is penalized by the higher background rates.

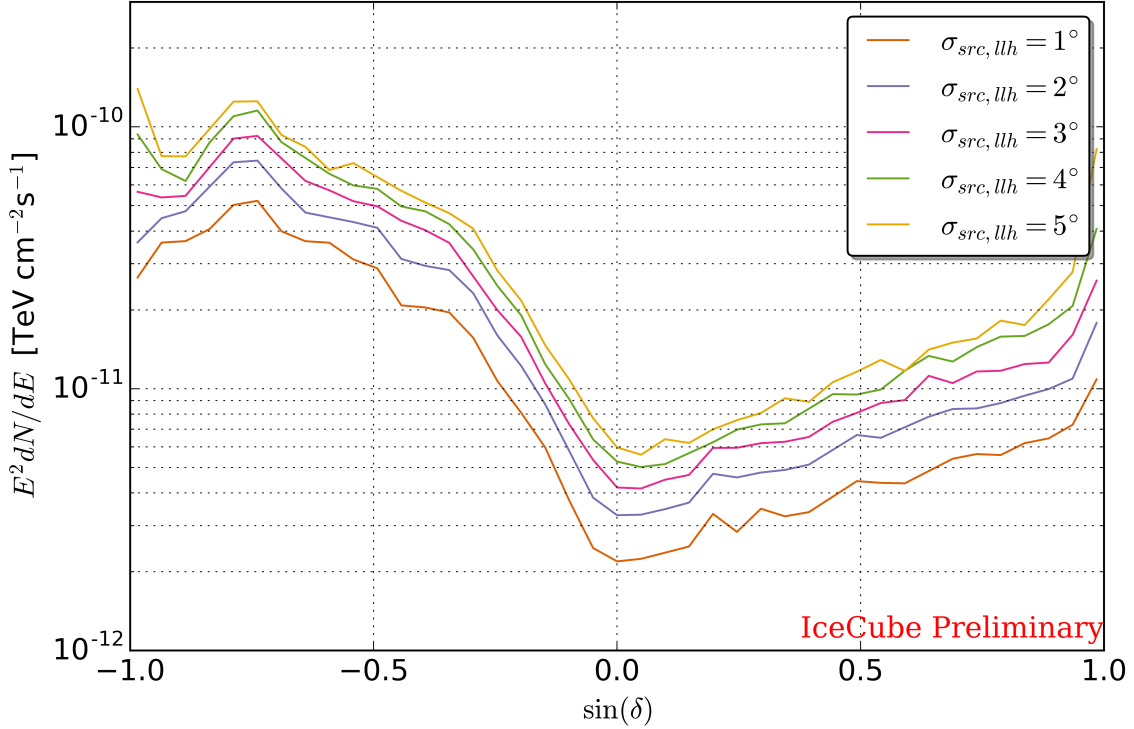


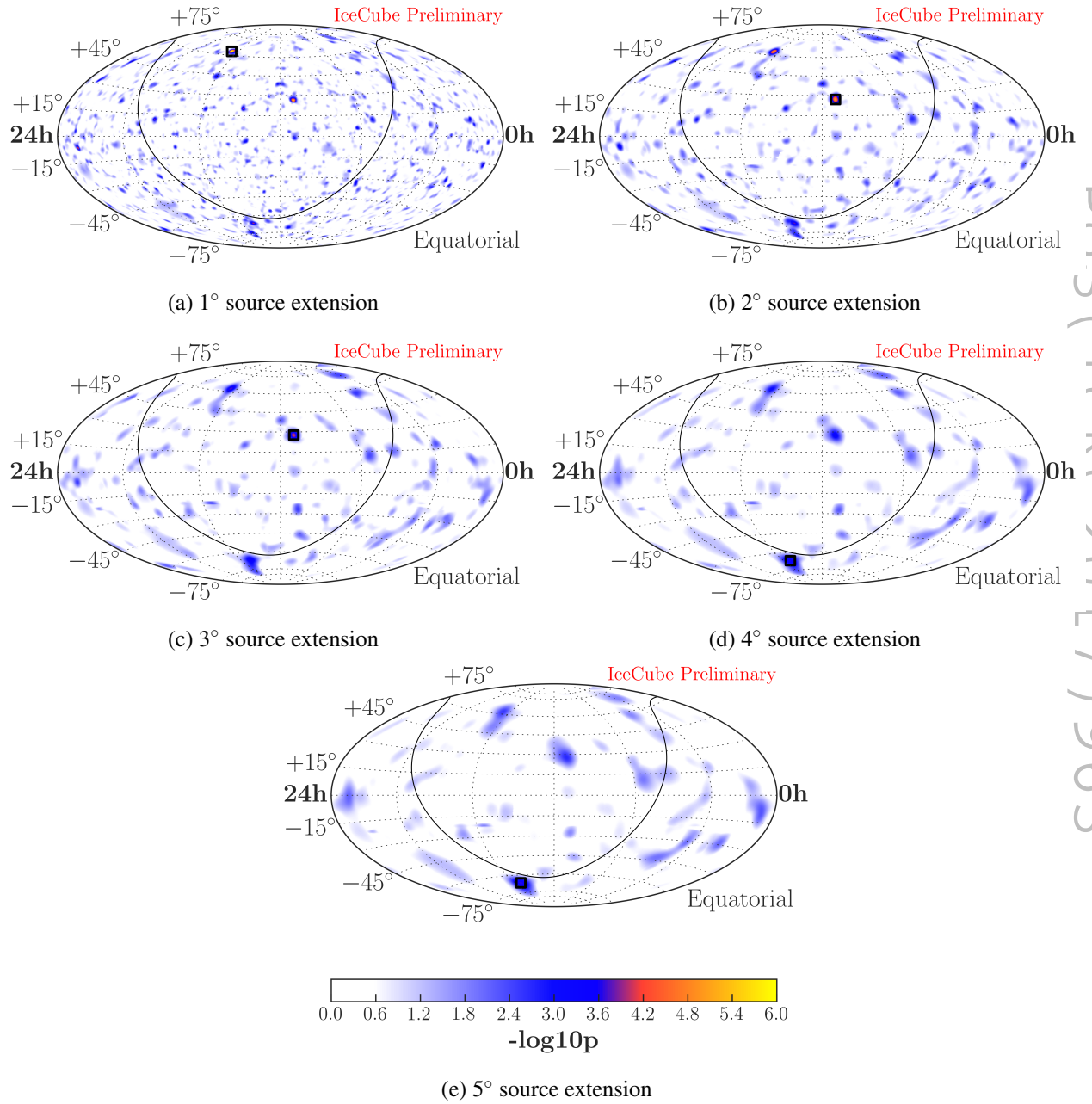
Figure 3: Discovery potential at 50% confidence level for the five extensions considered and an  $E^{-2}$  power law spectrum. The best case scenario is assumed, that is when the simulated source extension ( $\sigma_{src}$ ) matches exactly the extension of the likelihood scan ( $\sigma_{llh}$ ).

## 5. Results

The aim of this analysis is to produce five significance skymaps. All-sky scans for source extensions of  $1^\circ$ ,  $2^\circ$ ,  $3^\circ$ ,  $4^\circ$  and  $5^\circ$  are shown in Figures 4a, 4b, 4c, 4d and 4e, respectively. For each extension scan, the direction with the highest significance (marked with a black box on the skymaps) has been selected and the post-trial p-value calculated by comparing the result to the distribution of hotspots obtained from background-scrambled maps for each extension. Due to Earth's rotation, the probability density of the background is uniform in right ascension. It is therefore possible to produce background pseudo-experiment by using data that have kept the information of the declination but have been assigned a random value for the right ascension. Results of each scan are grouped in Table 1. All the results are consistent with the background-only hypothesis. The most significant among the maps is the  $1^\circ$  extension with a post-trial p-value of 0.1. This result is however not significant, especially if considering a conservative trial factor of 5 to account for the fact that the maps are not independent. This is also the reason why hotspot locations for the  $2^\circ$  and  $3^\circ$  extensions and also for the  $4^\circ$  and  $5^\circ$  ones are the same. However, these locations have been checked and do not correspond to any know cataloged astrophysical object.

## 6. Conclusions

A search for extended sources has been performed using seven years of throughgoing muons.



DOI: 10.1088/1741-4221/17/9/0963

Figure 4: Pre-trial significance skymaps for different source extension and seven years of through-going muons. The solid black line represents the galactic plane. The hottest spot is highlighted with a black box in each skymap.

Extension [°]	RA [°]	DEC [°]	$\hat{n}_s$	$\hat{\gamma}$	p-value (pre-trial)	p-value (post-trial)
1°	249.32	63.28	73.32	1.85	$8.20 \times 10^{-7}$	0.10
2°	169.44	27.04	102.92	2.19	$9.04 \times 10^{-6}$	0.30
3°	169.37	27.68	119.18	2.16	$7.31 \times 10^{-5}$	0.58
4°	229.82	-66.64	140.05	1.63	$2.23 \times 10^{-4}$	0.78
5°	231.56	-66.44	160.83	1.68	$1.99 \times 10^{-4}$	0.60

Table 1: Summary of the results from the extended all-sky survey. The coordinates of the most significant spots located for each source extension hypothesis are given together with the respective p-values. The post-trial p-values are all consistent with the background-only hypothesis.

Data have been taken with different detector configurations, from the 40-string to the final 86-string layout. Given the source extension is not known *a priori*, five extensions from 1° to 5° have been considered. A novel likelihood method has been implemented, that accounts and corrects for the signal contamination in the background obtained by scrambling technique. Five different significance skymaps have been produced, and a p-value has been calculated for the hottest spot of each map. All the five maps are consistent with the background-only hypothesis.

## References

- [1] **IceCube** Collaboration, M. G. Aartsen et al., *JINST* **12** (2017) P03012.
- [2] **IceCube** Collaboration, [PoS \(ICRC2015\) 1081](#) (2016).
- [3] **IceCube** Collaboration, M. G. Aartsen et al., *ApJ* **833** (2016) 3.
- [4] **IceCube** Collaboration, M. G. Aartsen et al., *ApJ* **835** (2017) 151.
- [5] **IceCube** Collaboration, M. G. Aartsen et al., *ApJ* **796** (2014) 109.
- [6] **H.E.S.S.** Collaboration, F. Aharonian et al., *A&A* **477** (2008) 353-363.
- [7] **Telescope Array** Collaboration, R. Abbasi et al., *ApJ* **790** (2014) L21.
- [8] **KASCADE-Grande** Collaboration, [PoS \(ICRC2015\) 812](#) (2016).
- [9] J. Braun et al., *ApJ* **29** (2008) 299-305.
- [10] **IceCube** Collaboration, M. G. Aartsen et al., *Phys. Rev. D* **91** (2015) 122004.

## Search for a cumulative neutrino signal from blazar flares using IceCube data

---

### The IceCube Collaboration<sup>†</sup>

<sup>†</sup> [http://icecube.wisc.edu/collaboration/authors/icrc17\\_icecube](http://icecube.wisc.edu/collaboration/authors/icrc17_icecube)

E-mail: [christoph.raab@ulb.ac.be](mailto:christoph.raab@ulb.ac.be)

Blazars are active galactic nuclei which have their relativistic particle jet pointing towards Earth and have been observed to emit gamma rays to very high energies. They are also candidates for the yet-unknown accelerators of ultra-high-energy cosmic rays. In such a scenario, their gamma-ray emission might be associated with neutrinos produced by hadronic interactions in the jet. Correlating the astrophysical neutrinos detected by IceCube, a cubic-kilometre neutrino telescope at the South Pole, with the gamma-ray emission from blazars could therefore reveal the origin of cosmic rays. In our method we focus on periods where blazars show an enhanced gamma-ray flux, as measured by Fermi, thereby reducing the background of the search. At the same time we test for the combined emission of a whole blazar population in a stacked search. A detection of such a neutrino flux could lead to the discovery of a source class responsible for cosmic-ray acceleration. We present sensitivities and discovery potentials for a selection of Fermi monitored sources and one year of IceCube data.

**Corresponding authors:** Christoph Raab and Kevin J. Meagher<sup>\*1</sup>

<sup>1</sup> *Université libre de Bruxelles, Science Faculty CP230, B-1050 Brussels, Belgium*

*35th International Cosmic Ray Conference — ICRC2017  
10–20 July, 2017  
Bexco, Busan, Korea*

---

\*Speaker.

## 1. Introduction

One hundred years after the discovery of ultra-high-energy cosmic rays (UHECR), their accelerators are still unknown. On their way from the source to Earth, CR get deflected by magnetic fields and thus do not point back to their origin. High-energy neutrinos are produced in cosmic-ray interactions in the dense and energetic environment of the sources, or along their path of propagation. Thanks to their small interaction cross-section and because they have no charge, they can escape these environments and pass undeflected through magnetic fields. Therefore, neutrino astronomy is one of the most promising avenues for identifying the origin of high-energy cosmic rays [1].

IceCube is a neutrino telescope instrumenting a cubic kilometre of glacial ice at the South Pole with 5160 light-detecting modules [2]. When a neutrino interacts in the ice or bedrock, its energy and arrival direction can be reconstructed from the measured Cherenkov radiation induced by the secondary charged particles produced in the interaction. In the case of a the charged-current interaction of a  $\nu_\mu/\bar{\nu}_\mu$ , this yields a median angular resolution smaller than  $1^\circ$  for energies exceeding 2 TeV [3].

IceCube has detected a diffuse flux of astrophysical neutrinos of that same flavour [4], but so far no spatial clustering around any particular point source. For IceCube to detect such a clustering by distinguishing individual sources from any source population, its density  $\rho$  must be sufficiently small. On the other hand, a sufficient luminosity  $L$  is required if a source class should have an emission per volume  $L \cdot \rho$  that contributes significantly to the astrophysical flux [5] [6].

As can be seen in [5], blazars do fulfil both these criteria. They are also known to be highly variable sources of gamma rays. The gamma rays on their own however do not prove cosmic-ray acceleration, since they could be leptonic or hadronic in origin. Several models predict hadron acceleration by internal shocks in blazar jets and predict emission of both gamma rays and high-energy neutrinos [7]. The discovery of a correlation between gamma-ray flares and a neutrino flux would imply at least a partially hadronic production mechanism of the observed gamma rays, and thus identify blazars as cosmic-ray accelerators.

Following the arguments in [5], the low source density of blazars also means that if they were responsible for the entire astrophysical neutrino flux, the closest one should already have been detected as a point source. A stacking analysis of 149 HBL<sup>1</sup> blazars from the 2FHL catalogue [8] excludes them from emitting more than 4.5%-5.7% of the astrophysical  $\nu_\mu/\bar{\nu}_\mu$  flux at 90% C.L.. However, if their emission in neutrinos is concentrated in flares like it is for gamma rays, an analysis that exploits this extreme variability might still detect a flux whose time integral is below this limit.

Here we present a search for high-energy neutrinos detected by IceCube correlated in time with the combined gamma-ray flux measured by the Fermi Large Area Telescope (LAT) from a set of blazars. Contrary to previous analyses which focused on individual flaring sources [9], we apply a stacking approach (see [10] for details on the stacking technique), which improves our sensitivity to a weak signal.

---

<sup>1</sup>high synchrotron peaked BL Lac

## 2. Analysis Method

### 2.1 Likelihood

Our analysis is based on a maximum likelihood ratio method, as has been used before in time-integrated searches for single point sources (e.g. [3]). The signal hypothesis represented in this likelihood depends on the position, strength and spectral index of a source's emission. For our search focused on flares, we augment the signal hypothesis for a source ( $k$ ) by a time distribution  $\mathcal{S}^{(k)}(t)$ . We derive this from Fermi-LAT light curves (see sec. 3) by applying a flux threshold  $\Phi_0^{(k)}$  and normalising the result. The likelihood then considers events where the flux is below threshold as entirely background-like.

$$\mathcal{L}^{(k)}(t|\text{LC}_k, \Phi_0^{(k)}) = \max \left\{ \left( \text{LC}_k(t) - \Phi_0^{(k)} \right) / \text{norm}, 0 \right\} \quad (2.1)$$

In previous time-dependent analyses such as [9], this threshold was left as a free parameter between 0 and the maximum of the light curve to reflect the fact that we expect enhanced neutrino emission to occur during the flaring states, but to an unknown degree. At a threshold of 0, all the gamma-ray emission would be related to neutrino emission and thus directly proportional.

In a stacked search as described in [10], the global signal hypothesis is a sum of the local hypotheses for a catalogue of sources. We assume these to have identical spectral indices and source strengths proportional to the global strength by a normalised weight  $w^{(k)}$ :

$$S(x, E|\gamma) = \sum_{k \in \text{sources}} w^{(k)}(\gamma) \mathcal{S}^{(k)}(\gamma) \quad (2.2)$$

Here,  $w^{(k)}$  expresses any assumptions about the relative brightness of each source's neutrino flux as well as the detector response at their respective declinations.

We choose to fix the spectral index in order to avoid an increased effective trial factor and numerical challenges. This can be partially justified by an analysis of bright blazar flares [11] which shows their spectral indices to be constrained to 1.9–2.6, with flares longer than  $\sim 1$  day converging to 2.3–2.4.

When applying this principle to a time-dependent analysis, we can make the equivalent argument for the flux threshold and assume that no source produces neutrinos during its quiescent period. We express this as a fixed threshold  $\{\Phi_0\}_{\text{est.}}^{(k)}$  estimated for each light curve individually, to accommodate their different brightness and variability characteristics.

$$\mathcal{S}_i(x, E, t|\gamma) = \sum_{k \in \text{sources}} w^{(k)}(\gamma) \mathcal{S}^{(k)}(x, E, t|\gamma, \{\Phi_0\}_{\text{est.}}^{(k)}) \quad (2.3)$$

We perform this threshold estimation starting from the denoised Bayesian block representation of the light curve (see sec. 3). We take the derivative, i.e. for each adjacent block the difference between their fluxes divided by the distance of their centres  $(\Phi_{i+1} - \Phi_i)/(t_{i+1} - t_i)$ . By taking the time-weighted median of this derivative, we can select one half of the observed time where the light curve is locally most steady, largely independent of the overall variability of the light curve. We then use fluxes measured during this time to compute a mean flux. As the goal is to exclude low and

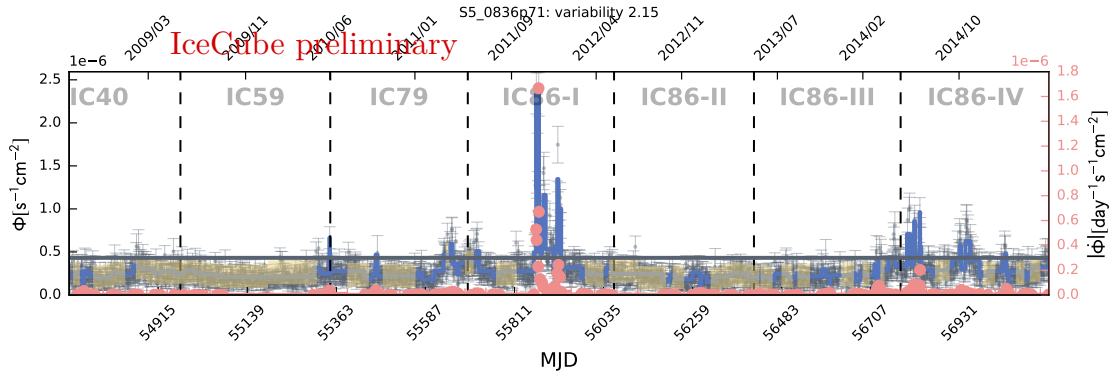


Figure 1: A light curve of the flat spectrum radio quasar S5 0836+71, covering the observation periods of the IceCube detector in its 40-string configuration, up to the fourth year of the completed detector with 86 strings (IC86-IV). The grey data points show the gamma-ray flux observed by the Fermi-LAT. The blue curve shows its denoised block representation. The time derivative between each two blocks is drawn as red points (right axis). We consider the time periods when the derivative does not exceed its median as quiescent (yellow bands). The mean flux during these time periods and the standard deviation determine the flux threshold (grey line).

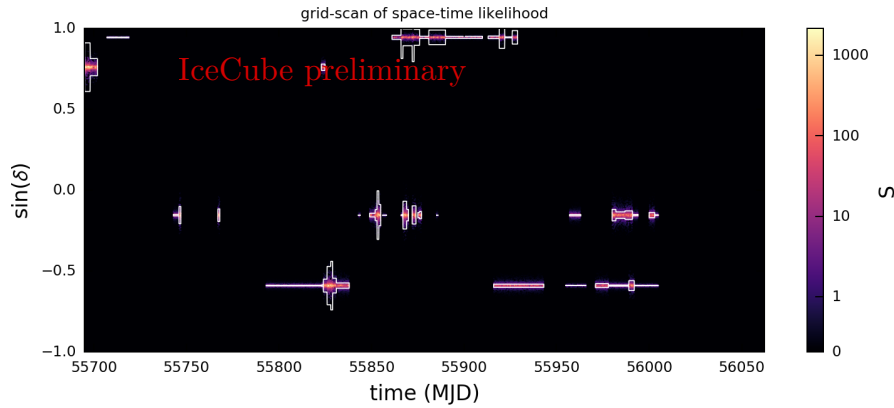


Figure 2: Illustration as the likelihood as a function of space and time for four sources, evaluated for a grid scan of the declination and time, maximised in right ascension. The time distributions for each source are drawn for comparison as white lines with an arbitrary scale.

steady fluxes in a robust way, we take the final threshold as this mean steady flux plus five times its root mean square deviation from the mean. We illustrate this procedure in figure 1. Figure 2 shows the space-time likelihood, i.e. the full likelihood without energy, evaluated for illustration on a grid scan given four arbitrary sources. Events which have a lower time likelihood need to be closer to the corresponding source in order to be treated equally.

## 2.2 Performance

In order to evaluate the sensitivity of the  $\log\mathcal{L}$ -derived test statistic to the addition of signal

events to pure-background data we use a toy Monte Carlo that generates background and signal events.

For the pure background case, we do this by choosing a random time for each event from within the **uptime** where the detector was taking data. These are equivalent, since seasonal variations do not play a role in the analysed sample [12]. For a neutrino entering the detector at the reconstructed local direction, and at the new, random time, we compute the new direction in equatorial coordinates. We keep all other event information, so that the data still describe the observed detector response. We call this procedure **time scrambling**, and it has been used previously in [9].

To generate signal data with an expected number of signal neutrinos  $\mu$ , each realisation is a mixture of a background time scrambling and a number of simulated events following a Poisson distribution of mean  $\mu$ . To simulate the point spread function, we consider Monte Carlo events from within a declination band for each source, and then rotate them so their true position is at the source. We draw events so that their energies follow a power-law flux (we use  $E^{-2}$  as a benchmark) from the sources in consideration. We also take the relative effective area of the detector at the respective declinations into account. We then assign every event belonging to a certain source a random time, again within the uptime but now weighted according to the time p.d.f. used for this source (we use the same as in the likelihood, see sec. 2.1).

Ultimately we can evaluate the performance of the method by determining the  $\mu$  at which the power  $\beta = 0.5$  of the hypothesis test corresponds to a certain significance. Specifically we determine the median  $5\sigma$  discovery potential with  $\alpha = 2.87 \times 10^{-7}$  by extrapolating the background-only test statistic distribution (see fig. 3).

### 3. Fermi Data and Source Selection

The analysis method described above requires continuous light curves for all sources. We therefore use data from the Fermi Large Area Telescope, which scans the entire sky every 3h [13]. The Fermi Monitored Source List<sup>2</sup> comprises 148 sources which at the time of writing have experienced a strong flare during the Fermi mission. We use the SIMBAD astronomy database<sup>3</sup> to remove non-AGN objects and assume that the rest are blazars. This includes eight sources not directly identified by SIMBAD of which three have been identified as blazars in literature: PKS 1510-08 9 [14], S5 0716+714<sup>4</sup> and 0FGL J0910.2-5044 [15]. This leaves 125 sources to be analysed for their variability. In the final analysis we will use source classification from the third Fermi catalogue, 3FGL<sup>5</sup>.

For each of these sources we derive the gamma-ray light curves with aperture photometry using the `Fermi Science Tools v10r0p5`<sup>6</sup>. We take photons above 100MeV in a  $2^\circ$  radius around the source location. This radius corresponds approximately to the 68% containment radius at 200MeV. We correct for the loss of photons outside the analysis region, an effect which decreases with energy [13]. We apply further selection criteria and processing according to [12] and

<sup>2</sup>[https://fermi.gsfc.nasa.gov/ssc/data/access/lat/mssl\\_lc/](https://fermi.gsfc.nasa.gov/ssc/data/access/lat/mssl_lc/)

<sup>3</sup><http://simbad.u-strasbg.fr/simbad/>

<sup>4</sup><http://tevcat.uchicago.edu/?mode=1&showsrc=172>

<sup>5</sup>[https://fermi.gsfc.nasa.gov/ssc/data/access/lat/4yr\\_catalog/](https://fermi.gsfc.nasa.gov/ssc/data/access/lat/4yr_catalog/)

<sup>6</sup><https://fermi.gsfc.nasa.gov/ssc/data/access/lat/>

0716+714	4C +28d07	OG 050	PKS 0521-36	S5 1803+78
1150+497	B2 1520+31	OJ 287	PKS 2247-131	TXS 1530-131
1510-089	BL Lac	PKS 0402-362	PMN J1038-5311	
1633+382	CTA 102	PKS 0454-234	PMN J2345-1555	
3C 279	NRAO 676	PKS 0502+049	S5 0836+71	

Table 1: Preliminary list of sources selected for the analysis.

count the photons in 1-day bins. After removing days without observations or low exposure, we then denoise the daily measurement using the Bayesian block algorithm [16] which seeks to combine those sequences of bins which are compatible with a constant emission. We also follow [12] in selecting the most variable light curves during the analysis period. The cut is described by

$$\frac{\Phi_{\max} - \Phi_{\min}^{(80)}}{\langle \Phi^{(80)} \rangle} > 1 \quad (3.1)$$

where  $\Phi_{\min}^{(80)}$  is the minimum flux within the central 80% of blocks, and  $\langle \Phi^{(80)} \rangle$  is the mean flux calculated over the same set. Since the Fermi Monitored Source List<sup>7</sup> is selected by applying a threshold of  $10^{-6} \text{ cm}^{-2} \text{ s}^{-1}$  to the observed flux without an absolute flux calibration, we also re-apply this cut to the calibrated fluxes. We therefore end up with a subset of 22 from the sources used in [12], which are listed in table 1.

#### 4. Discovery Potentials

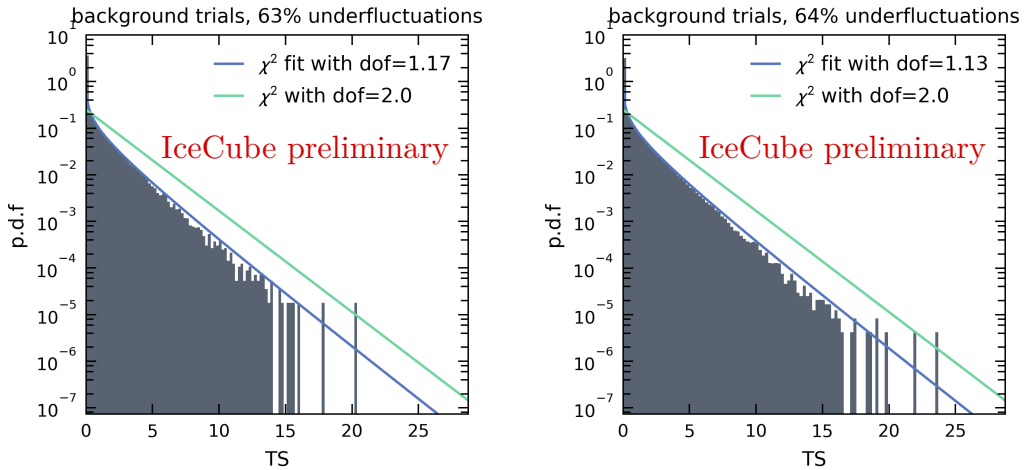


Figure 3: Distribution of the test statistic for trials on realisations of the background-only hypothesis (**grey**), with (**left**) and without (**right**) relative source weights in the likelihood. To compute the discovery potentials, we extrapolate with the fit  $\chi^2$  distribution (**blue line**); we show the classical assumption of  $n_{\text{dof}} = 2$  for comparison.

<sup>7</sup>[https://fermi.gsfc.nasa.gov/ssc/data/access/lat/msl\\_lc/](https://fermi.gsfc.nasa.gov/ssc/data/access/lat/msl_lc/)

We use the same sample of events as [3] during the first season of IceCube data-taking in its full configuration. In figure 4 (**left**) we show  $5\sigma$  median discovery potentials for an individual source while varying the threshold of the light curve. This shows how the discovery potential depends on the amount of background that is removed by the time-dependency; assuming a higher threshold, fewer events are needed. In the stacked case, we instead predefined the threshold using the light curve data (see sec. 2.1). In the following we use two different signal hypotheses. First, we assume that the neutrino flux is proportional to the gamma-ray flux above the threshold, and weight the likelihood for each source according to the integrated gamma-ray flux. This reflects the case where for each source the fraction of hadronically produced gamma rays is equal. Second we assume equal weighting such that each source has the same neutrino fluence. The resulting background test statistic distributions and their respective extrapolations are shown in 3. The effective degrees of freedom are now closer to 1 than to 2, as the fit shows. For each signal hypothesis we use the respective model in the signal injection, which is the most optimistic case, to arrive at the discovery potentials in figure 4 (**right**). There, we have done this calculation not only for the full source list, but also for any subset of the  $N$  brightest sources, according to the integrated gamma-ray flux. We show that many sources that are individually undetectable can sum up to a discovery in the stacking. Typically we can expect a discovery for stacking 10 sources if  $\sim 1$  neutrino is detected from each.

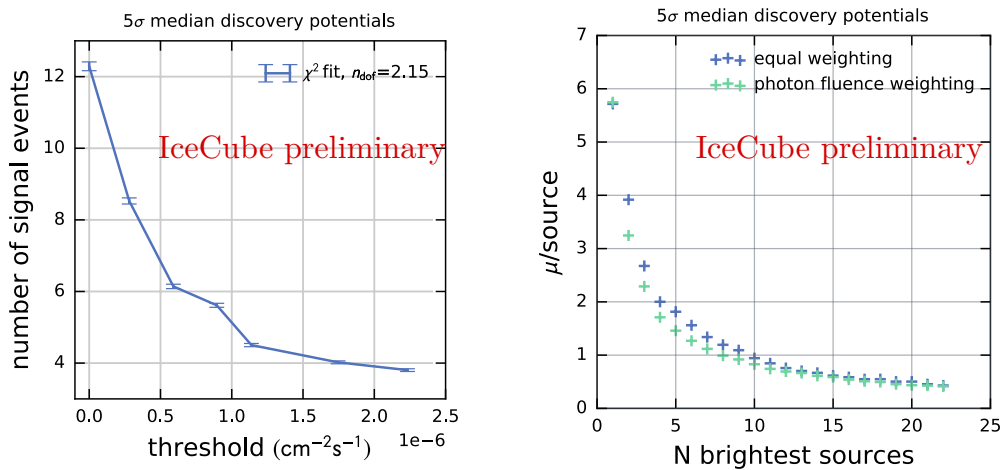


Figure 4: **Left:**  $5\sigma$  median discovery potentials in terms of detected neutrinos per source, for a single source, varying the flux threshold in the definition of the time distribution (see eq. 2.1). **Right:** The same for several possible combinations out of the total 22 sources by taking the  $N$  sources with the highest fluence integrated above the light curve threshold, for  $N \in \{1, \dots, 22\}$ . Points in blue assume the neutrino emission is equal for each source, and points in green assume it is proportional to the same total fluence as used for the ordering.

## 5. Conclusions and Outlook

We have shown that our implementation of the method fulfils its goals with respect to reducing background via time-dependence, and increasing sensitivity via stacking. Nevertheless, several

enhancements are possible both for the method itself and its application. The former includes an improved extrapolation of the TS distribution that gives less conservative discovery potentials than the currently used fit, a more realistic estimation of the thresholds, with a possible common parameter analogous to figure 4 (left). For the weights, the existing assumptions could be more closely motivated by the expected hadronic character of the source according to astrophysical arguments. Alternatively we could fit the weights, which in the case of non-detection might improve the limits provided the expected weighting varies by orders of magnitude. We further need to characterise the biases of the  $\log\mathcal{L}$  fit, especially to allow interpretation in case of a discovery. In either case, we should ultimately express the number of signal events in terms of a flux in order to allow comparisons to astrophysical models as well as other analyses.

Once the analysis method is finalised we will apply it to all years of available IceCube data. This will in turn lead to a longer source list. We can then apply more stringent criteria on the object type, using other catalogues such as 3FGL<sup>8</sup>, to facilitate interpretation of limits or discoveries. To the same end, we could split up the source list into subsets according to their weight. Their light curves should be derived using likelihood analysis instead of aperture photometry. Then astrophysical models can be used where appropriate to give the neutrino time profile. Finally, it is important to keep in mind that so far we are using IceCube data optimised for time-integrated searches. It is possible that a data sample with a higher background contamination but also higher signal efficiency will prove more suitable.

## References

- [1] M. Kowalski, *arXiv:1411.4385 [astro-ph.HE]* (2014).
- [2] **IceCube** Collaboration, M. G. Aartsen, et al., *JINST* **12** (2017) P03012.
- [3] **IceCube** Collaboration, M. G. Aartsen, et al., *Astrophys. J.* **835** (2017), 2 151.
- [4] **IceCube** Collaboration, M. G. Aartsen, et al., *Astrophys. J.* **833** (2016), 1 3.
- [5] P. Mertsch, M. Rameez, and I. Tamborra, *JCAP* **1703** (03, 2017).
- [6] P. Lipari, *Phys. Rev.* **D78** (2008), 083011.
- [7] W. Essey, et al., *AAS Meeting* **224** (2009), 407.06.
- [8] **IceCube** Collaboration, *POS (ICRC2017) 994* (2017).
- [9] **IceCube** Collaboration, M. G. Aartsen, et al., *Astrophys. J.* **807** (2015), 46.
- [10] **IceCube** Collaboration, M. G. Aartsen, et al., *Astrophys. J.* **835** (2017), 1 45.
- [11] K. Nalewajko, *MNRAS* **430** (2012), 2 1324–1333.
- [12] A. Christov. PhD thesis, Université de Genève, 11/01, 2016. ID: unige:91766.
- [13] **Fermi** Collaboration, W. B. Atwood, et al., *Astrophys. J.* **697** (2009) 1071–1102.
- [14] D. C. Homan, et al., *Astrophys. J.* **580** (12, 2002) 742–748.
- [15] N. Mirabal, *arXiv:0908.1389 [astro-ph.HE]* (2009).
- [16] J. D. Scargle, et al., *Astrophys. J.* **764** (02, 2013) 26 pp. ID 167.

---

<sup>8</sup>[https://fermi.gsfc.nasa.gov/ssc/data/access/lat/4yr\\_catalog/](https://fermi.gsfc.nasa.gov/ssc/data/access/lat/4yr_catalog/)

## Investigation of Obscured Flat Spectrum Radio AGN with the IceCube Neutrino Observatory

---

### The IceCube Collaboration<sup>†</sup>

<sup>†</sup> [http://icecube.wisc.edu/collaboration/authors/icrc17\\_icecube](http://icecube.wisc.edu/collaboration/authors/icrc17_icecube)

E-mail: [giuliano.maggi.olmedo@gmail.com](mailto:giuliano.maggi.olmedo@gmail.com)

The IceCube Collaboration recently reported the first detection of high-energy extraterrestrial neutrinos. Nonetheless, their origins are still unknown. In view of the IceCube discovery, active galactic nuclei (AGN) and gamma-ray bursts (GRBs) have been explored as possible sources, but no significant neutrino flux from these objects has been observed yet. The AGN that have previously been investigated by IceCube are characterized by a large gamma-ray flux as observed by dedicated instruments like the Fermi Space Telescope. In these bright AGN, neutrinos are expected to be generated via charged pion decay, as counterparts of the  $\gamma$ -rays produced by the decay of neutral pions. In contrast to the previously studied objects, it is also possible to target a specific class of AGN that show weak emission at the highest frequencies. These so-called “Obscured Flat Spectrum Radio AGN” show indications for a radio jet pointing towards Earth, as well as a column of matter in our line of sight that blocks high-energy electromagnetic emission from the central engine of the source. In addition to the blocked electromagnetic emission, a possible hadronic component will also be blocked by the obscuring material. This hadron beam dump is expected to give rise to an additional neutrino flux. Here we present results of a search for neutrino emission from selected AGN of this type using IceCube data.

**Corresponding authors:** Giuliano Maggi, Krijn D. de Vries, Nick van Eijndhoven\*  
Vrije Universiteit Brussel, Dienst ELEM, IIHE, Pleinlaan 2, 1050 Brussels, Belgium

*35th International Cosmic Ray Conference — ICRC2017*  
*10–20 July, 2017*  
*Bexco, Busan, Korea*

---

\*Speaker.

## 1. Introduction

Several neutrino astronomy analyses have been performed in order to find the origin of astrophysical high-energy ( $\sim$  TeV-PeV) neutrinos as the ones discovered by IceCube [1, 2]. Nevertheless, so far no significant evidence has been reported for a link between high-energy neutrino emission and a certain astrophysical source. The main source candidates for high-energy neutrino emission belong to two classes of astrophysical objects, Gamma Ray Bursts (GRBs) and Active Galactic Nuclei (AGN).

The main characteristic of the investigated subclasses of AGN [3, 4, 5] is that they have a large  $\gamma$ -ray flux as observed by dedicated telescopes. In this scenario, the neutrino production is expected to be dominated by the interaction of accelerated protons with ambient photons ( $p\gamma$ ) in the AGN environment. These interactions produce neutrinos via the decay of various charged mesons, where the decay of neutrons and muons can also contribute to the neutrino production (see for example [6]). The  $\gamma$ -ray flux could have a hadronic origination, which is dominated by the decay of various neutral mesons that are produced as a consequence of the  $p\gamma$  interaction. Therefore, one can argue that the larger the charged meson multiplicity is, the larger is the neutral meson production, and consequently the neutrino -  $\gamma$ -ray correlation can be established.

The efficiency of the expected neutrino production in bright AGN via  $p\gamma$  interactions depends on several factors, as for example, the photon field density in the AGN environment, and the fraction of  $p\gamma$  interactions that indeed produces neutrinos [7]. However, another channel to produce high-energy neutrinos in AGN could be via hadronuclear interactions ( $pp$ ) [6, 8]. In this context, the existence of hidden Cosmic-Ray accelerators has been proposed [9], where by comparing the neutrino flux detected by IceCube with the  $\gamma$ -rays observed with the Fermi telescope, a tension is observed, if one considers only neutrino production from  $p\gamma$  interactions.

In this work, we present the results of a search for high-energy neutrinos ( $\nu_\mu + \bar{\nu}_\mu$ ) with the IceCube neutrino observatory from a specific class of AGN, called ‘‘Obscured Flat Spectrum Radio AGN’’ (OFSR-AGN) [10]. OFSR-AGN, that fall into the category of hidden cosmic-ray accelerators, show indications of a possible radio jet which is pointing towards Earth and a surrounding column of matter in our line of sight, which blocks the electromagnetic emission at the highest frequencies, as in the X-ray domain. Therefore, instead of being bright objects, OFSR-AGN are opaque at short wavelengths, whereas emission of long wavelengths, as radio, is not affected by the obscuring material. If hadronic acceleration takes place at OFSR-AGN, neutrino production is expected via the ‘‘standard’’  $p\gamma$  interaction. However, a second component is expected to enhance the neutrino production in OFSR-AGN via hadron-column of matter interactions. The hadrons that interact with matter are expected to be the primary ones that did not interact with the ambient photons, or the ones that follow from the  $p\gamma$  interactions.

The current analysis is based on the investigation of 14 OFSR-AGN with four years of data collected at the IceCube neutrino observatory at the South Pole, between 2012 April 26 and 2016 May 20. We specifically search for muons induced by muon-neutrino ( $\nu_\mu + \bar{\nu}_\mu$ ) interactions in or nearby the IceCube detector, because these provide the best directional information. Our data as obtained at the South Pole is dominated by atmospheric muons, nonetheless, after several event selection procedures, we obtain an irreducible atmospheric neutrino event rate. Subsequently, to distinguish atmospheric neutrinos from astrophysical neutrinos, we use an unbinned likelihood

method as described in [11]. The results obtained from the current analysis show no significant neutrino emission from the investigated population of OFSR-AGN. We present a 90% upper limit for each investigated source, for an  $E^{-2}$  power-law neutrino emission spectrum.

## 2. Obscured Flat Spectrum Radio AGN

OFSR-AGN are characterized by having a flat spectrum radio emission, and by being obscured by a column of matter that blocks our line of sight at frequencies in the  $X$ -ray domain. The latter could be a consequence of a tilted AGN torus, a misaligned disc or any column of matter in the AGN environment that causes the AGN obscuration phenomenon [12, 13].

An OFSR-AGN catalog based on radio and  $X$ -ray observations was constructed in [10]. The selection procedure started from an initial sample of 735 objects obtained from the second catalog of AGN detected by *Fermi*-LAT (2LAC) [14], and from a catalog of strong radio-emitting galaxies (referred to as the Nijmegen radio catalog) [15]. A first selection was made by selecting objects that are not expected to have an  $X$ -ray flux attenuation due to intergalactic medium or redshift effects. After applying a redshift selection  $z < 0.17$ , the initial sample of 735 objects is reduced to 209 sources.

In OFSR-AGN, a particle emission is required to be directed towards Earth, consequently, we require that the AGN radio jet points towards the observer, which is usually indicated by a flat radio spectrum. As outlined in [10], this can be determined by the value of the radio spectral index  $\alpha_R$  in the power law  $F_\nu \propto \nu^{\alpha_R}$ , where objects with  $\alpha_R > -0.5$  are typically classified as Flat Spectrum Radio Quasars or BL Lac objects. After selecting objects with  $\alpha_R > -0.5$ , a total of 98 sources remain.

In order to discriminate OFSR-AGN from non obscured AGN, the luminosity intensity at a frequency of  $\nu_{X\text{-ray}} = 3.03 \cdot 10^{17}$  Hz is analyzed, as explained below. Using the NASA/IPAC Extragalactic Dataset (NED) [16], 62 objects out of 98 sources have measurements at  $\nu_{X\text{-ray}}$ .

As outlined in [10], for the remaining 62 objects, three source categories are distinguished according to various signatures in the electromagnetic domain. The categories are Flat Spectrum Radio Quasars (FSRQs) (14), BL Lacertae (BL Lac) objects (45) and Ultra Luminous Infrared Galaxies (ULIRGs) (3).

In the FSRQ sample composed of 14 sources, the galaxy 3C273 is excluded from the analysis because of the exceptionally strong  $X$ -ray and radio emission, which implies that 3C273 does not qualify as an obscured source.

The ULIRG sample is composed of 3 objects, including the galaxy NGC 3628, also known as the ‘‘Hamburger Galaxy’’. For this galaxy, the  $X$ -ray measurements given in NED are unsuitable for further analysis of the corresponding  $X$ -ray frequency. The large uncertainties of the two fluxes given by Chandra and XMM telescopes as presented in [16], make these measurements compatible with background, which would imply that these space telescopes did not have the capability to detect a clear signal at  $\nu_{X\text{-ray}} = 3.03 \cdot 10^{17}$  Hz, or indeed this object has a very low  $X$ -ray emission. However, the latter fact in addition to detailed telescopic views as shown in Fig. 1, make it worthwhile to investigate this object as a possible neutrino source powered by proton-matter interactions. Consequently, this object was also studied using IceCube data.



**Figure 1:** The galaxy NGC 3628, which is categorized as an Ultra Luminosity Infra Red Galaxy (ULIRG) in [10]. Credits: [16]

After excluding the galaxy 3C273, and the separate treatment of NGC 3628, 60 objects remain, which are grouped in two categories, BL Lac and FSRQ-ULIRG. The latter contains FSRQ and ULIRG galaxies, which are treated in a similar way due to the similarity in radio and X-ray emission. To determine whether a source has low emission compared with objects in the same category, source intensities at  $\nu_{X\text{-ray}}$  are compared.

To avoid the classification of OFSR-AGN as a consequence of low X-ray emission due to a weak central engine instead of a weak X-ray emission due to absorption by a column of matter in our line of sight, the X-ray luminosity is normalized to the radio luminosity for the FSRQ-ULIRG category. For objects in the BL Lac category, no correlation between X-ray and radio is observed [10], therefore, no further normalization is applied to the X-ray intensity of objects in the BL Lac category.

Considering the two categories and a normalization factor for FSRQ-ULIRG objects, the intensity  $I$  for the selection of OFSR-AGN is given by  $I_B = L_{X\text{-ray}}$  for objects in BL Lac category, and  $I_{F-U} = L_{X\text{-ray}}^\beta / L_{\text{radio}}$  for objects classified as FSRQ-ULIRG, where  $\beta$  is the normalization factor as computed in [10],  $L_{X\text{-ray}}$  is the X-ray luminosity at  $3.03 \cdot 10^{17}$  Hz and  $L_{\text{radio}}$  is the radio luminosity at  $1.4 \cdot 10^9$  Hz. The final procedure to select OFSR-AGN considers the objects that have the lowest intensity  $I$  in each population, which are taken from the lowest quartile in each population [10].

The list of resulting OFSR-AGN objects as selected in [10], is presented in Table 1 together with the results obtained in the current work, which will be described later on.

### 3. The IceCube Detector and the Data Sample

The IceCube neutrino observatory is a cubic kilometer detector located at the geographic South Pole [18], which is buried 1450 meters under the ice surface (called InIce detector). The instrumented volume consists of an array of 86 vertical strings, where the data collection is performed by 5160 Digital Optical Modules (DOMs) that are attached to the strings. These DOMs are placed between 1450 and 2415 meters under the ice surface.

The horizontal string spacing corresponds to  $\sim 125$  meters, except for a denser core where the spacing amounts to about 70 meters. This denser IceCube instrumentation is called DeepCore,

which differs from the rest of the detector in order to perform neutrino studies at lower energy. The vertical spacing between DOMs in the DeepCore array corresponds to  $\sim 7$  meters, whereas the spacing in the rest of the instrumentation is  $\sim 17$  meters. Furthermore, the IceCube observatory has a dedicated instrumentation for studying cosmic-ray interactions with the terrestrial atmosphere. The latter is an array composed of 162 tanks of ice, located on the ice surface, which is called IceTop detector.

The IceCube event rate at South Pole amounts to  $\sim 2700$  Hz, which is highly dominated by atmospheric muons induced by cosmic-ray interactions with the terrestrial atmosphere. An IceCube event (InIce) is defined when at least four pairs of neighboring DOMs are fired within a time window of  $5 \mu\text{s}$ . If this condition to create an event is fulfilled, the times of the first ( $t_{init}$ ) and last ( $t_{last}$ ) trigger pulse are extended to read out the whole event in a time window of:  $[t_{init} - 10\mu\text{s}, t_{last} + 22\mu\text{s}]$  [19].

After a first data processing at the South Pole to reject atmospheric muon events in the IceCube detector, the event rate is reduced to  $\sim 600$  Hz. These events are then transmitted to the North via satellite, where further reconstructions and event selections are performed as in [4], until a final sample dominated by neutrinos with a rate on the order of 2.5 mHz is obtained. These events are predominantly atmospheric neutrino events, with a small contribution  $\lesssim 1\%$  estimated to be astrophysical neutrinos.

In the current analysis, we have used an energy estimator to improve the angular resolution, which acts as a “weight” for determining how likely the recorded pulses are created by a certain track hypothesis. This slight improvement in the angular resolution with respect to the one used in [4], is enhanced by the likelihood formula used in the analysis method as described in Section 4, which results in an improved sensitivity.

The sample used for this analysis contains tracks with a declination  $\delta > -5^\circ$ , such that we cover the region of the sky where the 14 OFSR-AGN are located. The total number of events in this IceCube data sample amounts to 315639 events, collected in 1414.7 days (2012-2015), that implies an event rate of 2.58 mHz.

#### 4. Analysis Method

In order to discriminate events caused by atmospheric neutrinos from their astrophysical counterpart, we apply the statistical method described in [11]. This is based on an unbinned likelihood ratio, where the likelihood function is given by,

$$\mathcal{L}(\vec{x}_s, n_s, \gamma) = \prod_i^N \left( \frac{n_s}{N} \mathcal{S}_i + \left(1 - \frac{n_s}{N}\right) \mathcal{B}_i \right), \quad (4.1)$$

where  $x_s$  is the source position, and  $n_s$  and  $\gamma$  are the best-fit values for the number of signal events and spectral index due to a neutrino source located at  $x_s$ . We will refer to  $\gamma$  as  $\gamma_\nu$ . The expressions  $\mathcal{S}$  and  $\mathcal{B}$  correspond to the signal and background probability density functions respectively, and  $N$  indicates the total number of events (signal plus background). The details of Eq. 4.1 can be found in [11].

The test statistic can be constructed from the likelihood function in Eq. 4.1, which can be written as,

$$\lambda = 2 \cdot \text{sign}(n_s) \log \left[ \frac{\mathcal{L}(\vec{x}_s, n_s, \gamma_v)}{\mathcal{L}(\vec{x}_s, 0)} \right], \quad (4.2)$$

where the larger  $\lambda$  is, the less compatible the observation is with the background only hypothesis.

The fit for the spectral index of the signal can help to distinguish astrophysical signal from atmospheric background, if the source energy spectrum is considerably harder than the background (approximately  $E^{-3.7}$ ). In the present analysis, we do not assume any particular model about the spectral index of the signal, so we let  $\gamma_v$  vary as a free parameter in the range  $1 \leq \gamma_v \leq 4$ .

## 5. Results

We perform the likelihood search method at each of the source locations in the catalog of OFSR-AGN objects, calculating  $\lambda$  for the choice of  $n_s$  and  $\gamma_v$  that maximize the value of the likelihood function. We estimate the significance (p-value) of each result by performing the same analysis on the data when it is scrambled in right ascension, and counting the fraction of such scrambled trials which yield a  $\lambda$  more significant than the one obtained for the real data. The results obtained from the IceCube search for high-energy neutrino emission ( $\nu_\mu + \bar{\nu}_\mu$ ) from OFSR-AGN, show that there is no significant evidence that indicates high-energy neutrino production at the investigated sources.

The search for  $\nu_\mu + \bar{\nu}_\mu$  inducing a muon as a consequence of a neutrino charged current interaction in or nearby the IceCube detector, was performed using four years of IceCube data. We have set a 90% upper limit  $\Phi^{90\%}$  on the neutrino flux ( $\nu_\mu + \bar{\nu}_\mu$ ) emitted from each source in the OFSR-AGN sample, as displayed in Table 1. This was calculated assuming a power-law of  $\frac{d\Phi_\nu}{dE} \propto E^{-2}$  for energies between 1 TeV - 1 PeV. Furthermore, in Table 1, we present the pre-trial p-values, the best-fitting spectral index  $\gamma_v$  and the number of signal-like events  $n_s$  as provided by the maximization of the likelihood formula. In addition, we give the position (declination  $\delta$  and right ascension ra) of each source.

As shown in Table 1, the two most significant pre-trial p-values are 0.034 and 0.037, which correspond to the objects NGC 3628 and 2MASXJ05581173+5328180 respectively. For the more significant source, NGC 3628, we determine the post-trial p-value, which amounts to 0.3. Nevertheless, since we obtain two sources with approximately equal pre-trial p-values, we also determine an a-posteriori p-value. This a-posteriori p-value reflects the probability of finding 2 out of 14 sources with such a p-value to be 0.08. This is also compatible with background.

## 6. Discussion

The IceCube investigation of 14 sources classified as Obscured Flat Spectrum Radio AGN shows no significant evidence for neutrino emission from the analyzed astrophysical objects. The two most significant sources belong to the same category (FSRQ-ULIRG), these galaxies are NGC 3628 and 2MASXJ05581173+5328180, where the former is classified as an ULIRG and the latter as an FSRQ.

Moreover, the two sources with the largest significance have been investigated in the Nijmegen radio catalog as possible ultra-high-energy cosmic-ray emitters [15]. In this catalog, four groups of

Source name	ra (°)	$\delta$ (°)	p-val	$n_s$	$\gamma_\nu$	$\Phi^{90\%}$	Object-Class
2MASXJ05581173+5328180	89.55	53.47	0.037	16.12	2.73	1.08	FSRQ-ULIRG
MRK0668	211.75	28.45	0.300	2.48	3.76	0.88	FSRQ-ULIRG
NGC3628	170.07	13.59	0.034	6.88	2.21	0.72	FSRQ-ULIRG
ARP220	233.74	23.50	1.0	0.0	4.0	0.75	FSRQ-ULIRG
3C371	271.71	69.82	0.242	5.35	4.0	1.18	BL Lac
4C+04.77	331.07	4.67	0.412	0.73	2.05	0.65	BL Lac
1H1720+117	261.27	11.87	1.0	0.0	3.11	0.70	BL Lac
B21811+31	273.40	31.74	0.076	11.93	2.85	0.85	BL Lac
CGCG186-048	176.84	35.02	1.0	0.0	2.88	0.86	BL Lac
GB6J1542+6129	235.74	61.50	1.0	0.0	2.68	1.07	BL Lac
PKS1717+177	259.80	17.75	0.142	7.81	2.97	0.75	BL Lac
RGBJ1534+372	233.70	37.27	0.318	3.95	3.05	0.90	BL Lac
SBS0812-578	124.09	57.65	0.386	1.70	3.84	1.09	BL Lac
SBS1200+608	180.76	60.52	1.0	0.0	2.46	1.09	BL Lac

**Table 1:** List of sources in the AGN population and the their position (ra, $\delta$ ) in Equatorial coordinates in degrees. The following values correspond to the fit result that are obtained by maximizing the likelihood formula. Here we show the pre-trial p-value, the best fit number of signal events  $n_s$  and the spectral index  $\gamma_\nu$ . The upper limit on the  $\nu_\mu + \bar{\nu}_\mu$  flux  $\Phi^{90\%}$  is given in units of  $10^{-12}$  [TeV cm $^{-2}$ s $^{-1}$ ].

galaxies have been investigated which have been constructed according the source morphology and observations in the electromagnetic domain. These groups are: Starforming galaxies, Jets & Lobes, Point sources and Unknown morphology. The galaxy 2MASXJ05581173+5328180 is classified as a Point source, whereas NGC 3628 belongs to the Starforming galaxy category.

In view of the current results, a follow up study could be made by investigating ULIRG objects, Starforming galaxies and Point Source, where the last two would belong to a classification as made in the Nijmegen radio catalog [15]. This study can be accomplished by performing stacking analyses of the same class of objects. Moreover, in order to obtain more sources, an investigation on how to correct the observed flux for far away objects would be needed, since the redshift selection was the hardest cut that was used to construct the OFSR-AGN catalog [10]. On the other hand, to have a conception about the expected neutrino spectral index from OFSR-AGN could help on the search for neutrinos from these kind of sources, which implies a full modeling of the  $p\gamma$  and  $pp$  interactions, including secondary hadrons propagation through the AGN medium.

## References

- [1] **IceCube** Collaboration, M. G. Aartsen et. al, Science **342**, 1242856 (2013).
- [2] **IceCube** Collaboration, M. G. Aartsen et. al, Phys. Rev. Lett. **113**, 101101 (2014).
- [3] **IceCube** Collaboration, M. G. Aartsen et. al, Astrophys. J. **796**, 109 (2014).

- [4] **IceCube** Collaboration, M. G. Aartsen et. al, *Astrophys. J.* **835**, 151 (2017).
- [5] **IceCube** Collaboration, M. G. Aartsen et. al, *Astrophys. J.* **807**, 46 (2015).
- [6] Gaisser T. and Stanev T., *Astroparticle Physics* **39-40**, 120-128 (2012).
- [7] Reimer A., *Journal of Physics: Conference Series* **355**, 012011 (2012).
- [8] Murase K. et. al, *Phys.Rev.D* **88**, 121301 (2013).
- [9] Murase K. et. al, *Phys.Rev.Lett.* **116**, 071101 (2016).
- [10] Maggi G. et. al, *Phys.Rev.D* **94**, 103007 (2016).
- [11] Braun J. et. al, *Astropart. Phys.* **29**, 299-305 (2008).
- [12] Lawrence A. and Elvis M., *The Astrophysical Journal* **714**, 1 (2010).
- [13] Bianchi S., Maiolino R. and Risaliti G., *Advances in Astronomy* **2012**, Article ID 782030, 17 pages, (2012).
- [14] **Fermi-LAT** Collaboration, M. Ackermann et. al, *The Astrophysical Journal* **743**, 2 (2011).
- [15] van Velzen S. et. al, *A&A* **544**, 19 (2012).
- [16] NASA/IPAC Extragalactic Database (NED), <https://ned.ipac.caltech.edu>
- [17] Netzer H., “The Physics and Evolution of Active Galactic Nuclei”, Cambridge University Press (2013).
- [18] **IceCube** Collaboration, M. G. Aartsen et. al, *JINST* **12**, P03012 (2017).
- [19] **IceCube** Collaboration, M. G. Aartsen et. al, *Astropart. Phys.* **78**, 1-27 (2016).

## Realtime neutrino alerts and follow-up in IceCube

---

### The IceCube Collaboration<sup>†</sup>

<sup>†</sup> [http://icecube.wisc.edu/collaboration/authors/icrc17\\_icecube](http://icecube.wisc.edu/collaboration/authors/icrc17_icecube)

E-mail: [blaufuss@icecube.umd.edu](mailto:blaufuss@icecube.umd.edu)

Since the detection of a diffuse flux of high-energy astrophysical neutrinos in 2013 by the IceCube neutrino observatory, their origin so far has remained unknown. With no steady sources of neutrinos observed in IceCube data, neutrinos produced during transient astrophysical events are a viable alternative. Identification of an electromagnetic counterpart that is coincident in time and space would be strong evidence of a source of neutrinos. To support these searches, IceCube has implemented a realtime search for potentially astrophysical neutrino candidates that includes alerts to the community for rapid follow-up observations. This contribution will highlight the realtime analysis system, the current realtime alerts now being produced, and some preliminary results from the first alerts.

**Corresponding author:** E. Blaufuss<sup>1\*</sup>

<sup>1</sup> *Dept. of Physics, University of Maryland, College Park, MD 20742, USA*

*35th International Cosmic Ray Conference – ICRC2017-  
10-20 July, 2017  
Bexco, Busan, Korea*

---

\*Presenter

## 1. Introduction

The detection of a diffuse flux of astrophysical neutrinos by IceCube [1, 2] represented the "first light" in the new field of high-energy neutrino astronomy. The detection of neutrinos from a source would be a telltale sign of high-energy hadronic interactions, and could add to the understanding of the acceleration mechanism which produces the most energetic particles observed in the Universe, the highest energy cosmic rays [3]. Searches for point sources [4] in the IceCube data and dedicated follow-up searches [5] have failed to locate a potential source. By observing the location of these neutrinos long after the arrival of the neutrino, these searches have assumed a steady state source flux. If these astrophysical neutrinos are from a class of transient sources, more immediate follow-up observations are required.

Multimessenger astronomy, the combined observations in cosmic rays, neutrinos, photons of all wavelengths, and gravitational waves, represents a powerful tool to study the physical processes driving the high-energy universe. Neutrinos play an important role in this emerging field. Unlike photons and charged cosmic rays, the neutrinos' small cross section and absence of electric charge allow them to travel the cosmological distances necessary to reach Earth from source regions without absorption or deflection. Observation of these astrophysical neutrinos can provide critical directional information that can be used to direct rapid, follow-up observations. Several models [7, 8] predict emission from flaring objects or other transient phenomena, requiring a fast start to follow-up observations.

IceCube is a cubic-kilometer neutrino detector [9] installed in the ice at the geographic South Pole, Antarctica between depths of 1450m and 2450m. Detector construction was completed in 2010, and the detector has operated with a  $\sim 99\%$  duty cycle since. IceCube does not directly observe neutrinos, but rather the secondary particles produced in the neutrino interaction with matter. IceCube detects these particles by observing the Cherenkov light emitted as they travel through the Antarctic glacial ice. The ability to accurately determine the direction of a neutrino event recorded in IceCube is highly dependent on the ability to reconstruct these secondary particles.

These secondary particles can produce two distinct classes of signals within IceCube: tracks and cascades. Track events are produced by muons, arising mainly from the charged current interaction of muon-type neutrinos, which produce  $\mathcal{O}(\text{few})\text{km}$  long light paths as they transit the detector. These tracks can be reconstructed with a directional uncertainty less than  $1^\circ$ , but with large energy uncertainty since an unmeasured fraction of their energy is deposited outside the instrumented volume. Shower events are produced by the charged current interaction of electron and tau-flavor neutrinos and by neutral current interactions of all neutrino flavors. Shower events tend to deposit all their energy within  $\mathcal{O}(10)\text{m}$ , producing a relatively isotropic light emission. These shower events tend to have good energy resolution ( $\delta E/E \sim 15\%$  [10]), but have typical angular resolutions on the order of  $10 - 15^\circ$  [11].

Given the depth and the size of IceCube, the observed event rate for penetrating atmospheric muons is approximately 2.7 kHz. The neutrino detection rate (a few mHz) is dominated by atmospheric neutrinos, created in the air showers when cosmic rays interact with the Earth's atmosphere. The first challenge for the realtime alert system is to find a pure sample of neutrino events, and the second is to identify the small fraction of these neutrinos that are likely to be astrophysical in origin.

IceCube is sensitive to astrophysical neutrinos from the entire sky ( $4\pi$  steradians), making it

an ideal trigger for follow-up observatories around the globe. Given the modest field of view of most follow-up instruments, track events from astrophysical neutrino interactions are preferred for realtime follow-up alerts. The smaller directional uncertainties of track events also help to limit coincidental discoveries when sensitive telescopes are pointed at unexplored regions of the sky.

This contribution presents a summary of IceCube realtime system, which has enabled rapid identification and public notification following the detection of neutrino event candidates. Two neutrino event selections are used to generate the public notifications. First, a search for track-like starting events [12] is used to identify high energy neutrino interactions that occur within the IceCube instrumented volume and produce an outgoing track (HESE track alerts). Second, a high-energy track search, adapted from a selection used to identify cosmogenic neutrino candidates [13] identifies through-going track events likely of astrophysical origin (EHE track alerts). Alerts issued in the first year of operation are presented, as well as an outlook toward future extensions of these alerts to new classes of astrophysical neutrinos.

## 2. IceCube Realtime Alert System and Active Alerts

Given the remote location of the IceCube detector, all data collection, processing and filtering is automated. The IceCube realtime alert system [14] is also fully automated, as shown in Figure 1. Neutrino selections are hosted in the online event filtering system and identify neutrino alert candidates in realtime. For each alert candidate, two messages are generated. The first contains a brief summary of the event information and the second, a larger message that can take longer to transfer north, contains the full event information.

Once the brief summary message is in the north, alerts are automatically issued to Gamma-Ray Coordinates Network (GCN<sup>1</sup>) via the Astrophysical Multimessenger Observatory Network (AMON<sup>2</sup>). The full event information is used to start data quality checks and refined direction reconstructions of the event. These refined reconstructions improve the angular resolution by more than 50% and provide a measure of the energy loss within the detector volume. Additionally, data quality and visual checks of the event information are used to ensure the event is consistent with an astrophysical neutrino signal and not rare backgrounds, such as atmospheric muons that are not detected in veto regions. Results from these checks and follow-up reconstructions are completed within a few hours of the alert and result in an updated alert notification in the form of a GCN circular.

### 2.1 HESE Track Alerts

The IceCube high-energy starting event (HESE) search has resulted in a clear detection ( $> 6.5\sigma$ ) of astrophysical neutrinos [6]. HESE events are identified as high-energy events that deposit a substantial amount of charge measured by the IceCube DOMs ( $\geq 6000$  photoelectrons), and reconstruct with an event vertex within the instrumented detector volume. In 4 years of data, 54 HESE neutrino events have been identified, with 14 of these being track-like. Given the better angular resolution of tracks, only the track-like events identified online are considered for HESE alerts.

---

<sup>1</sup><https://gcn.gsfc.nasa.gov/>

<sup>2</sup><http://amon.gravity.psu.edu/>

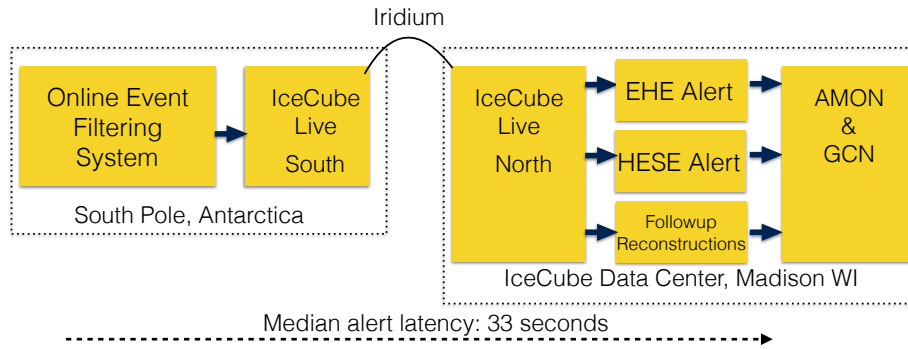


**Figure 1:** Overview of the realtime alert system. Events satisfying alert criteria are identified in the online event filtering system that operates in realtime at the detector site in Antarctica. Event summaries and event data are transferred to the north via the IceCube Live experiment control system [9] over an Iridium satellite connection. Once in the north, alerts are formatted for distribution to GCN via the AMON network. Additionally, full event information for each alert is used to trigger automated followup event reconstructions. Median latency for alerts, comparing the time of the neutrino event to the alert being issued, is 33 seconds.

Track events are classified online by a "signal-trackness" parameter [14] that uses the likelihood values returned from track and shower reconstructions to assign a numerical measure of how consistent each HESE event is with being a track. Events with a signal-trackness value  $\geq 0.1$  are classified as tracks.

Based on measured background event rates, and expectations based on the measured HESE neutrino flux [6], 4.8 alerts are expected per year. Of these, 1.1 are expected to be astrophysical, while 3.7 are from atmospheric background events, primarily rare cosmic ray muon events. Given their track nature these events have good angular uncertainty, as shown in Figure 2, based on simulated HESE event samples. Here, the median angular difference between the alert direction and true direction is  $0.55^\circ$  ( $1.89^\circ$  for 90% inclusion) for tracks with a reconstructed track length  $> 200$  m.

## 2.2 EHE Track Alerts

The extremely-high-energy (EHE) neutrino alert stream is based on an offline search for cosmogenic neutrinos that resulted in the serendipitous discovery of the first observed PeV-scale neutrinos [15]. The standard EHE analysis searches for neutrinos with energies of  $\sim 10$  PeV to 1 EeV, where the expected event rate in the most optimistic case is  $\sim 1$  event per year [13]. To move this analysis into the realtime framework the event selection was modified in order to increase the sensitivity to astrophysical neutrinos, specifically neutrino energies in the 500 TeV to 10 PeV range, which are track events with good angular resolution.

The EHE alert selection requires a minimum deposited charge of  $\sim 4000$  photoelectrons (NPE) detected in IceCube DOMs, as well as at least 300 DOMs registering a signal. A cut on deposited charge that strengthens with zenith angle for well reconstructed tracks is then applied [14] (see Figure 3) to reject events likely to be from atmospheric origins.

A "signalness" value is calculated for each track event, which reflects how likely each event is to be of astrophysical origin relative to the total background rate. This value is calculated from the

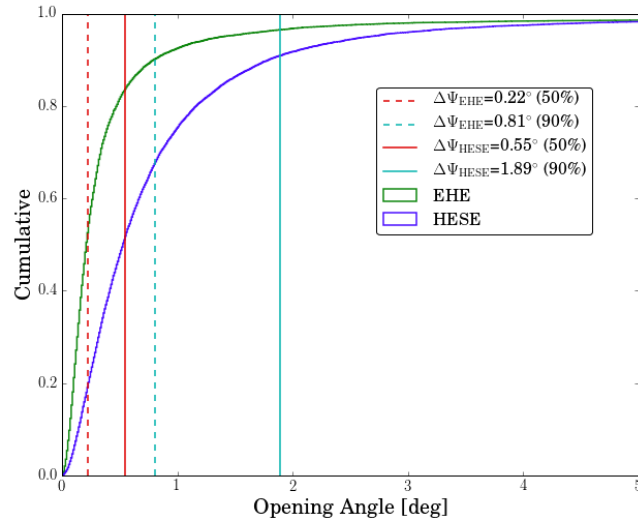


**Figure 2:** The cumulative distribution for the opening angle showing the radius containing 50% and 90% of simulated events for the HESE and EHE selected neutrino events. Figure adapted from [14].

expected number of astrophysical signal events for each energy and zenith combination relative to the total expected number (signal and background) of events, and is shown in Figure 3.

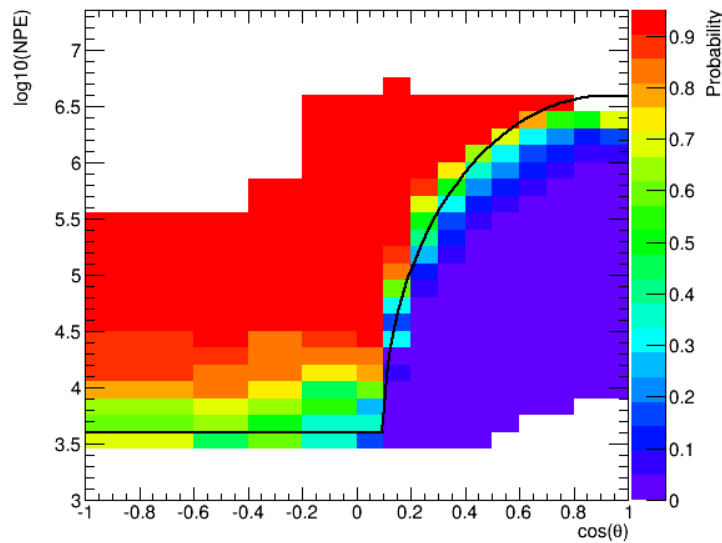


**Figure 3:** The two-dimensional signalness parameter depending on the reconstructed zenith angle ( $\cos(\theta)$ ) and total deposited charge ( $\log_{10}(\text{NPE})$ ) derived from simulated EHE alerts. Bins are only filled if a minimum threshold of signal events is met, and empty bins are indicated by white space. The black line represents the event selection criteria, with events above the line generating alerts. Figure adapted from [14].

The EHE track alerts are expected to issue  $\sim 5$  alerts per year. Of these alerts, 1.9 events will be from background events, primarily from high-energy atmospheric neutrino events, are expected.

2.5 - 4 alerts per year are expected from astrophysical neutrino events, depending on the assumed neutrino spectral index. As these events are through-going track events, the angular resolution is quite good. The median angular difference between the reported direction and true direction for a simulated sample of EHE alert candidates is  $0.22^\circ$  ( $0.81^\circ$  for 90% inclusion).

### **3. Alerts Issued**

Both the EHE and HESE event selections, as well as the software needed to handle the alerts were deployed to the IceCube detector site in early 2016. HESE alerts began operation in April 2016, and EHE alerts followed in July 2016. Since they began, nine alerts have been issued and are summarized in Table 1.

Each alert has generated follow-up observations that have been publicly reported to GCN or by Astronomer's Telegrams. No significant association with a transient source has yet been reported. Given the small cross section for neutrino interactions compared to other astronomical messengers, neutrinos that are created at extreme cosmological distances are still detectable at Earth. In this case signals in photons or gravitational waves are potentially too weak to be detected or show overlap with unrelated foreground objects that are detected in follow-up observations, but exhibit no flaring signal that would be expected from a transient source. Further follow-up observations will hopefully lead to a clear transient source detection, and a powerful hint to the underlying physics that drive the high-energy universe.

### **4. Future Outlook**

Now that the alert system is in stable operation, new alerts are being considered beyond the HESE and EHE channels. Additional through-going track candidates are found in the diffuse muon-neutrinos searches [17], and are being investigated as a supplement to the EHE track alerts. A new class of starting events is also being developed that will identify 1-2 additional starting tracks per year as an addition to the HESE track alerts. The non-track HESE shower events are also potentially interesting to wide field observatories like HAWC and Fermi. Even though the angular uncertainties of these events is  $\sim 10 - 15^\circ$ , a coincidence in time and space could still constitute a significant detection.

In addition to these public alerts, IceCube also has several agreements with optical, x-ray, and gamma-ray observatories to perform observations based on IceCube observed multiplets. These multiplets, observed as a cluster of events from the same direction on timescales of seconds to weeks, are dominated by accidental coincidences in the atmospheric background events. However, a neutrino detection from a gamma-ray burst, or an AGN flare would also trigger these follow-up observations. Searches for bursts of low energy neutrinos from nearby Supernova [18] are also performed as part of the SNEWS network [19]. Additionally, a fast-response neutrino point source analysis has been developed [20] to respond to external alerts from the wider astronomical community.

With the start of operation of the IceCube realtime alert system, the alerts generated by IceCube, and the potential discovery of transient astronomical sources in conjunction with them, the era of multi-messenger time domain astronomy has arrived. A clear multi-messenger detection

of a source holds the potential to enrich our understanding of the most energetic cosmic phenomena, shed light on the mysterious origins of the highest energy cosmic rays, and provide a unique window into the cosmos.

Additional information regarding the alerts from IceCube is at <https://gcn.gsfc.nasa.gov/amon.html>, and requests for additional information should be directed to the IceCube realtime coordination group ([roc@icecube.wisc.edu](mailto:roc@icecube.wisc.edu))

## References

- [1] **IceCube** Collaboration, M.G. Aartsen et al., *Phys. Rev. Lett.*, **115** (2015) 081102
- [2] **IceCube** Collaboration, M.G. Aartsen et al., *Astrophys. J.*, **833** (2016) 3
- [3] K.A. Olive et al., *Chin. Phys.*, **C38** (2014) 090001
- [4] **IceCube** Collaboration, [PoS \(ICRC2017\) 997](#), *These proceedings*
- [5] M. Santander, K. Satalecka, J. Dumm, et al., [PoS \(ICRC2017\) 618](#), *These proceedings*
- [6] **IceCube** Collaboration, [PoS \(ICRC2015\) 1081](#) (2016)
- [7] E. Waxman and J.N. Bahcall, *Phys. Rev. Lett.*, **78** (1997) 2292
- [8] S. Razzaque, P. Meszaros, and E. Waxman, *Mod. Phys. Lett. A***20** (2005) 2351
- [9] **IceCube** Collaboration, M.G. Aartsen et al. *JINST*, **12** (2017) P03012
- [10] **IceCube** Collaboration, M.G. Aartsen et al., *JINST*, **9** (2014) P03009
- [11] **IceCube** Collaboration, M.G. Aartsen et al., *Phys. Rev. Lett.*, **113** (2014) 101101
- [12] **IceCube** Collaboration, [PoS \(ICRC2017\) 981](#), *These proceedings*
- [13] **IceCube** Collaboration, [PoS \(ICRC2017\) 975](#), *These proceedings*
- [14] **IceCube** Collaboration, M.G. Aartsen, et al., *Astropart. Phys.*, **92**, (2017) 30
- [15] **IceCube** Collaboration, M.G. Aartsen, et al., *Phys. Rev. Lett.*, **111** (2013) 021103
- [16] **IceCube** Collaboration, M.G. Aartsen, et al., *Astrophys. J.*, **811** (2015) 52
- [17] **IceCube** Collaboration, [PoS \(ICRC2017\) 1005](#), *These proceedings*
- [18] **IceCube** Collaboration, R. Abbasi et al., *Aanda*, **535** (2011) A109
- [19] C Vigorito et al., *J. Phys.: Conf. Ser.*, **309** (2011) 012026
- [20] **IceCube** Collaboration, [PoS \(ICRC2017\) 1007](#), *These proceedings*

Alert:	160427A	160731A	160806A	160814A	161103A	161210A	170312A	170321A	170506A
Date	16/04/27	16/07/31	16/08/06	16/08/14	16/11/03	16/12/10	17/03/12	17/03/21	17/05/06
Time	05:52:32	01:55:04	12:21:33	21:45:54	09:07:31	20:06:40	13:49:39	07:32:20	12:36:56
RA (deg, J2000)	250.6	214.5	122.8	200.3	40.8	46.6	305.2	98.3	221.8
DEC (deg, J2000)	+9.3	-0.33	-0.8	-32.4	+12.6	+15.0	-26.6	-15.0	-26.0
Ang. Uncertainty (deg)	0.6	0.75	0.5	1.5	0.9	0.7	0.5	1.2	2.5
Dep. Energy	150 TeV	130 TeV	62 TeV	97 TeV	47 TeV	56 TeV	55 TeV	16 TeV	38 TeV
Alert Type	HESE	HESE/EHE	EHE	HESE	HESE	EHE	HESE	EHE	HESE
Signalness	0.92	0.91/0.85	0.28	0.12	0.30	0.49	0.78 <sup>†</sup>	0.28	0.35 <sup>†</sup>
Latency (sec)	81	41	37	42	37	27	59	13	1465
GCN Circular	19363	NA	19787	NA	20119	20247	20857	20929	21075

**Table 1:** Summary table of alert information from all IceCube EHE and HESE alerts sent since April, 2016. Name, date, time, right ascension (RA), declination (DEC), angular uncertainty, deposited energy, alert type, signalness measure, latency, and GCN circular reference is included for all alerts. Angular uncertainty values are listed for 90% containment radius, and any asymmetric error regions (available in the GCN circulars) have been averaged to a single value. Deposited energy is a preliminary measure of the energy detected within the IceCube instrumented volume [1] from the offline, follow-up reconstructions. Signalness values are the "signal-trackness" values for HESE alerts and the astrophysical signalness measure for EHE alerts. Signalness values marked with a † show signs of being consistent with expected non-astrophysical backgrounds. The large latency of 170506A was caused by a communication network outage. GCN circulars are available at [gcn.gsfc.nasa.gov](http://gcn.gsfc.nasa.gov).

## Search for High-Energy Neutrino Emission from Fast Radio Bursts

---

### The IceCube Collaboration<sup>†</sup>

<sup>†</sup>[http://icecube.wisc.edu/collaboration/authors/icrc17\\_icecube](http://icecube.wisc.edu/collaboration/authors/icrc17_icecube)

E-mail: [dxu@icecube.wisc.edu](mailto:dxu@icecube.wisc.edu)

Fast radio bursts (FRBs) are irregular millisecond radio outbursts that are thought to be of astrophysical origin. The first FRB was discovered by the Parkes Radio Telescope in 2007. During this search period from May 2010 to May 2016, a total of 29 FRBs with 13 unique locations (FRB 121102 has repeated 17 times) have been observed, with addition of the Green Bank and Arecibo radio telescopes to the discovery facilities. Although the nature of the FRBs is still largely unknown, the high dispersion measures of the FRBs indicate that they are most likely originating from extragalactic sources. A multitude of models have been proposed to explain the FRB phenomena, most of which involve strong magnetic fields and are of leptonic nature. Currently, there are no concrete models predicting high-energy neutrinos from FRBs, while in principle a strongly magnetized environment such as that from a magnetar could produce short radio bursts due to the volatility of the magnetic fields, and having hadronic processes present at the same time. We will present the results from a recent search for high-energy neutrinos coincident spatially and temporally with FRBs in 6 years of IceCube data.

**Corresponding authors:** <sup>1</sup>Sam Fahey, <sup>1</sup>Justin Vandenbroucke and <sup>1</sup>Donglian Xu\*

<sup>1</sup> *Wisconsin IceCube Particle Astrophysics Center and Department of Physics, University of Wisconsin, Madison, WI 53706, USA*

*35th International Cosmic Ray Conference - ICRC2017-  
10-20 July, 2017  
Bexco, Busan, Korea*

---

\*Speaker.

## 1. Introduction

Fast radio bursts (FRBs) are a new category of bright, broadband, transient astrophysical radio outbursts which typically last a few milliseconds. The first FRB, FRB 010724, was discovered in 2007 in the archival data collected on January 7, 2001 by the Parkes Radio Telescope [1]. More FRBs were found later by several different instruments including the Green Bank Telescope and the Arecibo Telescope, eliminating the instrumental origin hypothesis [2, 3]. To date, a total of 23 FRBs with unique locations have been detected, of which only FRB 121102 has been observed to repeat by multiple instruments [4, 5]. The nature of FRB progenitors is largely unknown. The sources are thought to be extremely compact ( $\sim$  hundreds of kilometers) due to causality. The majority of FRBs are detected at high Galactic latitudes due to limited telescope coverage bias, with much higher dispersion measures (DM) than expected from a Galactic contribution, indicating extragalactic origin. Despite the limited number of detected bursts, the all-sky occurrence rate for FRBs is estimated to be a few thousand per day, consistent with the supernova rate [3, 6]. There exists a multitude of models for FRB progenitors, the majority of which involve strong magnetic fields and leptonic process. Some models associate FRBs with cataclysmic events such as dying stars [7], neutron star mergers [8] or evaporating black holes [9]. The repeated FRB 121102, however, refuted the cataclysmic cause for this burst. Because of its repeating nature, a multi-wavelength follow-up campaign was able to locate this burst's origin to a dwarf galaxy at a redshift of  $z = 0.19$ , at a distance of  $\sim 1$  Gpc [5]. No convincing models exist to explain the repeating burst, although a millisecond magnetar has been recently proposed [10]. It is unclear whether the repeating burst is typical for the FRB population or not, as no other FRBs have been localized to their host galaxies. Multi-wavelength and multi-messenger follow ups would provide additional information and help shed light on the FRB progenitor puzzle. One such follow up study would be a search for high-energy neutrino counterparts with the IceCube neutrino observatory.

IceCube is a cubic-kilometer neutrino detector installed in the ice at the geographic South Pole [11] between depths of 1450 m and 2450 m, completed in 2010. Reconstruction of the direction, energy and to some extent the flavor of the neutrinos relies on the optical detection of Cherenkov radiation emitted by charged particles produced in the interactions of neutrinos in the surrounding ice or the nearby bedrock. IceCube collects data from the whole sky with greater than 99% up time per year, enabling real-time alerts to other instruments and archival data follow ups on interesting signals from other detectors.

## 2. Data Samples

The data samples used in this analysis were based on track-like muon neutrino candidate events selected from previous analyses in search for coincident neutrinos with gamma ray bursts [12, 13]. Specifically, the first year sample from the northern hemisphere (declination  $> -5^\circ$ ) was from [12] and the rest of both northern and southern hemisphere (declination  $< -5^\circ$ ) samples were from [13]. The data taking period for these data samples was from May 31, 2010 to May 20, 2016. During this time, there were 4 unique FRBs detected in the northern hemisphere, namely FRB 110523 (Green Bank Telescope), FRB 110703 (Parkes Telescope), FRB 121102 (Arecibo Telescope) and FRB 130628 (Parkes Telescope). Only 17 of the repeated bursts from FRB 121102 are included in

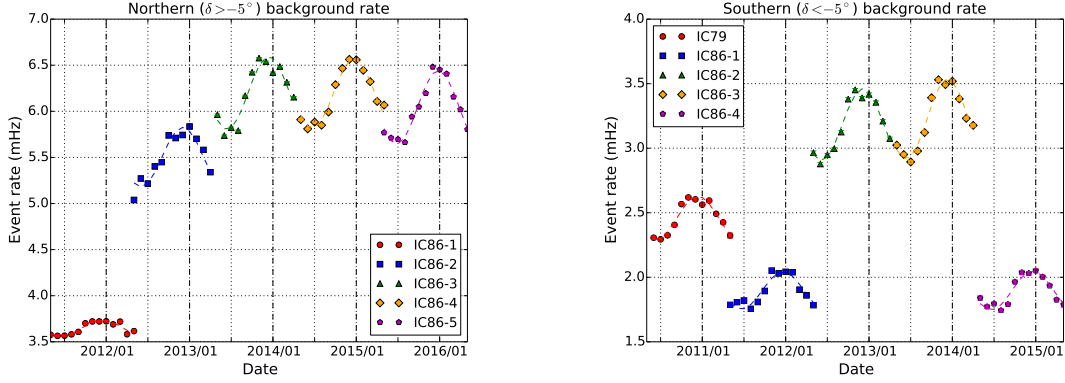


Figure 1: Left: northern hemisphere event distributions. The label “IC86-1“ indicates the first year when IceCube was taking data with the full 86 string configuration in 2011. Right: southern hemisphere event distributions. The label “IC79“ denotes the year when IceCube was taking data with the 79 string configuration in 2010.

this analysis and treated as unique bursts in space and time. In the southern hemisphere, there are 9 unique FRBs, all of which were detected by the Parkes Telescope. The northern event samples consist primarily of atmospheric muon neutrinos because the Earth acts as a filter for cosmic-ray induced atmospheric muons. On the other hand, the southern samples are dominated by down-going atmospheric muons despite a higher energy threshold in the event selection to reduce the enormous atmospheric muon background. As shown in Fig. 1, the first year northern sample has an overall event rate  $\sim 3.5$  mHz, while the rest of the later four year samples have a rate  $\sim 6$  mHz. The southern samples have event rates  $\sim 2 - 3$  mHz. The year to year event rate variation was a combined effect of initial event selections treating each year of the IceCube data sample independently due to frequent filter and data processing scheme updates in the early years of IceCube operation, and optimization to the per year sensitivity which was dependent on the amount of selected GRBs. The annual seasonal variations for both atmospheric muon and neutrino rates are thought to be caused by a combination of temperature and column density of air nuclei changes in the atmosphere over different seasons. The seasonal variations on event rates were taken into account when constructing background ensembles.

The events that are within  $\pm 2$  days from any FRB burst time are defined as the *on time* samples, which will be used to search for correlations once the analysis methods are finalized (see Section 3). The rest of the events are called *off time* samples, and were used in background modeling.

### 3. Analysis Methods

This analysis is designed to search for spatial and temporal correlation between observed fast radio bursts and neutrinos detected by IceCube. An unbinned maximum likelihood method is employed in the search, during which a Poissonian time distribution is assumed. The likelihood for observing  $N$  events with properties  $\{x_i\}$  for  $(n_s + n_b)$  expected number of events is

$$L(N, \{x_i\}; n_s + n_b) = \frac{(n_s + n_b)^N}{N!} \cdot \exp(-(n_s + n_b)) \cdot \prod_{i=1}^N \frac{n_s S(x_i) + n_b B(x_i)}{n_s + n_b} \quad (3.1)$$

where  $n_s$  and  $n_b$  are the expected number of signal and background events, and  $S(x_i)$  and  $B(x_i)$  are the signal and background PDFs. The piecewise contributions to the signal and background PDFs are only spatial and temporal, so no energy dependent PDF is included. A generic test statistic used in this analysis is defined as the logarithmic ratio of the alternative hypothesis and the null hypothesis,  $TS := \ln L(N, \{x_i\}; n_s + n_b) / L_0(N, \{x_i\}; n_b)$ , which can be simplified as

$$TS := -\hat{n}_s + \sum_{i=1}^N \ln\left(1 + \frac{\hat{n}_s S_i}{\langle n_b \rangle B_i}\right) \quad (3.2)$$

To find the most probable number of signal-like events  $n_s$  from  $N$  observed events, one needs to maximize the likelihood function  $L$  with respect to  $\hat{n}_s$ , which is equivalent to maximizing the test statistic  $TS$  because  $L_0$  is a constant.

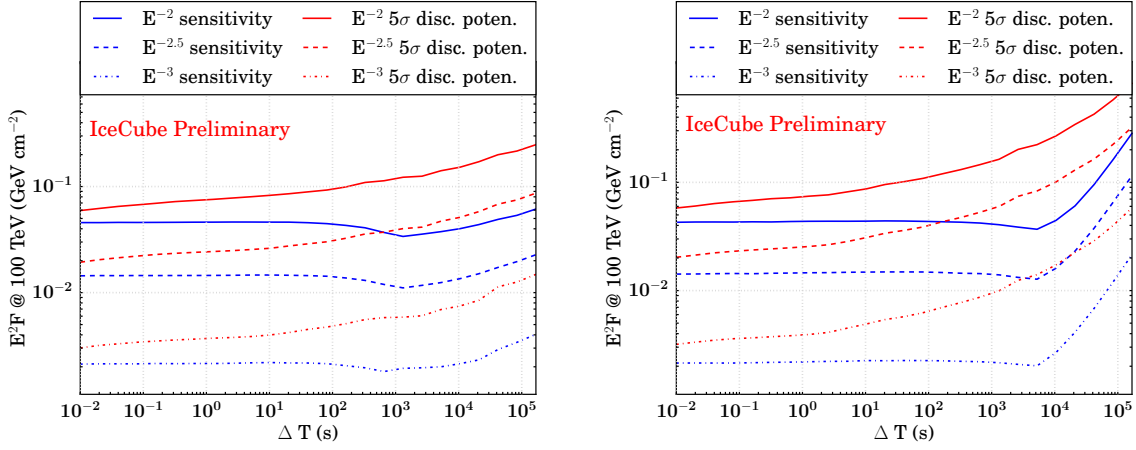


Figure 2: Left: the 90% confidence level pre-trial sensitivity and  $5\sigma$  discovery potential in fluence (time integrated flux) as a function of searched time windows for the max burst search in the northern sky. Right: the 90% confidence level pre-trial sensitivity and  $5\sigma$  discovery potential for the stacking search as a function of searched time windows in the northern sky. Three signal energy spectra are considered here,  $E^{-2}$  in solid lines,  $E^{-2.5}$  in dashed lines, and  $E^{-3}$  in dot dashed lines.

Two search strategies were carried out based on the test statistic defined in Equation 3.2. One is called the *stacking* search, which tests the hypothesis that FRBs emit neutrinos as a class of astrophysical sources; the other is called the *max burst* search, which tests the hypothesis that one or a few FRBs emit neutrinos. In the stacking search,  $n_s$  and  $\langle n_b \rangle$  are the total number of expected signal and background events, respectively, from all FRBs considered. One  $TS$  (with its corresponding  $n_s$ ) value will be returned in one ensemble of events. In the max burst search,  $n_s$  and  $\langle n_b \rangle$  are treated as expected signal and background events, respectively, at a given FRB location, and the  $TS$  will be evaluated for each burst with the most optimal one returned in one ensemble of events. The expected background events  $\langle n_b \rangle$  are obtained from off time data samples as discussed in Section 2.

As the potential neutrino arrival time difference with respect to photons is model dependent and unknown, we employed a model independent search using expanding time windows, each of which is centered at the burst times, similar to [14]. A total of 25 time windows were considered, starting from  $\Delta T = 10$  ms to about 2 days, following an exponential expansion  $\Delta T = 2^i \cdot 10$  ms ( $i = 0, 1, \dots, 24$ ). The various time windows are overlapping, so cross time window trial factors must be accounted for when computing significance values.

#### 4. Sensitivity and Discovery Potential

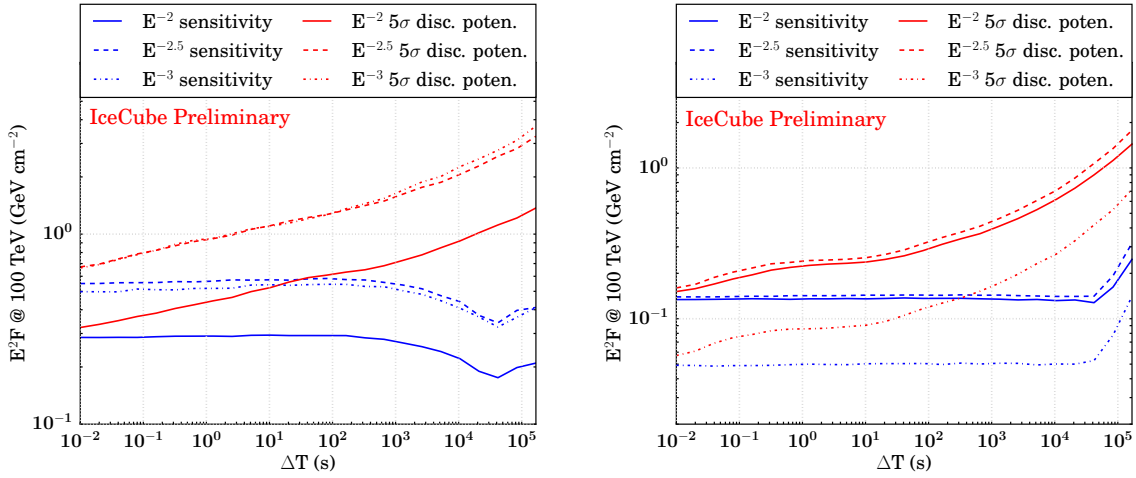


Figure 3: Left: the 90% confidence level pre-trial sensitivity and  $5\sigma$  discovery potential in fluence (time integrated flux) as a function of searched time windows for the max burst search in the southern sky. Right: the 90% confidence level pre-trial sensitivity and  $5\sigma$  discovery potential for the stacking search as a function of searched time windows in the southern sky. Three signal energy spectra are considered here,  $E^{-2}$  in solid lines,  $E^{-2.5}$  in dashed lines, and  $E^{-3}$  in dot dashed lines.

Background ensembles were constructed by injecting fake events following a Poissonian distribution with mean  $\mu = \langle n_b \rangle$  and event properties that follow their corresponding distributions from the off time event samples. The sensitivity and discovery potential were then calculated by injecting signal events following an assumed energy spectrum on top of injected background events: the injected signal fluence (time integrated flux, denoted as  $F$ ) is iterated over until a minimum value is obtained to reach the thresholds set for sensitivity and discovery potential. Here, sensitivity and discovery potential are defined as the minimum signal fluences required to surpass, respectively, the median in 90% of the trials and  $5\sigma$  point in 90% of the trials of a background only test statistic distribution. Shown in Fig. 2 and Fig. 3 are the sensitivity and discovery potentials for the northern and southern hemisphere searches, respectively. For both the stacking and max burst searches in both hemispheres, the sensitivity stays flat in the short time windows that are nearly background free. In the longer time windows where background becomes relevant, however, both the sensitivity and discovery potential are rapidly worsening.

## 5. Results

To avoid artificially introducing a bias for a weak signal search, a *blind* procedure was employed in this analysis. The on time events were put aside during the analysis development, and only analyzed after unblinding, i.e. after the methods were reviewed and approved by the collaboration. The overall analysis procedure returns the most optimal time window for coincident IceCube events with FRBs and the corresponding pre-trial  $p$  values. No significant correlations between neutrinos and FRBs were found. The most significant pre-trial  $p$ -value ( $p = 0.034$ ) among all the searches is in the time window of 655.36 s of the northern max burst search, and the post-trial  $p$ -value is  $p = 0.25$ . The corresponding  $TS$  and  $n_s$  are 3.90 and 0.99, respectively. The most significant pre-trial  $p$ -value for the southern hemisphere is  $p = 0.412$ , which is post-trialled to be  $p = 0.84$ , from the largest time window searched, 167772.16 s. The corresponding  $TS$  and  $n_s$  are 0.64 and 0.78, respectively. The post-trial  $p$ -values were obtained by investigating more background only ensembles. In each such ensemble, a set of expected background events for the largest time window were injected and pre-trial  $p$ -values were calculated for each time window with expected events randomly selected from this set of injected events for the specific time window. The most significant pre-trial  $p$ -value across all time windows is then selected in each ensemble, and hence form a pre-trial  $p$ -value distribution for a set of ensembles. Such a distribution is used to correct for cross time window trial factors. Fig. 4 shows the sky maps of the events that contributed most significantly to their associated nearby FRBs in both the northern and southern max burst searches. The stacking search evaluates all the burst contributions simultaneously so the overall threshold for the scenario that only a few bursts are contributing is higher than the max burst search. The most significant pre-trial  $p$ -value for the stacking search in the northern hemisphere is  $p = 0.074$ , corresponding to a post-trial  $p$ -value of  $p = 0.38$ , in the same optimal time window of 655.36 s as the max burst search. The stacking search for the southern hemisphere yielded a null result, i.e.  $TS$  and  $n_s$  equals to zero, across all time windows. The unblinding results are summarized in Table 1.

## 6. Conclusion and Outlook

A search for a high-energy neutrino signal correlated in time and direction with FRBs has been performed, using a maximum likelihood method applied to 6 years of all sky IceCube data. No significant correlation was found for either the northern or southern hemispheres. The most stringent upper limits on neutrino fluence from FRBs for the prompt time window of  $\Delta T = 10$  ms centered at the burst times are  $E^2 F @ 100 \text{ TeV} = 0.049 \text{ GeVcm}^{-2}$  and  $0.134 \text{ GeVcm}^{-2}$  for the northern and southern hemispheres, respectively. These limits are much improved, especially in the northern hemisphere, compared to a previous search using only one year of IceCube data which searched only 4 bursts, which also resulted in no correlations [15]. With future radio telescopes with a large instantaneous field of view such as CHIME [16] turning on, on the order of thousands of FRBs per year are expected to be detected. IceCube will continue to follow up on the neutrino correlations with FRBs with similar techniques as discussed in these proceedings.

Northern ( $\delta > -5^\circ$ )	$TS$	$n_s$	most significant events ( $t-t_{FRB}, \Delta\Psi$ )	pre-trial $p$ (post-trial $p$ )	optimal $\Delta T$	coincident FRBs
max-burst	3.90	0.99	(+200.806 s, $2.31^\circ$ )	0.034 (0.25)	655.36 s	FRB121102 repeater 2015/06/02 16:38:07.575 UTC
stacking	1.41	1.01	(+200.806 s, $2.31^\circ$ )	0.074 (0.38)	655.36 s	FRB121102 repeater 2015/06/02 16:38:07.575 UTC
Southern ( $\delta < -5^\circ$ )	$TS$	$n_s$	most significant events ( $t-t_{FRB}, \Delta\Psi$ )	pre-trial $p$ (post-trial $p$ )	optimal $\Delta T$	coincident FRBs
max-burst	0.64	0.78	(-16.9 hrs, $0.20^\circ$ )	0.412 (0.84)	167772.16 s	FRB 140514 2014/05/14 17:14:11.06 UTC
stacking	0	0	–	1.0 (1.0)	–	–

Table 1: Unblinding results for four searches in both the northern and southern hemispheres. Only shown in this table are the most significant bursts with the most significantly contributing IceCube events.

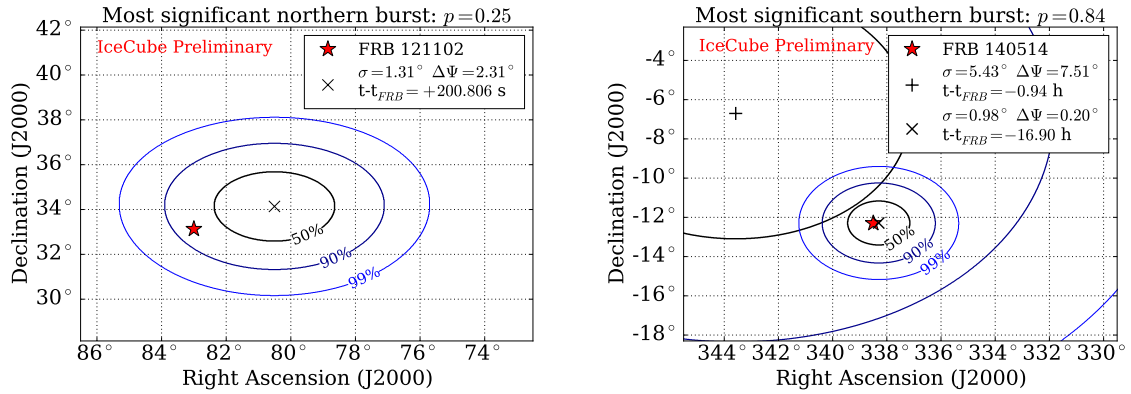


Figure 4: Left: most significant burst and the associated IceCube event from the northern sky max burst search. Right: most significant burst and associated IceCube events from the southern sky max burst search.

## References

- [1] D. R. Lorimer, M. Bailes, M. A. McLaughlin, D. J. Narkevic, and F. Crawford, *Science* **318** (2007) 777–780.
- [2] K. Masui et al., *Nature* **528** (2015) 523.
- [3] L. G. Spitler et al., *Astrophys. J.* **790** (2014) 101.
- [4] P. Scholz et al., *Astrophys. J.* **833** (2016) 177.
- [5] S. Chatterjee et al., *Nature* **541** (2017) 58.

- [6] D. Thornton, B. Stappers, M. Bailes, B. Barsdell, S. Bates, N. Bhat, M. Burgay, S. Burke-Spolaor, D. Champion, P. Coster, et al., *Science* **341** (2013) 53–56.
- [7] H. Falcke and L. Rezzolla, *Astron. Astrophys.* **562** (2014) A137.
- [8] T. Totani, *Publications of the Astronomical Society of Japan* **65** (2013) L12.
- [9] M. J. REES, *Nature* **266** (1977) 333–334.
- [10] B. D. Metzger, E. Berger, and B. Margalit, *Astrophys. J.* **841** (2017) 14.
- [11] **IceCube** Collaboration, M. G. Aartsen et al., *JINST* **12** (2017) P03012.
- [12] **IceCube** Collaboration, M. G. Aartsen et al., *The Astrophysical Journal Letters* **805** (2015) L5.
- [13] **IceCube** Collaboration, M. G. Aartsen et al., [arXiv:1702.06868](https://arxiv.org/abs/1702.06868).
- [14] **IceCube** Collaboration, R. Abbasi et al., *Nature* **484** (2012) 351–353.
- [15] S. Fahey, A. Kheirandish, J. Vandenbroucke, and D. Xu, *arXiv preprint arXiv:1611.03062* (2016).
- [16] **CHIME Scientific** Collaboration, M. Amiri et al., [arXiv:1702.08040](https://arxiv.org/abs/1702.08040).

## IceCube as a Neutrino Follow-up Observatory for Astronomical Transients

---

### The IceCube Collaboration<sup>†</sup>

<sup>†</sup> [http://icecube.wisc.edu/collaboration/authors/icrc17\\_icecube](http://icecube.wisc.edu/collaboration/authors/icrc17_icecube)

E-mail: [kmeagher@ulb.ac.be](mailto:kmeagher@ulb.ac.be)

The IceCube Neutrino Observatory is a cubic kilometer neutrino telescope located at the geographic South Pole which can observe neutrinos at energies from GeV to above a PeV. Now that IceCube has realized its primary goal, the detection of high-energy astrophysical neutrinos, the task remains to identify the sources of these neutrinos. Observing neutrinos in coincidence with transient astrophysical events would be a smoking gun for hadronic acceleration and provide other valuable insights into the nature of the sources. This contribution discusses a new approach to investigate transient phenomena by performing a rapid follow-up analysis. This is done by searching for neutrinos in coincidence with detections by other observatories so that the results can be distributed rapidly to the rest of the astronomical community. In order to accomplish this with minimum delay, the data must be processed immediately at the South Pole and be transmitted to the Northern Hemisphere via the Iridium satellite network. The data processing pipelines, maximum likelihood analysis, and sensitivity of this analysis will be discussed.

**Corresponding authors:** Kevin Meagher<sup>\*1</sup>

<sup>1</sup> *Université Libre de Bruxelles, Science Faculty CP230, B-1050 Brussels, Belgium*

*35th International Cosmic Ray Conference — ICRC2017  
12–20 July, 2017  
Bexco, Busan, Korea*

---

<sup>\*</sup>Speaker.

## 1. Introduction

Multimessenger astronomy is the combination of observations of cosmic rays, neutrinos, gravitational waves, and photons of all wavelengths, and it represents a powerful tool to study the non-thermal universe. For quite some time, the IceCube Neutrino Observatory[1] has contributed to multimessenger astronomy by searching for neutrino events correlated with transient astrophysical events observed by other messengers such as gamma-ray bursts[2], active galactic nuclei[3], and gravitational wave events[4]. Despite the fact that IceCube has observed a diffuse flux of astrophysical neutrinos [5], the source of this flux has yet to be identified. Past efforts to correlate IceCube neutrinos with astrophysical transients were hindered by long delays between the original observation and the completion of the IceCube analysis, with results too late to contribute to the observation efforts. This contribution describes a new program to respond to astronomical transients observed by other instruments. These analyses will be performed quickly so that IceCube can issue follow-up notices to the rest of the astronomical community. With this program in place, IceCube will become a full member of the astrophysical community contributing fully to the rapid analysis of astronomical transients. This program is separate from other efforts by the IceCube collaboration to issue circulars generated solely from IceCube data to astronomers[6]. These real-time efforts, such as the Optical, X-ray, and gamma-ray follow-up programs, are documented elsewhere[7, 8, 9].

## 2. Selection of Astronomical Transients

Astronomical transients will be selected from publicly available circulars such as the Astronomer’s Telegram (ATEL)<sup>1</sup> or the Gamma-ray Coordinate Network (GCN)<sup>2</sup>. Analyses may also be initiated upon request by IceCube’s MOU partners, and the results will be shared only with the partners according to the rules of the MOU. Transients will be selected based on the following criteria: 1) Potential to generate TeV neutrinos—the source must exhibit at least one of the following: observation of neutrinos by IceCube or another neutrino telescope, evidence for high energy particle acceleration such as VHE gamma rays or cosmic rays, or theoretical predictions of hadronic acceleration. 2) New or unexpected behavior—The discovery of a new class of astronomical events or unusual behaviors by an otherwise well understood class of events. 3) Brightness—unusually bright or close transients where the probability of neutrino detection is significantly greater than the typical event in its class. 4) General interest—an unusual amount of ATEL or GCN notices for a source of its class. Since this analysis will not be tailored to any specific class of events, it will be capable of being used to investigate any type of sources, particularly new classes which have not been observed yet.

The IceCube Realtime Oversight Committee (ROC) is mandated with oversight and coordinating of IceCube’s realtime programs, both those initiated solely with IceCube data such as the optical follow-up [8], gamma-ray follow-up [9] and high-energy starting event (HESE) [10] programs as well as externally triggered analyses such as described in this paper. The members of the ROC were specifically chosen from disparate time zones to ensure that at least one member will be

---

<sup>1</sup><http://www.astronomerstelegam.org/>

<sup>2</sup><https://gcn.gsfc.nasa.gov/>

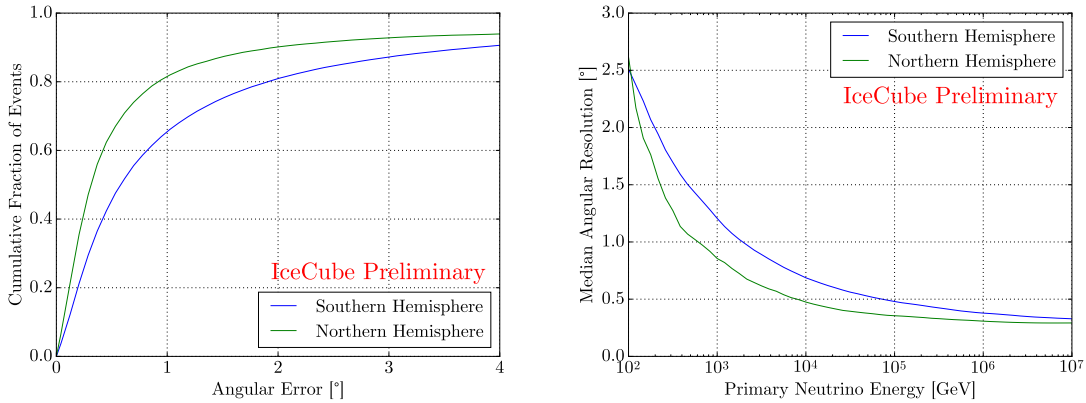


**Figure 1:** Angular error of events in the online neutrino event selection assuming an  $E^{-2}$  energy spectrum. The angular error is the opening angle between the online reconstructed neutrino direction and the true direction in the simulation. The left plot shows the cumulative distribution. The right plot shows the median angular error as a function of the true primary neutrino energy.

active at all times of the day. In order to initiate a realtime analysis the observer will contact the committee with the right ascension, declination, start and stop time, and source extension of the proposed analysis. The approval of at least one ROC member is necessary to initiate the analysis. Upon reception, the ROC will determine whether to issue a circular. In general, for analyses which favor the null-hypothesis, a follow-up circular will not be issued.

### 3. Data Processing and Event Selection

The remote location of IceCube at the Geographical South Pole presents a number of challenges to analyzing data quickly after it is collected. To overcome these obstacles, the IceCube collaboration has developed a realtime data processing pipeline described in detail in references [7, 8, 9] and summarized here. The IceCube online filtering system contains a computing cluster with  $\sim 400$  CPU cores which continuously calibrates and reconstructs events as they are recorded by the data acquisition system. This system includes several reconstruction algorithms that characterize each event's extracted light arrival information against the expected patterns from muon neutrino events to determine the direction, position and energy of each event [11]. IceCube has many detection channels to reconstruct different types of events based on their flavor and energy. Because of their superior angular resolution  $< 1^\circ$ , the muon channel is the most important for multimessenger astronomy. Based on initial reconstructions, approximately 0.2% of events are selected to be potentially of neutrino origin and are processed with additional, more sophisticated and computationally intensive reconstructions. The selection targets well-reconstructed events with a charge threshold that depends on the reconstructed direction, and with more stringent cuts applied in the atmospheric muon dominated down-going region [9]. The this online event selection has been in operation since 2011, with each year seeing incremental improvements that bring better tools developed offline to the online system.

The results of these reconstructions are used as the input to a multivariate classifier. Further reduction of the atmospheric muon background and separation of an astrophysical signal is achieved

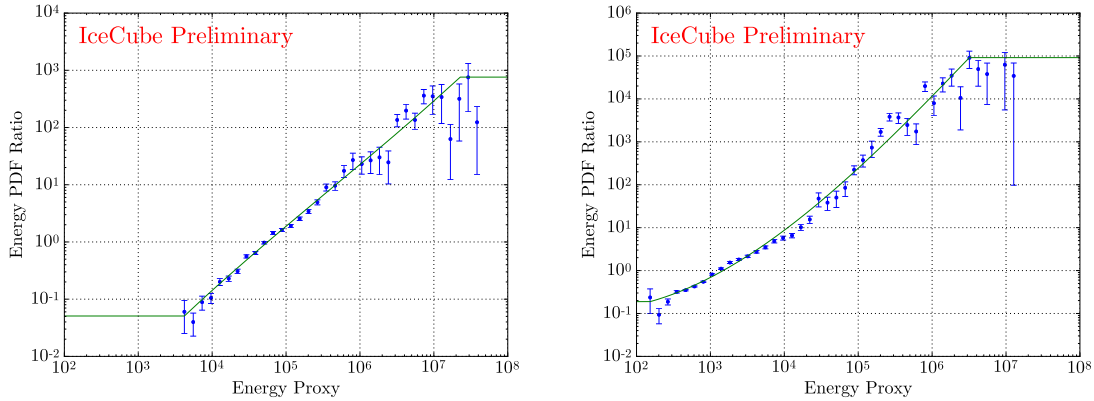


**Figure 2:** Examples of energy probability distribution function (PDF) ratios. The ratio of the Signal Energy PDF to the Background Energy PDF is shown for two different declinations:  $\delta = -15^\circ$  (Left) and  $\delta = +15^\circ$  (Right). The ratio is fit to a 3<sup>rd</sup> order polynomial (shown in green) for use in the likelihood analysis.

by training boosted decision trees (BDTs) [12]. The training is done separately for the Northern and Southern Hemisphere to account for the different kinds of background encountered in each region, yielding a final event selection rate of 5 mHz, equally divided between both hemispheres. A description of the variables entering the BDTs can be found in [9]. Two different subsamples are defined from the output of the BDTs: one for the Northern Hemisphere and a second for the Southern Hemisphere. The neutrino effective area, as used in this analysis, is shown in Fig. 3. The angular error for selected neutrino events, and its dependence on the energy of the neutrino, is shown in Fig. 1. All events selected by the BDT are immediately transferred from the South Pole to the North, where they are made available in a database.

#### 4. Analysis Method

This analysis uses an unbinned likelihood method to evaluate if neutrino candidates observed by IceCube are coincident with an astronomical transient. The technique is based on previous work done by the IceCube collaboration for off-line analyses of gamma-ray burst studies [2]. These studies showed that the unbinned likelihood method was more sensitive than simple binned methods. The likelihood of observing  $n_s$  signal events and  $n_b$  background events is:

$$\Lambda(\mathbf{x}_i; n_s) = -n_s + \sum_i^N \ln \left( \frac{n_s S(\mathbf{x}_i)}{\langle n_b \rangle B(\mathbf{x}_i)} + 1 \right) \quad (4.1)$$

where  $N = n_s + n_b$ ,  $S(\mathbf{x})$  is the probability density function (PDF) for signal events and  $B(\mathbf{x})$  is the background PDF.  $\mathbf{x}_i$  represents the properties of the  $i^{\text{th}}$  event.  $n_b$  can be replaced with  $\langle n_b \rangle$ , the measured background rate from off-source data to make this a one dimensional likelihood function. For this analysis, the PDFs will include both a spatial and an energy component.

For the spatial signal PDF, the Kent distribution is used. This distribution is the analog of a bivariate normal distribution when projected on to the surface of a unit sphere [13]. The distance from the reconstructed neutrino direction to the source is used as the random variable and the estimated angular uncertainty of the neutrino is used as the width parameter. The error parameter is

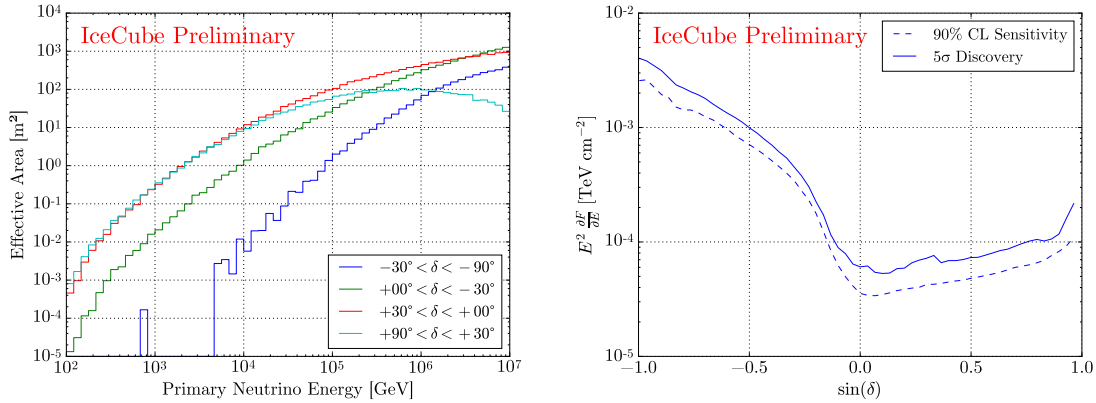


**Figure 3:** **Left** Effective areas for the online neutrino event selection. Four different declination bands are shown. At low energies, the Northern Hemisphere has a higher effective area due to the more permissive cuts. However, at high energies, the effective area in the Northern Hemisphere decreases due to absorption in the Earth. **Right** The performance as a function of declination, using an analysis lasting  $10^5$  seconds with no source extension.  $10^5$  seconds is slightly longer than 1 day and is considered the typical timescale for this analysis. Most of the declination dependence is a result of changing background rates. The solid line shows the discovery potential: the minimum flux required to make a  $5\sigma$  discovery 50% of the time. The dotted line shows the sensitivity: the 90% confidence upper-limit on the flux at the median value of the test statistic for the background only hypothesis.

the estimated angular uncertainty of the neutrino added in quadrature with the source extension if present. Since the selected events are nearly symmetric in azimuthal directions, a uniform distribution will be used for the spatial background PDF (there is a significant deviation from uniform in the zenith direction but this does not affect the results for an analysis at a single point.)

The shape of the energy PDFs is highly dependent on zenith angle, requiring that the PDF calculation is performed separately for each trigger. For a given trigger, the energy PDFs are constructed empirically from both simulation and off-time data using events from within a  $\pm 4^\circ$  declination band about the source declination. The signal PDF is calculated using simulated neutrino events weighted to an  $E^{-2}$  energy spectrum incident on Earth’s surface. Off-time data is used to calculate the background PDF and is augmented with neutrino simulation weighted to an atmospheric spectrum in high-energy bins where there is insufficient statistics from data. The ratio of signal to background is histogrammed and fit to a third order polynomial. In order to avoid unphysical behavior at the highest and lowest energies, the PDF are flattened out above and below the highest and lowest bin respectively. Example energy PDFs are shown in Figure 2. Unlike IceCube GRB analyses, this analysis does not use time PDFs; instead cuts removing data outside the time window of interest are used.

The likelihood analysis provides an estimate of the number of signal events in the data sample  $n_s$ . The analysis will only select events with a signal-to-background ratio greater than 0.1. For an analysis with a single event, the event needs a signal-to-background ratio of greater than 1 in order to result in a non-zero  $n_s$ . For comparison a typical 100 TeV neutrino within the  $1\sigma$  error circle will have a signal-to-background ratio of 100 and a 1 PeV event could have a ratio as high as  $10^5$ . To calculate the significance of a given analysis, the likelihood value  $\Lambda$  is used as a

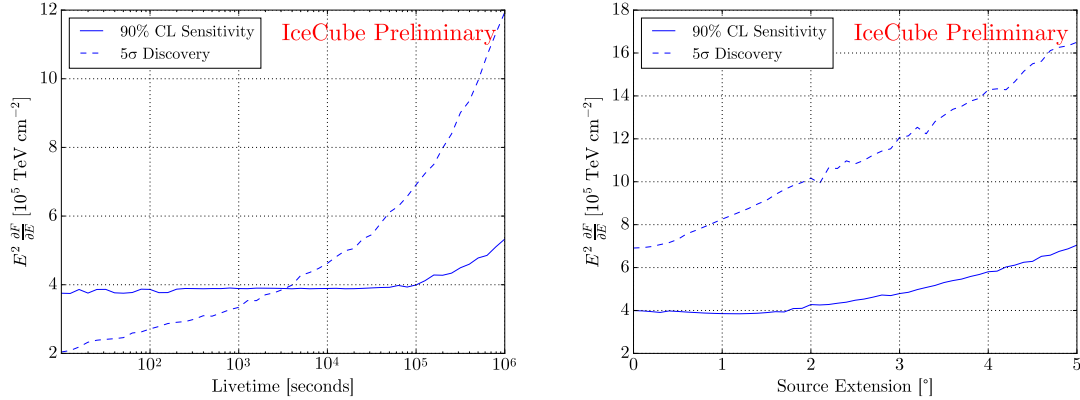


**Figure 4:** **Left:** The time dependence of the analysis sensitivity and discovery potential as a function of duration, for a declination of  $\delta = +15^\circ$  and no source extension. Since the background is low, the sensitivity remains flat for timescales less than  $10^5$  seconds. **Right:** Performance as a function of source extension for an analysis with a duration of  $10^5$  seconds and a declination of  $\delta = +15^\circ$ .

test statistic. Pseudo-experiments with azimuthally scrambled off-time data are used to empirically determine the survival function. Point estimates of the flux or upper-limits are then performed using an iterative search method of pseudo-experiments with both injected off-time data and simulated neutrino events.

To evaluate the performance of the analysis, two figures of merit were defined: the sensitivity and the model discovery potential. The sensitivity is defined as the 90% confidence upper limit on the median value of the background only test statistic. The discovery potential is defined as the flux in which a  $5\sigma$  discovery will be made 50% of the time. Plots of these performance metrics are shown in Figures 3 and 4.

## 5. Results

Six transient analyses have been performed to date. This section describes each one briefly.

*PS16cgx* — On 27 April, 2016 IceCube detected a HESE event with track-like characteristics at location  $\alpha = 240.57^\circ$  and  $\delta = +9.34^\circ$  with a positional uncertainty of  $\Delta\Psi = 0.6^\circ$  [14]. The Pan-STARRS optical telescope followed up this event three days after the detection and observed 7 supernova candidates consistent with the IceCube event: 6 of them showed flat light curves across 5 days of monitoring consistent with being after peak. However, PS16cgx showed a rising light curve consistent with an explosion at the time of the IceCube event [15]. The trigger time was taken from the IceCube event (05:52:32 UTC) and the position from the Pan-STARRS candidate ( $\alpha = 16^{\text{H}}01^{\text{M}}18.60^{\text{S}}$ ,  $\delta = +09^\circ 51' 53.1''$ ) and a duration of  $10^5$  seconds (1.16 days) was selected with the trigger time at the center of the time window. The HESE event (RunID = 127853, EventID = 67093193) was excluded from the likelihood analysis. Only one other event was observed, and it had a large positional uncertainty and a low energy, and therefore  $n_s = 0$ .

*Cygnus X-3* — In conjunction with a major radio flare, the *Fermi*-LAT observed an increase in the gamma-ray emission of the microquasar at a significance level of nearly  $5\sigma$  [16]. Using the

Source	Start Time [UTC]	Duration [D:H:M:S]	RA	Dec	Extension
PS16cgx	2016-04-26 15:59:12	1:03:46:40	240.33°	+09.86°	0.0°
Cygnus X-3	2017-04-03 00:00:00	1:00:00:00	308.11°	+40.96°	0.0°
GRB 170405A	2017-04-05 18:35:49	0:00:20:02	219.83°	-25.24°	0.0°
AGL J0523+0646	2017-04-15 11:50:00	2:00:00:00	080.86°	+06.78°	0.6°
IceCube 170506A	2017-05-06 00:36:55	1:00:00:00	221.80°	-26.00°	1.0°
AT2017eaw	2017-05-10 12:00:00	3:00:00:00	308.68°	+60.19°	0.0°

**Table 1:** The parameters of each transient analysis performed to date.

catalog location of Cygnus X-3 microquasar and the time window of the Fermi emission (2017-04-03 00:00:00 to 2017-04-04 00:00:00 UTC), a transient analysis was performed. Three events were identified by the unbinned analysis. However, all three were low-energy events with the source outside their 68% confidence contour, and the final result of the analysis was  $n_s = 0$ .

*GRB 170405A* — *Fermi*-LAT observed a hard GRB with more than 13 events observed above 100 MeV spatially and temporally correlated with the GRB. The highest-energy photon was a 900 MeV event which is observed 445 seconds after the GBM trigger[17]. Normally, IceCube follow-up analyses are handled by the dedicated gamma-ray burst analyses. But, in this case, due to the interesting nature of this burst, a transient analysis was requested as a cross-check to the GRB analysis. The analysis was performed using the same time windows as the *Swift*-BAT refined analysis ( $T - 239$ s to  $T + 963$ s where T is the *Swift* trigger time) [18] and the Enhanced *Swift*-XRT position ( $\alpha = 14^{\text{H}} 39^{\text{M}} 18.64^{\text{S}}$ ,  $\delta = -25^{\circ} 14' 37.3''$ ) [19]. No events were observed in conjunction with this burst.

*AGL J0523+0646* — AGILE reported the appearance of intense gamma-ray emission above 100 MeV located at  $\alpha = 80.855^{\circ}$ ,  $\delta = +6.777^{\circ}$  for a period of two days at greater than  $6\sigma$  [20]. Using the same time window as reported by AGILE (2017-04-16 11:50 UT to 2017-04-18 11:50 UT) and the same coordinates ( $\alpha = 80.855^{\circ}$ ,  $\delta = +6.777^{\circ} \pm 0.6^{\circ}$ ) a transient analysis was performed. No events were identified.

*IceCube-170506A* — on 2017-05-06 12:36:55.80 UT IceCube observed a HESE track-like event[21]. The offline reconstruction yielded a best fit position of  $\alpha = 221.8^{\circ} \pm 3.0^{\circ}$ ,  $\delta = -26.0^{\circ} \pm 2.0^{\circ}$ , where the error circles represent 90% containment. To observe any potential clustering of neutrinos a transient analysis was performed, using a time window of  $\pm 12$  hours from the HESE event. The event (RunID = 129474, EventID = 32674593) removed from consideration in the analysis. No further events were observed consistent with the source position.

*AT2017eaw* — A Supernova candidate was observed on 2017-05-14 located about 2.4' from the center of NGC 6946, a nearby galaxy at  $z = 0.000133$  and distance  $\sim 5.5$  Mpc [22]. Although the supernova does not show evidence of strong interactions with the circumstellar medium, the mostly likely scenario for neutrino emission from supernovae, due to its extreme closeness it was deemed interesting enough for a transient analysis. A three day time window was selected from May 10.5 to May 13.5. Four events were observed in coincidence, all of them were low-energy with large positional uncertainty. The likelihood analysis estimated the number of signal events to be  $n_s = 0.742$ , with a p-value of 10% ( $1.28\sigma$ ).

Source	$n_s$	p-value	Significance	90% upper limit [TeV cm <sup>-2</sup> ]
PS16cgx	0.00	1.00	0.00 $\sigma$	$3.698 \times 10^{-5}$
CygnusX3	0.00	1.00	0.00 $\sigma$	$5.613 \times 10^{-5}$
GRB 170405A	0.00	1.00	0.00 $\sigma$	$5.659 \times 10^{-4}$
AGL J0523+0646	0.00	1.00	0.00 $\sigma$	$4.124 \times 10^{-4}$
IceCube 170506A	0.00	1.00	0.00 $\sigma$	$5.482 \times 10^{-5}$
AT2017eaw	0.74	0.10	1.28 $\sigma$	$8.871 \times 10^{-5}$

**Table 2:** The results of the likelihood method analysis for each of the transients to date is summarized in this Table.  $n_s$  is the estimator for the number of signal events.

The parameters of these analyses are summarized in Table 1 and the results are summarized in Table 2. All of the analyses presented here were performed with the 2016-2017 event selection. On May 18, 2017 IceCube began a new data run with an improved BDT for the online event selection. This new selection has improved acceptance to downgoing signal events resulting in a significant improvement in sensitivity in the Southern Hemisphere. In addition, there is an improvement in rejecting poorly-localized background events in both hemispheres, resulting in an improvement in the discovery potential.

## References

- [1] **IceCube** Collaboration, M. G. Aartsen et al., *J. Inst.* **12** (2017) P03012.
- [2] **IceCube** Collaboration, M. G. Aartsen et al., *ApJ* **824** (2016) 115.
- [3] **IceCube** Collaboration, M. G. Aartsen et al., *ApJ* **835** (2017) 45.
- [4] **ANTARES, IceCube, LIGO Scientific, & Virgo** Collaboration, *PRD* **93** (2016) 122010.
- [5] **IceCube** Collaboration, M. G. Aartsen et al., *ApJ* **833** (2016) 3.
- [6] **IceCube** Collaboration, [PoS \(ICRC2017\) 982](#) (these proceedings).
- [7] **IceCube** Collaboration, M. G. Aartsen et al., *Astropart. Phys.* **92** (2017) 30.
- [8] **IceCube** Collaboration, M. G. Aartsen et al., *A&A* **539** (2012) A60.
- [9] **IceCube, MAGIC, & VERITAS** Collaboration, M. G. Aartsen et al., *J. Inst.* (2016) P11009.
- [10] **IceCube** Collaboration, M. G. Aartsen et al., *PRL* **113** (2014) 101101.
- [11] **IceCube** Collaboration, M. G. Aartsen et al., *J. Inst.* **9** (2014) P03009.
- [12] Y. Freund & R. E. Schapire, *J. Comput. Syst. Sci.* **55** (1997) 119.
- [13] J. T. Kent, *J. Royal. Stat. Soc.* **44** (1982) 71.
- [14] E. Blaufuss, *GCN Circ.* **19363** (2016).
- [15] S. Smartt, *GCN Circ.* **19381** (2016).
- [16] A. Loh & S. Corbel, *ATEL* **10243** (2017).
- [17] G. Vianello, *GCN Circ.* **20987** (2017).
- [18] A. Lien, *GCN Circ.* **20999** (2017).
- [19] P. Evans et al., *GCN Circ.* **20985** (2017).
- [20] F. Lucarelli, *ATEL* **10282** (2017).
- [21] E. Blaufuss, *GCN Circ.* **21075** (2017).
- [22] S. Dong & K. Z. Stanek, *ATEL* **10372** (2017).